5-2021

Out-of-Plane Behavior of Concrete Insulated Wall Panels with 2-Inch, 8-Inch, and 10-Inch Insulation

Jacob Luebke
University of Nebraska-Lincoln, jluebke3@huskers.unl.edu

OUT-OF-PLANE BEHAVIOR OF CONCRETE INSULATED WALL PANELS WITH 2-INCH, 8-INCH, AND 10-INCH INSULATION

By

Jacob A. Luebke

A THESIS

Presented to the Faculty of

The Graduate College at the University of Nebraska

In Partial Fulfillment of Requirements

For the Degree of Master of Science

Major: Architectural Engineering

Under the Supervision of Professor Marc Maguire

Lincoln, Nebraska

May 2021

OUT-OF-PLANE BEHAVIOR OF CONCRETE INSULATED WALL PANELS WITH 2-INCH, 8-INCH, AND 10-INCH INSULATION

Jacob A. Luebke, M.S.

University of Nebraska, 2021

Advisor: Marc Maguire

Insulated concrete sandwich wall panels provide structurally and thermally efficient building envelopes and are becoming more popular as energy regulations tighten. To continually adapt to an ever-changing building market and new energy regulations, insulated concrete wall panels are being constructed with thinner wythes, thicker insulation, and relying on partial composite action to decrease material costs and increase thermal and structural efficiency. Numerous methods of the design of partially composite insulated concrete sandwich wall panels have been introduced in recent decades and have been verified by comparing their results to existing experimental testing. Existing testing data for insulated concrete sandwich wall panels does not contain adequate experimental testing for thin wythe and thick insulation sandwich wall panels; therefore, the current methods of design have not been adequately verified for the design of such sandwich wall panels.

This project aimed to validate current methods of design of sandwich wall panels for the use of thin wythe and thick insulation concrete sandwich wall panels. The study concluded that current methods of design adequately predict behavior of thin wythe and thick insulation concrete sandwich wall panels within the elastic region but do not adequately predict the ultimate capacity of thin wythe and thick insulation concrete sandwich wall panels.

The predictions of two existing methods, which predict elastic shear stiffness of connectors, were compared to the results of 15 double shear tests for three unique connectors with agreeable results. The predictions of three methods, which predict elastic behavior and two

methods, which calculate ultimate capacity, were compared to the testing results of six full-scale panels. All methods predicting elastic behavior proved to be accurate and one method adequately predicted ultimate panel capacities.

(143 pages)

DEDICATION

I dedicate this thesis to my loving and ever-supporting wife, Bayli Luebke. Thank you for your patience, encouragement, and faith in me that made the completion of this long-term goal possible.

ACKNOWLEDGMENTS

The author would like to thank the Portland Cement Association for their financial support which helped fund this research. Also, appreciation is extended to Fibergrate Composite Structures who provided material at no cost for this research.

The author would also like to express sincere gratitude to Dr. Marc Maguire for his guidance, patience, and encouragement throughout this process. Several graduate and undergraduate students donated their time and efforts, as well, for which the author would like to express appreciation. Thanks goes out to Salam Al-Rubaye, Fray Pozo-Lora, Zach Benson, Mathew Henggeler, Nathaniel Colton, Liam Baker, Mike Horn, Huy Nguyen, Isaiah Rose, Griffin Anderson. The author would also like to thank Jose Lopez.

Jacob A. Luebke

TABLE OF CONTENTS

LIST OF TABLES

Table Page

LIST OF FIGURES

Figure Page

LIST OF SYMBOLS AND NOTATION

A_a, A_{sc}	cross sectional area of connector
A_{in}	area of foam subject to shear
b	panel width
E_a	modulus of elasticity of connector
F_E	elastic load limit
f_r	concrete modulus of rupture
F_u	ultimate capacity
f_{uc}, F_{uc}	ultimate shear capacity of a single connector
G_{in}	insulation shear modulus
I	moment of inertia
I_{exp}	equivalent moment of inertia obtained from testing
I_{FC}	fully composite moment of inertia
I_{NC}	non-composite moment of inertia
I_{sc}	connector moment of inertia
K_E	elastic shear stiffness
$K_{E.Panel}$	uniform shear stiffness of panel
K_{IE}	inelastic shear stiffness
l	span length
L_{ac}	initial connector length
M_{cr}	cracking moment
M_{crFC}	fully composite cracking moment
M_{crNC}	non-composite cracking moment
M_u	ultimate moment

M_{uFC}	fully composite ultimate moment
M_{uNC}	non-composite ultimate moment
N	number of connectors
P_2	applied shear force
Q_{FC}	first moment of area considered fully composite section properties
$q_{baseline}$	100 lb/in [based on shear flow strength of grid alone]
q_{demand}	shear flow demand
q_n	shear flow capacity
r	distance from center of wythe to center of panel
V_{demand}	shear demand based on shear flow
V_{dw}	shear carried by connector dowel action
V_{in}	shear carried by the insulation
V_{max}	maximum shear force due to applied load
V_{nc}	shear capacity at connector location
V_{sc}	total shear strength
V_t	distance to neutral axis
V_{tr}	shear carried by connector truss action
w_{tribv}	tributary width for shear flow
X	insulation thickness
γ	initial insertion angle of connector
γ_{type}	gamma factor for insulation type [EPS or XPS]
$\gamma_{thickness}$	gamma factor for insulation thickness
$\gamma_{spacing}$	gamma factor for grid spacing
$\gamma_{orientation}$	gamma factor for grid orientation [vertical or transverse]
δ_s	relative slip of the wythes

ΔE	elastic deflection limit
ΔL_{ac}	change of connector length
Δu	ultimate deflection limit
Δ_2	change in length of the truss element
ε_{sc}	axial strain in connector
θ	connector insertion angle
θ'	adjusted connector insertion angle
κ	percent or degree of composite action
ϕ	relative slip of the wythes

CHAPTER 1. INTRODUCTION

Insulated concrete sandwich wall panels (ICSWPs) are becoming more popular as the industry continues to move toward Leadership in Energy and Environmental Design (LEED) certified buildings. ICSWPs consist of two wythes of concrete sandwiching a layer of insulation. The sandwiched layer of insulation provides the increased thermal efficiency sought after in LEED certified buildings. A shear connector bridges the two wythes and transfers shear forces through its connection.

ICSWPs can be designed as non-composite, fully composite, or partially composite. These categories indicate the degree to which the two concrete wythes act in unison to resist loads. Partially composite ICSWPs can be designed to a certain degree of composite action necessary to resist the expected load, allowing engineers to optimize the structural capacity of the panels and reduce construction costs.

As partially composite ICSWPs become more popular, more effort has been made in developing methods to design and analyze these structural panels with increased efficiency to ensure safety and to reduce costs. Many of the current and past methods of analysis and design have been verified by comparing their results to existing ICSWP testing in academic literature. Due to the complex nature of many of the design methods, a simplified approach has been taken and is currently used for the design of ICSWPs in practice. In practice, engineers from precast plants or other specialized firms will use the complex methods of design to determine what is known as *percent* or *degree of composite* action. Effective section properties, such as an effective moment of inertia, are provided to the structural engineers on a project who use these effective section properties to design the panels using common design principles for solid concrete wall panels.

As ICSWPs evolve, they continue to be constructed in increasingly different ways and dimensions. Concrete wythes are being constructed thinner to reduce cost, waste, and to create

lighter building systems. Insulation thicknesses are increasing to improve the thermal efficiency of building envelopes. As insulation thicknesses increase, the FRP connectors need to be modified to account for the larger bridging distance between concrete wythes.

The shear connectors, which were commonly made of steel, are increasingly comprised of fiber reinforced polymer (FRP) in place of steel connectors to mitigate the problem of thermal bridging between the two concrete wythes. Most concrete sandwich wall panels are constructed with commercially available connectors, which vary widely in shape, size, and shear transfer mechanism; currently, none span the insulation thicknesses of eight and ten inches that are investigated within this research. Due to this, non-proprietary shear connectors were constructed using glass fiber reinforced polymer (GFRP) grating.

The testing data in literature lacks data on panels with thin wythes or thick insulation. Because of the lack of testing, the current methods of design and analysis for ICSWPs have not been adequately verified against physical testing for panels with thin wythes or thick insulation. This thesis has two purposes:

- Verify that these current design methods can accurately predict the behavior of thin wythe and thick insulation panels so engineers can have confidence in designing thin wythe and thick insulation panels with these methods.
- Verify that thin wythe and thick insulation panels are viable structural wall panels and can resist expected real-world loading. Thin and thick are subjective measurements; however, for the purposes of this thesis, thin wythes will be defined as wythes measuring two inches or less, and thick insulation will be defined as six inches or thicker.

1.1 Objectives and Scope

The primary research objectives are to:

1. Verify the accuracy of current design and analysis methods for transverse loads against testing data of ICSWPs with dimensions that lie beyond the bounds of the existing testing data including thin wythes and thick insulation.
2. Verify the viability of ICSWPs with thin wythe and thick insulation for use in real-world applications.

This thesis contains a thorough literature review, which focuses on identifying the current methods of design and analysis of ICSWPs and the corresponding testing data that has been used to verify them. Fifteen double shear tests were performed, and the specimens' deflections were recorded to determine the shear stiffnesses of various connectors. Six large-scale panels were loaded in flexure until failure. The deflection and relative wythe slips at various connector locations of the panels were measured, recorded, and compared to the predicted results of current design methods.

Among the full-scale panels are two panels with two-inch-thick wythes, two panels with eight-inch-thick insulation, and two panels with 10-inch-thick insulation. The two-inch-thick wythe panels were constructed and tested to represent the thin wythes described in the objectives, and the eight and 10-inch-thick insulation panels comprise the thick insulation panels described in the objectives.

The shear stiffness values obtained from the double shear tests are necessary for the evaluation of many of the current design and analysis methods for ICSWPs. Five double shear specimens were tested for each of the three connectors used in the three different groups of full-scale panels described above.

1.2 Thesis Organization

This thesis contains six chapters including the introduction, literature review, experimental program, experimental results, discussion, and conclusions. A summary of each chapter and how it helps to meet the objective of this thesis is provided below.

- In chapter 1, the introduction, the real-world applications, and implications of research on thick insulation and thin wythe ICSWPs is described to provide context to all readers for the purpose of the research. In addition, the objectives and scope of the research is outlined. The purpose of each chapter of the thesis is also explained in context of the research objectives.
- In chapter 2, a review of relevant literature on the topic of ICSWPs is provided. Specifically, two topics comprise the focus of the chapter. The first is listing and describing the various methods of analysis that are being and have been used to predict ICSWP behavior, which provides background to the methods used later in chapter 5. The second is an in-depth review of the scope of existing testing data on ICSWPs which highlights the need of the testing and discussion in this thesis.
- In chapter 3, the experimental program is outlined. The creation of all testing specimens, their configurations, and the methods of their testing are illustrated to the degree that replication of all testing could be accomplished. All deviations from testing procedures and errors in specimen creation are listed to provide all relevant information for the latter discussion of data.
- In chapter 4, the results of the experimental program are provided. This section provides all relevant testing data recorded necessary for the latter discussion. In addition, failure mechanisms for each specimen are described.
- In chapter 5, the results of the experimental program are compared to predictions from several methods outlined in the literature review. A discussion is included

discussing the accuracy of the various methods in predicting the behavior of the panels tested. A discussion about the viability of thick insulation and thin wythe ICSWP in real-world applications is also included.

- In chapter 6, conclusions about the viability of existing methods to predict behavior of thick insulation and thin wythe panels and the viability of the use of such panels in real-world applications are summarized.

CHAPTER 2. LITERATURE REVIEW

This section provides background information on ICSWPs, which is pertinent to this research. Basic background information on ICSWPs and their behavior and common classifications are included in this chapter. However, this chapter focuses on two primary topics. The first focus is on current methods of the design and analysis of ICSWPs. A number of these methods are used in chapter 5 for comparison of testing data within this research. The second focus is the scope of the existing testing data available in literature. This section is included to illustrate the lack of available testing data for ICSWPs with thick insulation and thin wythes.

ICSWPs are comprised of two wythes of concrete, insulation, shear connectors, and reinforcement. ICSWPs are used primarily as exterior walls to increase the thermal efficiency of the building envelope and can be used as both bearing and non-bearing wall systems.
As panels are subjected to flexural forces, internal forces perpendicular to the external forces develop in both tension and compression to create an internal moment that resists the external flexural forces. As is well understood with steel beam and concrete slab composite systems, it is possible to achieve varying degrees of composite action if these internal forces are capable of being transferred to different sections. In steel beam and concrete slab systems this force transfer is achieved using steel studs. In ICSWPs, this force transfer is facilitated by shear connectors, which bridge both wythes of concrete.

2.1 Percent Composite Action

ICSWPs are categorized by behavior into one of three categories: non-composite, partially composite, and fully composite based on their behavior. (Maguire & Pozo-Lora, 2020) The concrete wythes in a panel act either independently, as a single unit, or partially together for non-composite, fully composite, and partially composite panels, respectively.

Non-composite panels are well understood and are easy to design but are structurally inefficient. Fully composite panels require moderate design efforts and may, at times, be structurally efficient; however, in many cases, they provide excessive structural capacity and are economically inefficient. A larger number of connectors are needed to create a fully composite panel, increasing the cost of the panel. Partially composite panels are frequently the most structurally and economically efficient, but the behavior of these panels is the most difficult to predict and can be more computationally heavy.

The percent of composite action (PCA) describes the degree to which the panel acts as a single unit. The primary factor that determines this behavior is the ability of the shear connectors to transfer the internal forces from one concrete wythe to the other. If the connectors' capacity to transfer these forces is equal to or larger than the internal forces resisting the external moment, then full composite action is achieved. If no shear force is transferred, the panel acts non-compositely and partially composite behavior is achieved when shear transfer lies between these two extremes. This behavior can also be visualized in terms of strain as seen in Figure 2-1.

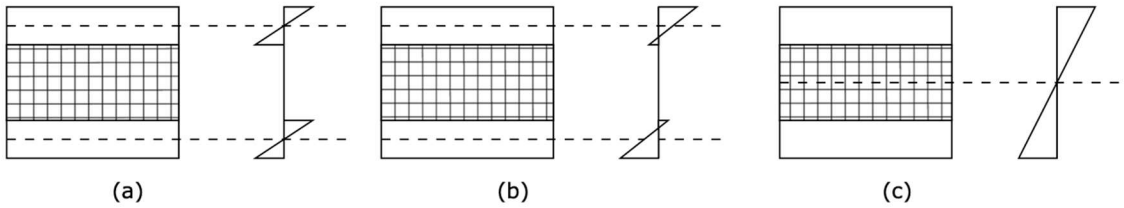

Figure 2-1 Composite Action Strain Assumptions for (a) Non-Composite (b) Partially Composite (c) Fully Composite Behavior

The classification of the behavior of ICSWPs is complicated further because each panel can be assigned three different values of PCA based on different elements of the panel's behavior. These elements of behavior include cracking strength, deflection (moment of inertia), and ultimate strength. A panel may perform at a different PCA in these three categories. The percent

composite action was defined by Pessiki and Mlynarczyk (2003) based on the moment of inertia is shown in equation (2-1).

$$\kappa = \frac{I_{exp} - I_{NC}}{I_{FC} - I_{NC}} \tag{2-1}$$

Where: κ = percent or degree of composite action

I_{exp} = equivalent moment of inertia obtained from testing

I_{NC} = non-composite moment of inertia

I_{FC} = fully composite moment of inertia

Similar equations are used to determine the percent of composite action based on cracking and ultimate strength. The non-composite moment of inertia is calculated by summing the moment of inertias of the two individual wythes. The fully composite moment of inertia is calculated by assuming the panel acts as one unit or comparable to a solid panel of the same dimensions.

The non-composite and fully composite cracking moments are determined using the same moment of inertias calculated for the percent composite defined by Pessiki and Mlynarczyk. The fully composite cracking moment can be found by using equation (2-2) and the fully composite moment of inertia. The non-composite cracking moment is found by summing the individual cracking moments of the two wythes, which are found using equation (2-2) and the section properties of the individual wythes.

$$M_{cr} = \frac{f_r * I}{y_t} \tag{2-2}$$

Where: M_{cr} = cracking moment

f_r = concrete modulus of rupture

I = moment of inertia

y_t = distance to the neutral axis

The non-composite and fully composite ultimate moment are calculated using strain compatibility and force equilibrium similar to reinforced concrete beams. Figure 2-2 below shows the typical strain compatibility and force equilibrium for non-composite and fully composite panels with mild reinforcement used to calculate the ultimate moment capacity for each.

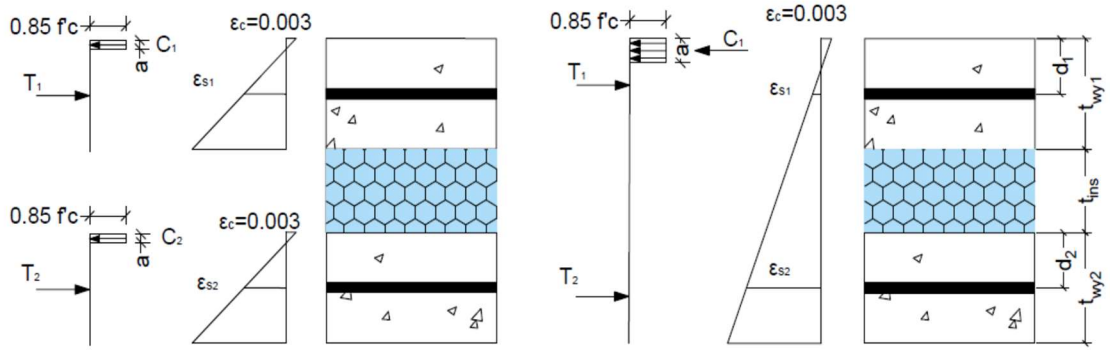

Figure 2-2 Strain and Load Profile for Non-Composite ICSWP (left) and Fully Composite ICSWP (right) (Olsen et al., 2017)

The process involves setting up a system of equations based on force equilibrium and solving for the distance to the neutral axis. Again, the non-composite ultimate moment requires solving the system of equations for both wythes and summing the ultimate moments of the two individual wythes.

Currently, many engineers rely on a percent composite action provided by a connector manufacturer for the design of precast ICSWPs. Al-Rubaye et al. (2017) conducted a study which determined that, of the commercial connectors tested, the percent composite provided was conservative for every panel within their testing.

2.2 Failure Mechanisms

2.2.1 Flexure

ICSWPs are used as both load bearing and non-load bearing walls. This means that some ICSWPs are subjected to in plane compressive forces while others are not. However, both bearing and non-bearing panels are subjected to flexural forces. These flexural forces originate from three primary sources: wind pressure, thermal gradients, and, for load bearing panels, P-delta effects.

Due to their increased thermal efficiencies, ICSWPs are used primarily as exterior wall systems or as a building envelope. This use case subjects the panels to outside wind pressures, which force the panels into flexure as they span between building stories. The thermal efficiency of the panels mitigates the transfer of heat into or out of the building provided thermal bridging does not occur (Sorensen et al., 2017). During times of extreme temperatures, the difference in temperature between the exterior wythe of concrete and the inner wythe can be significant. As the concrete is heated or cooled, it will expand or contract. This expansion and contraction of the concrete results in internal stresses as the connectors resist this movement and force the panel into flexural stresses (Pozo-Lora & Maguire, 2019). This is only of concern in partially composite or fully composite panels as non-composite panels will not transfer these forces.

Flexural failure occurs when either the reinforcement yields or connector failure. Reinforcement yielding occurs in the same manner as a reinforced concrete beam. After the concrete cracks, the tension forces previously carried by the concrete are transferred to the steel, and the steel is assumed to carry all tensile forces at this point. Connector failure occurs when the shear force in the connector exceeds the connector's ultimate shear capacity. Typically, the ultimate shear capacity of a shear connector is found through double shear or push through testing. The failure mechanism is indicative of whether the panel reached full composite action for ultimate strength. A fully composite panel based on ultimate strength contains enough connectors to ensure that the reinforcement yields before the connectors reach their limit. If the

connectors do fail before the reinforcement yields, the panel will not be fully composite based on ultimate strength.

Load-bearing panels are subjected to in plane compressive forces and, like all other wall or column systems, are never truly loaded concentrically. In many cases, wall panel systems incorporate corbels to transfer the roof or floor loads to the wall system, resulting in an eccentrically applied compressive force. This eccentricity leads to P-delta effects and the introduction of flexural stresses. As the system deflects under this and other flexural forces, the panel is subjected to P-little-delta effects. P-little-delta effects are flexural forces that result from the compressive forces being applied with additional eccentricity caused by the half sine-wave deflection behavior of columns and walls in compression. Typically, during design, stresses in the panel are limited to elastic limits so an elastic second order analysis can be completed.

2.2.2 Deflection

Deflection in ICSWPs subjected to the flexural stresses described above frequently can exceed deflection limits. Experimental testing has shown frequently that the slender nature of ICSWPs often lead to excessive deflection prior to other failure criteria. Various deflection limitations have been proposed, which are based on serviceability considerations.

2.3 Current Methods of Design and Analysis

Various methods and models have been created and used to predict the behavior of ICSWPs. Among these methods include analytical approaches based on mechanics of materials and statics and finite element models. These methods differ in a variety of ways; some methods predict behavior only within the elastic response region, and others predict up to ultimate capacity; some are analytical methods, while others employ finite element methods. The methods primarily focus on simply supported single span wall panels, but some research has been conducted on multiple span sandwich wall panels (Pozo-Lora & Maguire, 2019a).

The methods of design and analysis focus predicting behavior surrounding the common loading conditions described previously with most methods focusing on longitudinal and transverse loading conditions. A few methods, such as the analytical SBT method developed by Pozo-Lora, focus on the stresses induced by thermal bowing (Pozo-Lora & Maguire, 2020).

2.3.1 Connector Behavior Prediction Methods

Holmberg and Plem (1965) were the first to develop a method for predicting the elastic behavior of sandwich wall panel connectors. The method describes the behavior specific to a steel truss connector and takes into consideration the behavior of a panel loaded in plane and out of plane.

Shear forces in the wythe are transferred to the connector. The connector resists these forces in two elements: one in tension and the other in compression thus creating truss-like behavior. The resulting tension and compression forces can be calculated using the geometry of the truss and method of joints. Assuming all shear forces are taken by the truss action, Holmberg and Plem (1965) assert that the slip of one wythe relative to the other is proportional to the elongation or contraction of the truss elements. Holmberg and Plem then use Hooke's law and the connector's cross-sectional area and modulus of elasticity to establish the relationship between the tension and compression forces within the truss elements and their elongation or contraction. Figure 2-3 shows the relationship between the slip and orientation of the truss connector.

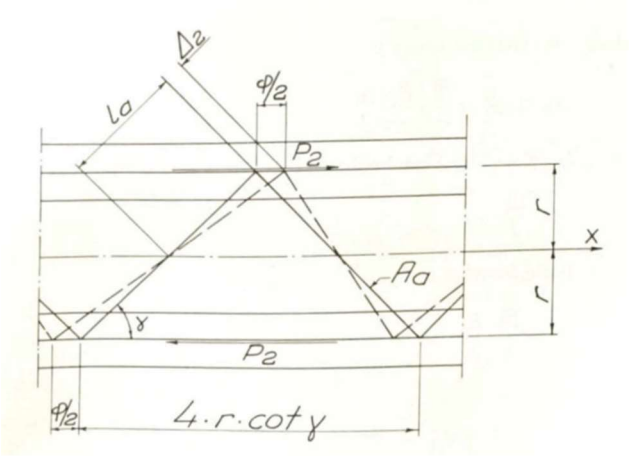

Figure 2-3 Elastic Truss Behavior of Connectors (Holmberg & Plem, 1965)

Combining Hooke's law and the truss force transfer from wythe to connector, a direct relationship is formed between the shear force applied and the slip relative to each wythe. This relationship is also known as the shear stiffness of the connector. The relationship between the slip and applied force can be found using equations (2-3) and (2-4). This method is limited to truss-like connectors within their material's linear-elastic region.

$$\Delta_2 = \pm \frac{P_2 * r}{2 * E_a * A_a} * \frac{1}{cos\,\gamma * sin\,\gamma} \tag{2-3}$$

$$\varphi = \frac{2 * \Delta_2}{cos\,\gamma} \tag{2-4}$$

Where: Δ_2 = change in length of the truss element

P_2 = applied shear force

r = one half the distance from edge of embedment in both wythes

E_a = modulus of elasticity of connector

A_a = cross sectional area of connector

γ = initial insertion angle of connector

φ = relative slip of the wythes

Salmon & Einea (1995) introduced another method to predict the shear stiffness of truss connectors like that of Holmberg and Plem. The method differs from Holmberg and Plem by introducing three separate cases based on the connector embedment which are shown in Figure 2-4. The three cases include truss action only, full embedment fixity, and lateral embedment restraint. This method, like Holmberg and Plem, uses Hooke's law and relates the expected tension and compression forces within the truss action to the elongation of the truss elements and subsequent relative slip between concrete wythes. The method is based on simple mechanics of materials and geometry of the truss-like connectors.

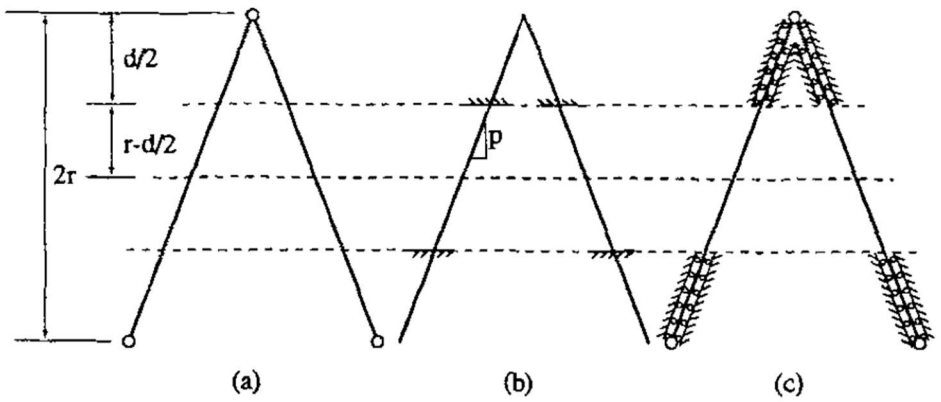

Figure 2-4 Connector-Embedment Types: (a) Pinned at Wythe Center; (b) Fixed at Wythe Embedment; (c) Laterally Supported within Wythe (Salmon & Einea 1995)

Years later, Tomlinson developed another method to predict connector behavior and shear transfer mechanics. This method considers shear carried by three components: insulation, connector truss action, and connector dowel action and is expressed in equation (2-5) (Tomlinson, 2015).

$$V_{sc} = V_{in} + V_{tr} + V_{dw} \quad (2\text{-}5)$$

Where: V_{sc} = total shear strength

V_{in} = shear carried by the insulation

V_{tr} = shear carried by connector truss action

V_{dw} = shear carried by connector dowel action

Assuming the insulation bonds to the concrete, shear forces are transferred through the insulation layer until either the insulation shear strength fails or the bond is broken. Tomlinson proposes that the shear strength contributed by the insulation is a function of the insulation thickness, shear modulus of the insulation, area of insulation subjected to shear, and the relative slip between wythes.

Shear contribution from dowel action for ICSWP connectors was introduced by Tomlinson in 2015. A dowel connector is a connector that bridges the insulation layer perpendicular to the wythes transferring all shear forces over its length. This behavior is similar to how wooden dowels or steel bolts transfer shear forces between elements.

The last factor Tomlinson considers is that of truss action from the connector. This is the same behavior described by Holmberg and Plem with some minor differences. Both methods use the same development of tension and compression members relative to the connector's angle of insertion. Additionally, both methods use Hooke's law to determine the elongation or contraction of the individual truss elements.

The first difference is Tomlinson considers geometric nonlinearity or that, as the wythes slip and the truss elements elongate or contract, the initial insertion angle changes. Holmberg and Plem use only the initial angle for their calculation. This difference results in Holmberg and Plem having a constant predicted shear stiffness for connectors regardless of the current slip, whereas

Tomlinson's model predicts that as the slip changes, the contribution of shear due to truss action changes.

The second significant difference is that Holmberg and Plem consider the length of the connector that is embedded into either wythe of concrete as part of the overall length of the truss element. Tomlinson uses only the thickness of the insulation and does not use the embedded portion of the truss elements as part of their calculation. The equations for calculating the shear contributions from the insulation, dowel action, and truss action from Tomlinson's model are proved below in equations (2-6) through (2-9).

$$V_{in} = \frac{G_{in}A_{in}}{X}\delta_s \tag{2-6}$$

$$V_{dw} = \frac{12E_{sc}I_{sc}}{X^3}\delta_s \tag{2-7}$$

$$\varepsilon_{sc,a} = \frac{\Delta L_{ac}}{L_{ac}} = \frac{\sqrt{(Xtan\theta + \delta_s)^2 + X^2} - L_{ac}}{L_{ac}} \tag{2-8}$$

$$V_{tr} = F_{ac}sin\theta' = E_{sc}\varepsilon_{sc,a}A_{sc}tan^{-1}\left(\frac{Xtan\theta + \delta_s}{X}\right) \tag{2-9}$$

Where: G_{in} = insulation shear modulus

A_{in} = area of foam subject to shear

X = insulation thickness

δ_s = relative slip of the two concrete wythes

I_{sc} = connector moment of inertia

ε_{sc} = axial strain in connector

ΔL_{ac} = change of connector length

L_{ac} = initial connector length

A_{sc} = connector cross sectional area

θ = connector insertion angle

θ' = adjusted angle

In addition to providing methods to predict the shear stiffness of the connector, Tomlinson included limits to the shear contribution for each of these factors. The calculations for these limits are simple for both the dowel action and insulation contributions. These calculations use the same methods as before to determine the shear stresses in either the insulation or dowel. However, instead of using the stress and Hooke's law to find elongation or slip, the stress is compared to the ultimate capacity of the material.

The determination of the maximum truss action is more involved as it considers three different failure mechanisms including strength failure, where the connector ruptures or yields; bond failure, where the connector breaks free of its embedment in the concrete; and buckling, where the angled truss elements either buckle or crush under compression.

2.3.2 Elastic Panel Behavior Prediction Methods

There are several methods of analysis for SWPs, some of which have been developed within the past few decades. Most of these methods focus only on predicting behavior within the panel's elastic limits. Newmark and Granholm are frequently cited as the first researchers to establish the foundation for composite beam behavior that was later adopted for SWPs.

Newmark et al. (1951) established equations for composite action of concrete slabs working in conjunction with steel beams. Granholm (1949) also developed similar equations for composite action but instead focused on composite timber beams. Holmberg and Plem, referencing Granholm, adopted these principles and equations of composite beam behavior to develop their method for analyzing and predicting sandwich wall panel behavior. Holmberg and Plem developed methods for analyzing the behavior of SWPs under longitudinal loads and transverse loads (Figure 2-5). The analysis of truss-like SWP connectors described earlier was developed by Holmberg and Plem in conjunction with these composite SWP analysis methods.

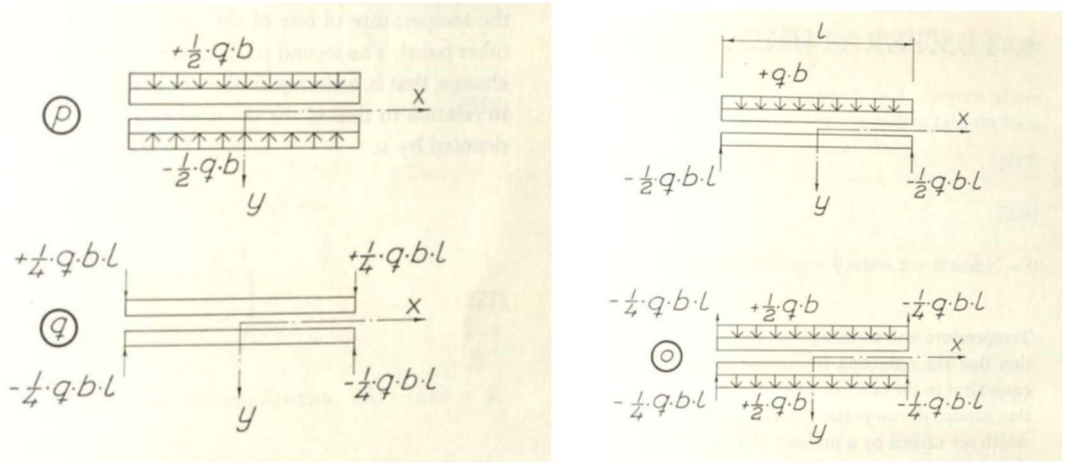

Figure 2-5 Sandwich Wall Panel under Uniform Transverse Loading (Holmberg and Plem, 1965)

The method developed by Holmberg and Plem has a number of limitations when compared to other methods. Specifically, for transverse loading, Holmberg and Plem assume uniform loading and no solution is derived for other loading conditions. In addition, only the solution for continuous connectors was derived. The method calculates a uniform panel stiffness based on the stiffness of the connectors, which can only be accurately modeled by continuous connectors. Within the derivation of the method, Holmberg and Plem additionally make the assumption that the wythes are of equal thicknesses. This assumption leads to the method being

incompatible with predicting behavior of partially composite panels with different compression and tension wythes.

A few years later Allen (1969) introduced another method for predicting elastic behavior of SWPs. The method introduced by Allen did not build on the work of Holmberg and Plem or even that of Newmark and Granholm. Instead, Allen compares building SWPs to sandwich wall panels incorporated in aircrafts, which are comprised of thin metal sheets that sandwich a lower density core. Allen outlined methods for predicting behavior for SWPs with thin and thick faces and also proposed a method for predicting behavior of SWPs with faces of unequal thicknesses.

Salmon and Einea (1997) were among the first to use finite element methods (FEM) to model SWP behavior. One of the finite element models utilized by Salmon & Einea incorporated the use of beam elements to model the concrete wythes and truss elements pinned at the wythe centroids to model the steel or FRP truss connectors (Figure 2-6). The model was used to verify the measured stresses in experimentally-tested panels, and the results between the model and experimental tests were agreeable.

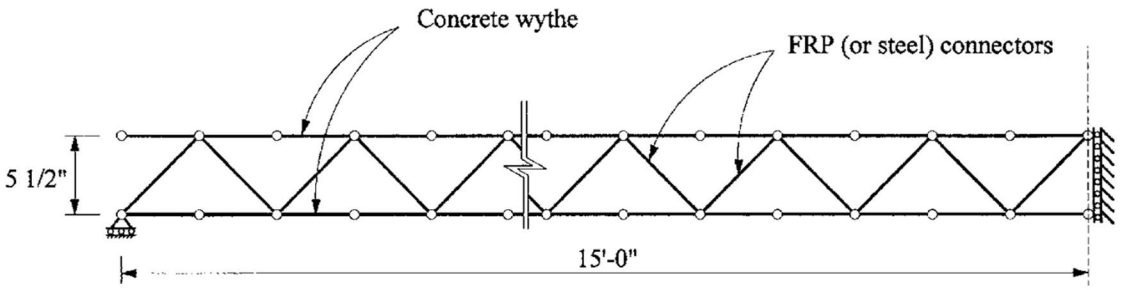

Figure 2-6 FEM Panel Model (Salmon & Einea, 1997)

Recognizing the complex nature of many of the existing methods, Al-Rubaye (2017) aspired to create a simplified analytical method for predicting SWP behavior. The method was originally introduced as the hand method. The researcher has since adapted the hand method into two separate methods known as the simplified sandwich beam theory (SSBT) and iterative sandwich beam theory (ISBT). Both the SSBT and ISBT methods are capable of predicting

elastic behavior of panels with various loading conditions, wythe thicknesses, and varying discrete connector placements.

The primary difference between the SSBT and ISBT methods is that the SSBT method assumes a linear slip profile whereas the ISBT method assumes a non-linear slip profile, and iterations are used to converge at the correct slip. The general procedure for both methods involves assuming end slips, calculating connector forces based on similar triangles (Figure 2-7), and checking the assumed slip using slip kinematic relationships, which are based on mechanics and the equilibrium of internal forces. The hand method, SSBT, and ISBT methods have all been verified against experimental testing data and compared with another method inroduced by Al-Rubaye, which utilizes finite element methods known as the Beam-Spring.

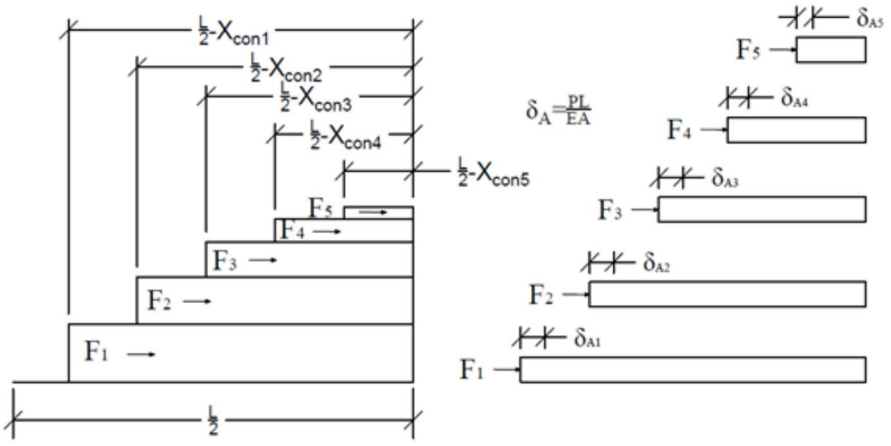

Figure 2-7 Hand Method: Connector Slip and Connector Internal Force Relationship (Al-Rubaye, 2017)

The Beam-Spring model was developed by Al-Rubaye et al. (2019) in conjunction with the hand method described above. This method introduces a simple method of modeling SWPs with discrete connectors using the basic FEM elements: beams and springs (Figure 2-8). The model is reminiscent of Salmon & Einea (1997) but is not applicable only to continuous truss connectors. This method uses beam elements to model the concrete wythes and connects the beam elements with spring elements, which are given specific shear stiffnesses. The shear stiffnesses used in the model can be calculated analytically using methods described previously,

such as Holmberg and Plem or Tomlinson, or found from experimental testing. This method can be used to predict elastic or ultimate behavior for arbitrary loading on SWPs in flexure. Despite not using more computationally intensive FEM elements, such as isoparametric elements as do other models, the model has proven to be an effective analysis method. Six panels were tested to validate the method. In addition, the method was verified against data from 19 other panel testings found within literature. All testing data correlated well with the Beam-Spring model.

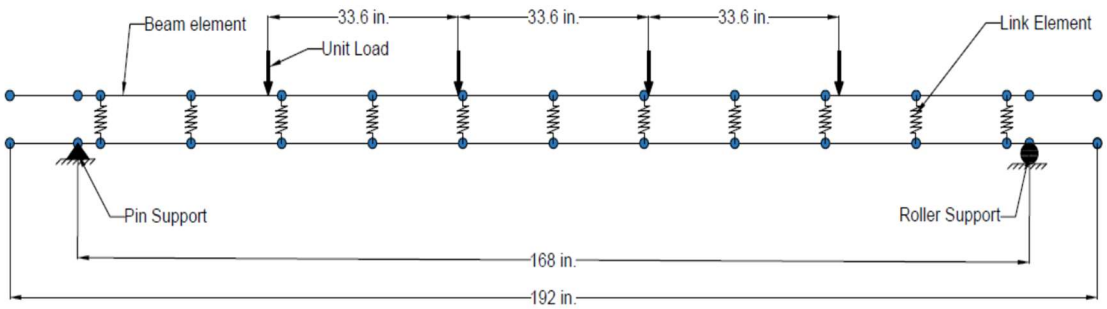

Figure 2-8 Beam-Spring Model (Al-Rubaye 2019)

The method is even capable of handling non-linear shear connector behavior, which was shown by verifying the method against testing by Mlynarczyk and Pessiki (2000). This was done by using non-linear spring elements within the model.

Jensen et al. (2020) also developed a mechanics-based model designated MBM that also can be used to predict elastic SWP behavior. The authors recognize that the method is computationally intensive and is best suited for use through a spreadsheet or computer program.

2.3.3 Ultimate Strength Analysis and Design Methods

A few methods that have been introduced over the years can be used to predict ultimate panel strength. Early models predicting ultimate behavior are few, as early models focused primarily on the elastic region. Unfortunately, many of models that predict ultimate strength are complicated and require computer programs to accomplish the iteration and integration frequently incorporated. Increased attempts have been made in more recent years to develop a simple

method for analysis of ultimate behavior. Finite Element Models have also been proposed to model SWP ultimate behavior and strength.

Naito et al. (2012) introduced a method which could predict panel ultimate behavior and strength. The model uses the relationship between tie force and slip to determine the slip and force of each shear tie. These forces and slips are used to determine the degree of partial composite action and the curvature at each shear tie location to determine the corresponding midspan displacement. This method was verified against experimental testing and proven to be accurate. Unfortunately, the method requires that the process described is repeated at load steps to develop a full load vs. displacement relationship of the panel.

Tomlinson's method was proposed in 2015. This method contains a process to develop the moment-curvature relationships of the SWP. This relationship, whose behavior lies between the response of a non-composite and fully composite panel is then used to determine the deflection of the panel under flexure and the relative slip between the wythes. Tomlinson's method was verified against test results of 27 panels from the available literature at the time and proven to be accurate. However, this method requires a computer model as iteration and integration are central to the method. This method also utilizes Tomlinson's previously described method of determining the relationship between shear flow and slip, where the total shear flow is calculated from the contributions of the insulation, connector dowel action, and connector truss action. Other methods use experimental results to determine this relationship instead of analytical models.

Gombeda (2017) also proposed a method for predicting ICSWP behavior, which could predict both elastic and ultimate behavior. In fact, Gombeda proposed two different methods in the same article. The first method consisted of computational modeling using finite elements. Gombeda recognized that "though effective for demonstrating partially composite action, the computational model is more suited to research applications rather than design due to its component-based assembly and computational effort" (Gombeda, 2017, p. 370). Because of this,

Gombeda presented yet another model that did not require the use of finite elements (Figure 2-9). While this method does not require finite elements, it would still not likely be completed without the aid of some coding or spreadsheet, as it requires numerous iterations that would be completed much easier with loops than by hand. This method was verified against testing data found in Naito et al. (2011), Trasborg (2014), and Tomlinson and Fam (2015).

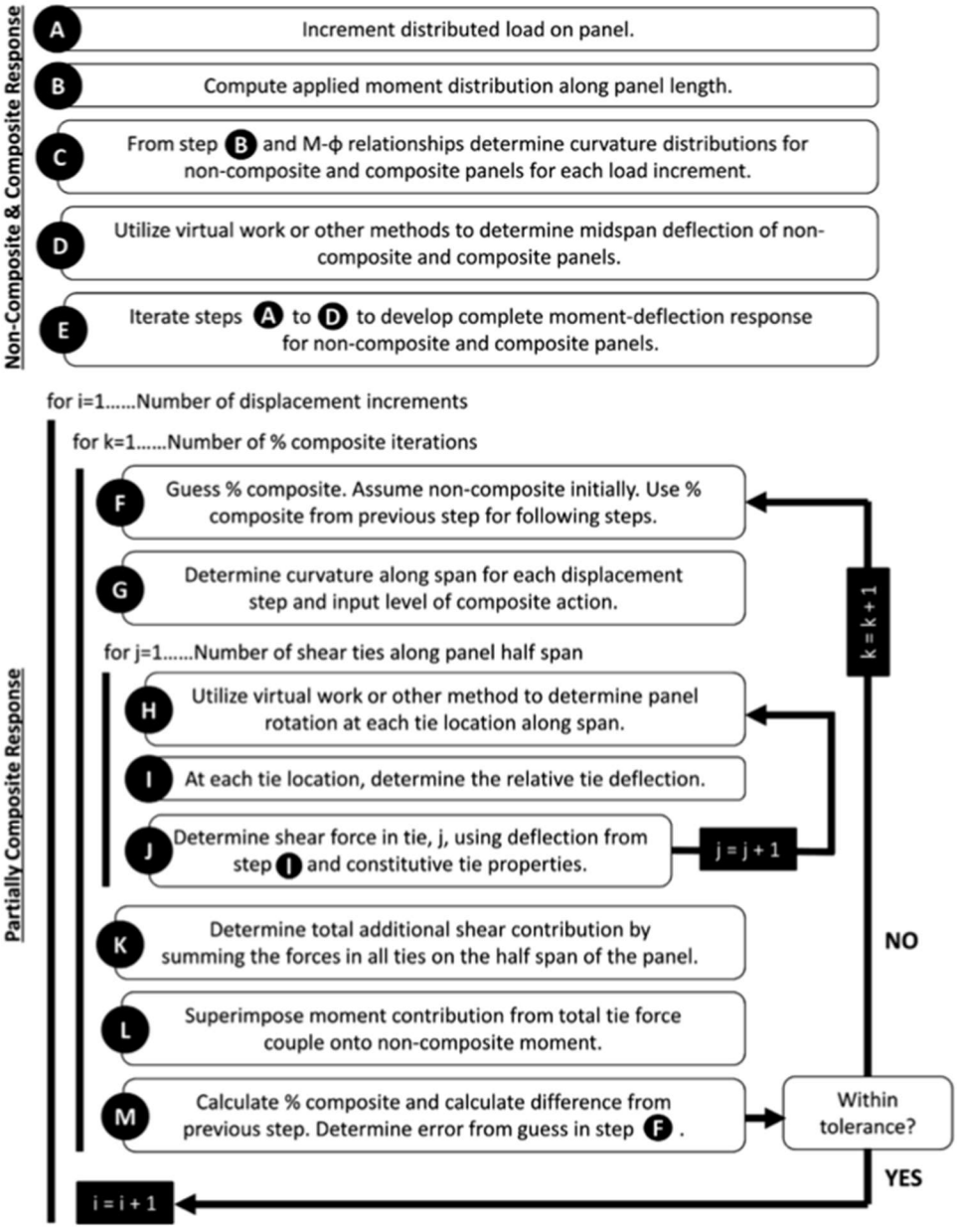

Figure 2-9 Gombeda ICSWP Model Flowchart (Gombeda, 2017)

The method of shear flow has been widely used to predict the ultimate strength of ICSWPs. Shear flow is among the most preferred method of ICSWP behavior prediction because it is simple to reproduce and straightforward to understand. Modified shear flow methods have been adopted by both the American Concrete Institute (ACI) and the Precast Concrete Institute (PCI) (Bunn, 2011). The method of shear flow is based on principles of mechanics and compares the shear flow demand within the panel wythes and the shear flow capacity of the connectors to predict connector failure. The shear flow demand and capacity based on basic principles of mechanics can be calculated using equations (2-10) and (2-11).

$$q_{demand} = \frac{V_{max} * Q_{FC}}{I_{FC}} \tag{2-10}$$

$$q_n = \frac{F_{uc} * N}{s} \tag{2-11}$$

Where: q_{demand} = shear flow demand

V_{max} = maximum shear force due to applied load

Q_{FC} = first moment of area calculated with fully composite section properties

I_{FC} = fully composite moment of inertia

q_n = shear flow capacity

F_{uc} = ultimate shear capacity of a single connector

N = number of shear connectors

The modified shear flow method introduced by PCI assumes the maximum shear force experienced will be the lesser of the tensile capacity of the reinforcement and the concrete

compressive force of the compression wythe. This shear force is then assumed to be distributed equally to shear connectors, which are placed between the panel support and the location of maximum moment. This approach is like that used by composite steel beams (Bunn, 2011).

The modified shear flow method from ACI calculated the shear demand as the maximum shear force divided by the distance between resultant tension and compression forces (Bunn, 2011). In addition to these two modified shear flow methods, Bunn (2011) also introduced a modified shear flow method, which used several gamma factors to determine the nominal shear flow capacity of the shear connector.

$$q_n = \gamma_{type} * \gamma_{thickness} * \gamma_{spacing} * \gamma_{orientation} * q_{baseline} \quad (2\text{-}12)$$

Where: q_n = nominal shear flow capacity of grid [lb/in]

γ_{type} = Gamma factor for insulation type [EPS or XPS]

$\gamma_{thickness}$ = Gamma factor for insulation thickness

$\gamma_{spacing}$ = Gamma factor for grid spacing

$\gamma_{orientation}$ = Gamma factor for grid orientation [vertical or transverse]

$q_{baseline}$ = 100 lb/in [based on shear flow strength of grid alone]

Al-Rubaye (2017) introduced a method, known simply as the ultimate method, to predict the ultimate strength and percent composite action of ICSWPs. The method is based on strain compatibility and force equilibrium. The method likens partially composite ICSWPs to two separate beams with identical curvature and applied axial loads. Within the analogy, the applied axial load in both beams is identical and represents the total force transferred between the wythes. To determine the total forces within the connectors, a linear slip relationship is assumed, and the force in each connector is calculated and summed. Because of the linear slip, relationship

connectors at different placements are assumed to experience different forces with the largest forces being found near the edge of the panel. The maximum connector force allowed in this calculation is limited to the measured maximum shear capacity of a single connector. The sum of forces within the connectors are then used in conjunction with the force equilibrium depicted in Figure 2-11 .

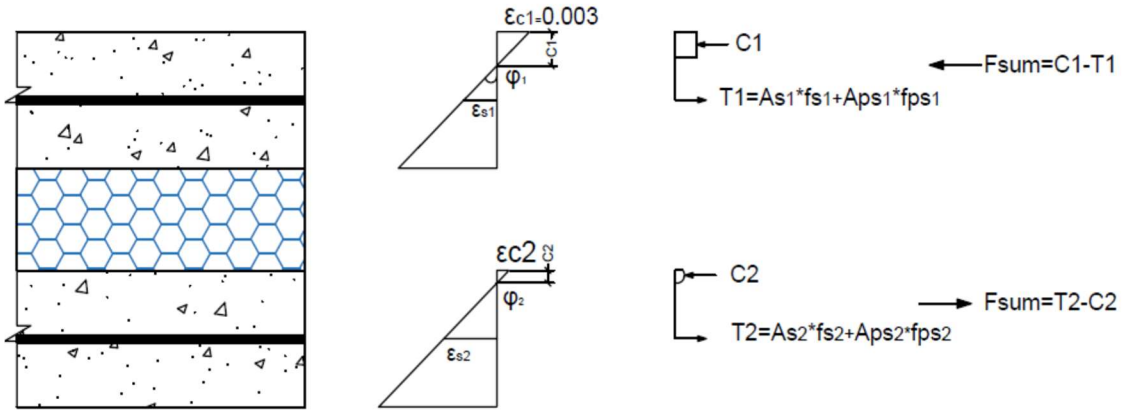

2-13 Ultimate Method Force Equilibrium (Al-Rubaye, 2017)

The ultimate moment can easily be calculated using the force equilibrium and compared to the non-composite and fully composite ultimate moments to determine percent composite. The method is robust and considers three possible ultimate failure mechanisms including connector failure, concrete crushing, and reinforcement yielding.

2.4 Scope of Existing Testing Data

Many of these methods have been verified using testing data from existing literature. Several the methods were verified at the time of introduction and others were not compared to experimental testing until many years later. The testing data regarding sandwich wall panels consists primarily of panels and push-through specimens. A variety of dimensions, connectors, insulation types, bonding condition, and reinforcements have been tested. This variety is a natural

outcropping showing the nature of research, as researchers seek out new and different aspects within a given field.

Among the available testing data in published literature are 365 double shear or push-through specimens and 137 panels. This list, which is not exhaustive, is provided in Table 6-1 and Table 6-2 in the appendix. This list was stratified by wythe thickness and insulation thickness to better understand the scope of the existing testing data available in literature with regards to wythe and insulation thicknesses. A breakdown of the results is shown in Table 2-1, including the average and median insulation and wythe thicknesses for panels and push-through specimens.

Much of the literature utilizes metric units to report specimen dimensions. The dimensions were rounded following conversion from metric to imperial units to keep the number of significant figures constant. For the purposes of this thesis, all thicknesses were rounded to the nearest tenth of an inch.

Table 2-1 Summary of Existing ICSWP Testing Data Stratified by Insulation and Wythe Thicknesses

Stratified by	Specimen Type	Minimum Thickness (in)	Maximum Thickness (in)	Median Thickness (in)	Average Thickness (in)	Range of Thickness (in)	Standard Deviation (in)
Insulation Thickness	Panel	1.6	4.0	3.0	2.9	2.0	0.9
	Push-Through	2.0	11.8	3.9	4.0	9.8	1.8
Wythe Thickness	Panel	1.6	6.0	3.00	2.8	4.0	0.61
	Push-Through	2.0	3.2	2.4	2.3	1.2	0.39

The median and average are within 0.2 inches for each data set evaluated. There are mild variations of average insulation and wythe thicknesses when comparing the panels and push-through specimens. Insulation thickness tended to be thicker for push-through specimens while wythe thickness for panels tended to be thinner for push-through specimens. Surprisingly, the range of insulation thicknesses tested with push-through specimens far exceeds the ranges of any other data set. The range of insulation thickness for push-through specimens was 9.8 inches, which is more than twice the range of any other data set examined. The range is exceptionally

large due to a few push-through specimens tested by He et al. 2020 whose insulation thicknesses reached a maximum of 11.8 inches. He et al. tested the shear capacity of a novel I-shaped GFRP shear connector in which the connector is not only restrained by embedment but by the longitudinal steel which runs through a hole within the embedded section of the connector. The research by He et al. was published after the research for this thesis began. Aside from the four push-through specimens tested by He et al., only two other push-through specimens, tested by Bunn (2011), have been tested with insulation thicknesses at or above the thicknesses examined in this thesis. In addition, no testing has been found for full-scale panels with the examined thicknesses of eight and 10 inches tested for the research of this thesis.

Figure 2-10 provides a more nuanced breakdown of the variation in insulation thicknesses in tested panels and push-through specimens in available literature. The figure shows that the variation in insulation thickness tested is far greater for push-through specimens than panels.

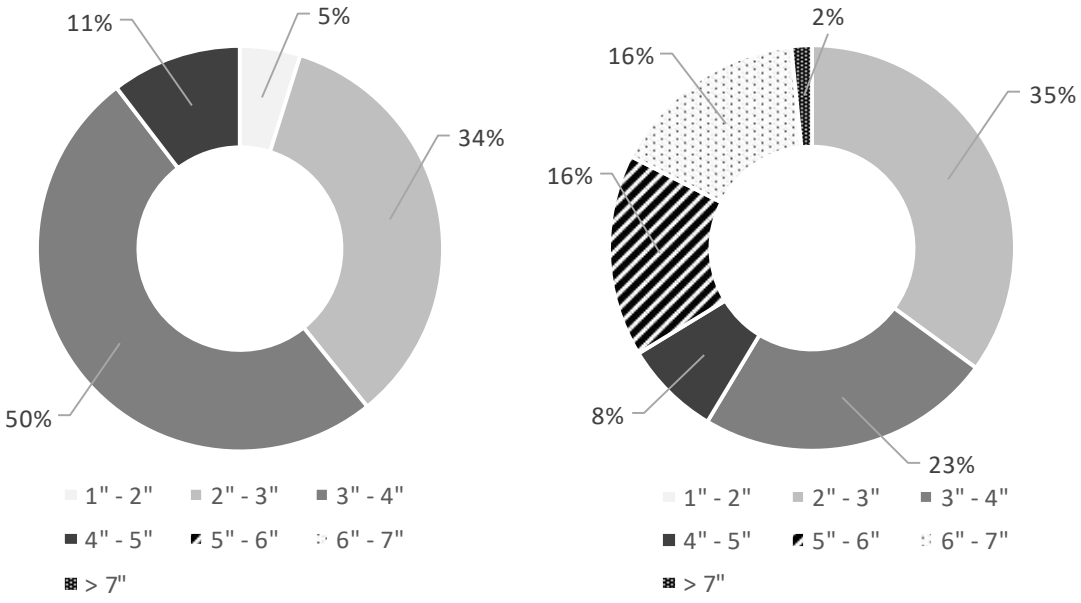

Figure 2-10 Available Testing Stratified by Insulation Thickness (panels left, push through right)

Only 16% of the panels in literature have insulation thicknesses that do not fall within two-to-four inches. This range of insulation thickness is still the most prevalent for push-through specimens, as well accounting for 58% of all push-through specimens tested.

Figure 2-11 provides a similar breakdown for the testing data based on wythe thicknesses. The wythe thicknesses did not have as large a range as the insulation thicknesses, so the wythe thicknesses were broken into half-inch increments compared to the one-inch increments used previously.

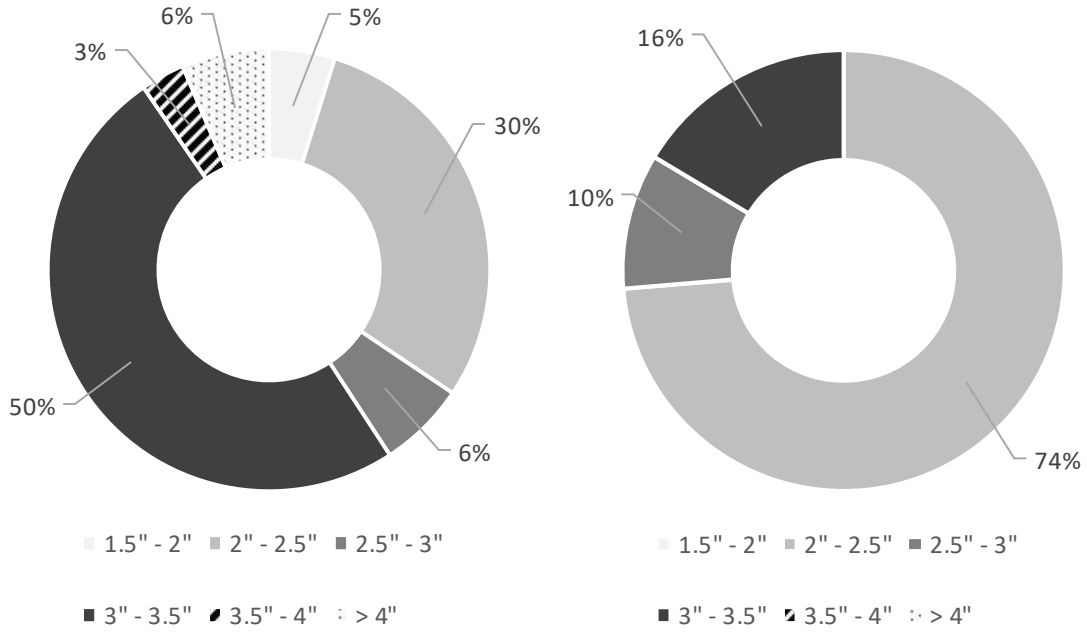

Figure 2-11 Available Testing Stratified by Wythe Thickness (panels left, push through right)

The opposite trend is seen for the data for wythe thickness than that of insulation thickness with a small range of thicknesses for the push-through specimens and a wider range found in the full-scale panel testing. Despite having a larger range, most of the specimens use the same wythe thicknesses of two-to 3.5-inches. Looking at the data further, it is apparent that all full-scale panels tested with wythe thicknesses ranging from 1.5-to-2.5 inches were constructed using continuous connectors and none with discrete connectors.

The existing testing data available in literature, while abundant, does not adequately cover panels with insulation thicknesses exceeding six inches or panels with thin wythes and discrete connectors. Testing data for full-scale panels is especially scarce for panels with insulation thicknesses exceeding four inches. Thin wythe panels, while common, primarily were constructed with a non-commercial continuous GFRP shear grid.

CHAPTER 3. EXPERIMENTAL PROGRAM

The experimental program included the testing of fifteen double shear tests and six full-scale partially composite concrete sandwich wall panels. These tests were conducted to analyze the viability of, and to verify current methods of design for, partially composite ICSWPs whose wythes and insulation thicknesses lie on the extreme ends of the current available testing data in literature. These extreme ends include wythe thicknesses of two-inches and insulation thicknesses of eight and ten-inches. This section outlines the testing procedure of these 21 tests and provides specimen configurations. This section also details the construction and fabrication of the specimens.

3.1 Fibergrate Connectors

Three different connectors were used for the double shear specimens. These connectors were classified and designed based on the thicknesses of insulation that they bridged. Custom connectors were created for the varying insulation thicknesses because commercially available connectors were unable to bridge the large insulation thicknesses desired. These connectors were all comprised of a GFRP grate that was cut into appropriate sizes to act as discrete connectors. Fibergrate's Multigrid GFRP grate was selected and provided by Fibergrate for the connectors. Dimensions of the GFRP grate spacing is shown in Figure 3-1 below from Fibergrate's website.

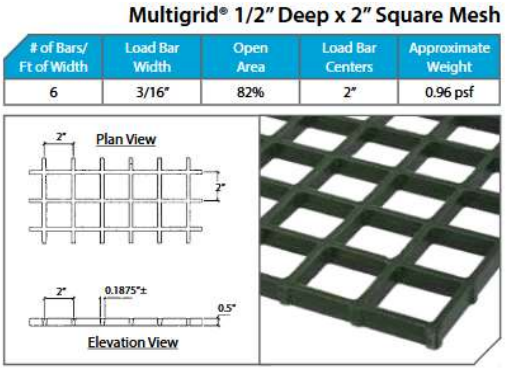

Figure 3-1 Multigrid GFRP Grate Dimensions

The three connectors are designated as F10, F8, and F2 for the connectors which span insulation thicknesses of 10 inches, eight inches, and two inches, respectively.

The size of the GFRP connectors was carefully considered, using methods created by Tomlinson, and Holmberg and Plem, approximate shear stiffnesses of the connectors were calculated. Both methods analyze a connector using the truss action of a connector to transfer the shear. Only the truss elements, which were to be fully embedded into concrete on both sides, were considered to contribute to the shear stiffness of the connector. Using these methods, it was decided that connectors which contained a minimum of eight truss elements would theoretically provide adequate shear stiffnesses.

Embedment depths were selected as 1.5 inches on each end for the F10 and F8 connectors and one inch for the F2 connector. These embedment depths and the thicknesses of the insulation bridged by the connector determined the width of the connectors. The length of the connector was determined by the geometry of the multigrid grating and the required minimum of eight truss elements fully embedded on each end. The dimensions of the three connectors are shown below in Figure 3-2.

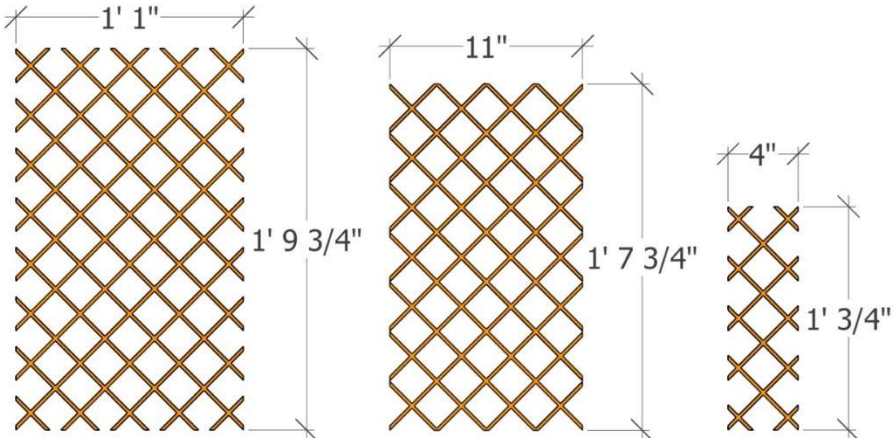

Figure 3-2 GFRP Connectors F10, F8, F2

All connectors were cut from three sheets of the GFRP grate measuring in 4’x12’x0.5”. Due to the limited amount of GFRP grating, a specific cutting schedule (Figure 3-3) was

established to obtain the maximum number of connectors possible from each sheet. The cutting schedule allowed for nine connectors of each size to be obtained from a single sheet of GFRP grating (Figure 3-3). This resulted in a total of 27 connectors of each size. It should be noted that small edges of certain connectors were missing due to the selected cutting schedule; it was assumed that the missing ends would not result in a lack of bonding of all truss elements. The edges of the connectors have been highlighted to illustrate the cutting schedule and should not be confused as solid GFRP sections along the connectors' borders.

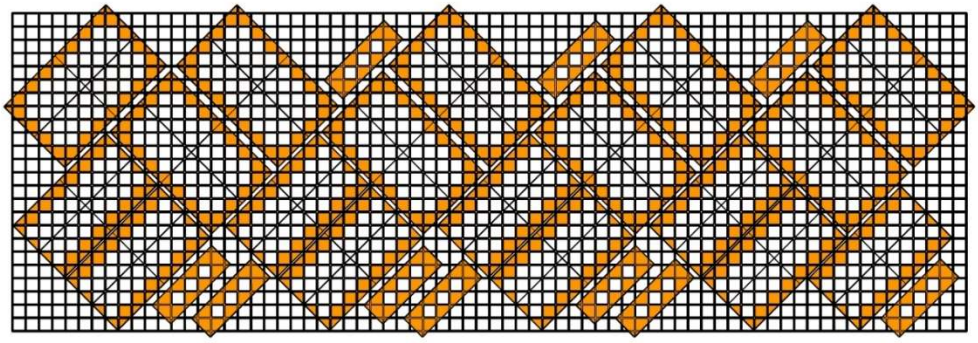

Figure 3-3 GFRP Grate Cutting Schedule

The GFRP grating was marked according to the cutting schedule, and the connectors were cut from the grid using a grinder. During cutting, PPE including masks rated N-95 or better, eyeglasses, and gloves were used. In addition to this, a shop vacuum was used to suction away the bulk of the GFRP dust that was produced as the grating was cut (Figure 3-4). Initially, only enough connectors were produced to construct the first nine double shear specimens. This was done so the viability of the novel shear connectors could be verified prior to the cutting of all available Fibergrate. Following preliminary analysis of the results of the first nine double shears the remaining Fibergrate was cut to manufacture all the connectors needed for the remainder of the testing.

Figure 3-4 Cutting of GFRP Grating

3.2 Double Shear Design and Construction

Fifteen double shear specimens were constructed and tested in order to determine the shear stiffness of the sandwich wall panel connectors. Three different connectors were tested, and each was made specifically for varying insulation thicknesses, including two-inch, eight-inch, and 10-inch thicknesses. The fabrication and construction of the connectors, double shear specimens, and formwork are described in this section.

3.2.1 Design

The design of the double shear specimens is similar to many of those described in the literature discussed in the previous chapter. Due to the limited number of connectors, it was determined that only two connectors would be placed in each double shear specimen, and these were placed in the center. Ideally two or more connectors are used connecting each wythe. The use of multiple connectors reduces the risk of excessive bending forces being introduced due to eccentricity. Great care was taken during construction and testing to place the connectors and to load the specimens at their center to reduce eccentricity. Figure 3-5 shows the configurations for each of the three double shear specimen series.

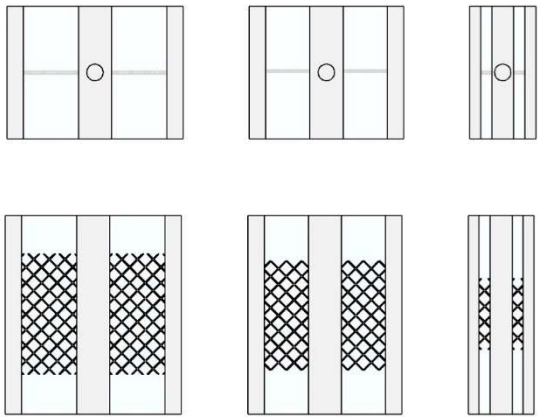

Figure 3-5 Double Shear Drawing

The double shear specimens all measured two feet in width and three feet in height. The thicknesses of each specimen and their wythes are listed in the table below. Connectors for the F2 series allowed for an embedment depth of one inch into each concrete wythe while series F8 and F10 allowed for 1.5 inches of embedment. A single lifting anchor was placed in the center wythe on the top of the specimens and was used to move the specimen before and after testing.

Table 3-1 Double Shear Wythe Thicknesses

Double Shear Designation	Thickness *(in)*	Outer Wythe Thickness (in)	Inner Wythe Thickness (in)
F2	12	2	4
F8	28	3	6
F10	32	3	6

3.2.2 Construction

XPS insulation sheets measuring four feet-by-eight feet were cut using box cutters into two feet-by-three feet rectangular sheets for double shear construction. A router with a half-inch diameter bit and one-inch depth was then used to rout a linear hole in each two feet-by-three feet sheet measuring the approximate length of the connectors. All foam sheets were cleaned of excess foam shavings using an air compressor, and the connectors were inserted into the foam sheets in preparation for the casting of the double shear specimens (shown in Figure 3-6).

Figure 3-6 Double Shear Insulation

Insulation sheets were trimmed to the correct dimensions to fit within the formwork. To ensure the consistency of the cuts, the insulation sheets were temporarily glued together using small dabs of liquid nail located just on the inside of each corner (Figure 3-7). After all foam sheets were adequately cut the liquid nail bonds were broken by sliding a thin serrated knife between each layer. The bonds of the liquid nail were broken so the shear strength of the connectors tested would not be altered by the increase given by the liquid nail. Corners of the insulation were also cut off to avoid excessive suction forces occurring when placing the insulation during the pouring of the specimens. This also aided in allowing visible confirmation during the pour that the insulation was placed far enough down to contact the concrete below. It did have the detrimental effect of allowing concrete sections to form connecting the independent wythe. These concrete sections had to later be removed with a hammer prior to testing to ensure only the connector would carry the applied shear forces during testing.

Figure 3-7 Double Shear Insulation Modifications

Formwork, depicted in Figure 3-8, Figure 3-9, and Figure 3-10 was designed, modeled and built for the pouring of the double shear specimens. The construction of the double shear specimens consisted of pouring concrete in three lifts. In the first lift, two-inch-or-three-inch thicknesses of concrete were poured dependent on the double shear configuration. Sheets of insulation and connectors were then inserted. The second lift consisted of four-inch-or-six-inch thicknesses of concrete, again dependent on the specimen configuration. During this second lift, a lifting anchor was glued to the formwork at center height. Following this, additional sheets of insulation and connectors were placed followed by a third and final lift of concrete.

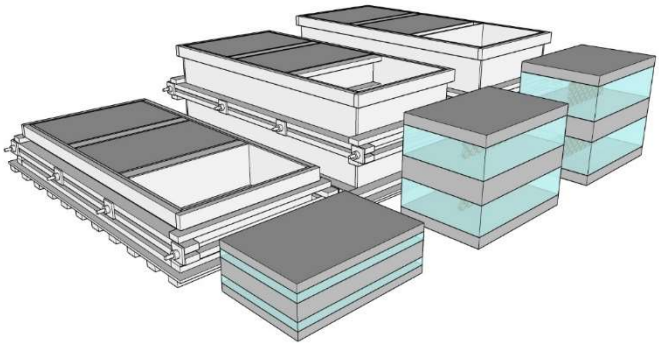

Figure 3-8 Formwork SketchUp Model

Depth gauges were used to ensure the correct thicknesses of each lift. The concrete used was self-consolidating concrete and, therefore, no vibration was necessary and was not conducted. The formwork, which could accommodate the construction of three specimens of each configuration (nine total), was reused for a second pour during which the final six double-shear specimens were constructed for a total of 15 double-shear specimens. The casting of the first, second, and final lifts are shown in Figure 3-9 and Figure 3-10.

Figure 3-9 Double Shear Construction (lift 1 left, lift 2 right)

Figure 3-10 Double Shear Construction (lift 3 left, finishing right)

3.3 Full-Scale Panel Design and Construction

Six full-scale panels measuring 22 ft in length and 2 ft in width were designed and constructed for testing. The panels were constructed to test the composite behavior of the panels both in strength and deflection. This section outlines the design and construction of the six panels.

3.3.1 Full-Scale Panel Design

Two panels were designed for an insulation thickness of 2", two for an insulation thickness of 8", and two for and insulation thickness of 10". These thicknesses correspond with the thicknesses of insulation tested with the double shear specimens. The same connectors were utilized in the full-scale panels as were used in their corresponding double shear specimens. All panels were designed to be 22 ft in length. This length was chosen to adequately model the approximate height of a 2-story tall wall panel. Each panel consists of two concrete thicknesses sandwiching a thickness of insulation. A table of the various dimensions of the panels is shown below in Table 3-2.

Table 3-2 Full-Scale Panel Dimensions

Panel Designation	Wythe Thicknesses *(in)*	Insulation Thickness *(in)*	Length (ft)	Width (in)	Longitudinal Rebar	Transverse Rebar
FS2-1	2	2	22	24	2 #3	#3@14"
FS2-2	2	2	22	24	2 #5	None
FS8-1	3	8	22	24	2 #3	#3@14"
FS8-2	3	8	22	24	2 #5	#3@14"
FS10-1	3	10	22	24	2 #3	#3@14"
FS10-2	3	10	22	24	2 #5	#3@14"

All panels were reinforced with steel rebar. All panels whose designations end with 1 contained #3 bars for both longitudinal and transverse reinforcement. The panels whose designations end with 2 contained #5 bars for longitudinal reinforcement. Panels FS8-2 and

FS10-2 contain transverse reinforcement consisting of #3 bars. Panel FS2-2 did not contain any transverse reinforcement because the longitudinal rebar's diameter was designed to be at the center of the two-inch wythe thickness, and it does not leave enough cover to allow for transverse reinforcement. The three dimensionally varied panels are shown in Figure 3-11.

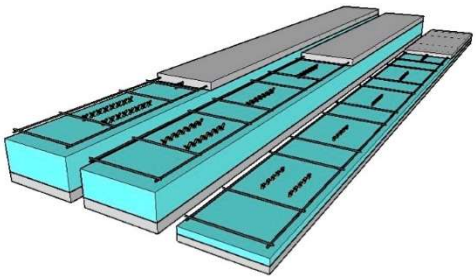

Figure 3-11 Full-Scale Panel Reveal

Each panel contained eight connectors with two rows of connectors at the ends and one row of connectors throughout the center of the panel. The end connectors were placed 32 in. from the end of the panel to the center of the connectors. The inner connectors were all placed 40 inches center to center. The dimensions showing where the cuts are located for each full-scale panel are shown below in Figure 3-12.

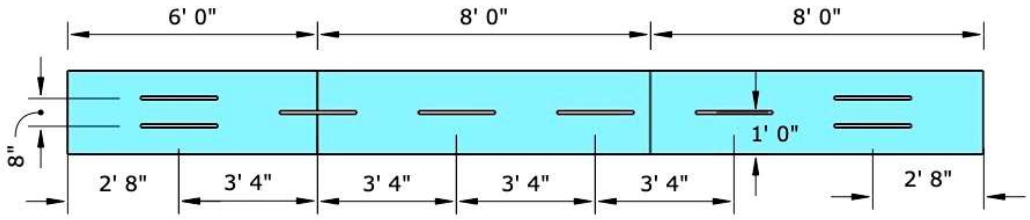

Figure 3-12 Full-Scale Panel Connector Insert Locations

Timber formwork was designed, modeled, and constructed for the casting of the full-scale panels. Insulation was also prepared by cutting 4'x8' insulation sheets similar to the double

shear specimens described previously. To fit the size of the full-scale panel for each 1” thickness of the insulation provided per panel, three sheets of insulation were cut. A router was used to create slots for the connectors to be placed at the correct locations along the length of the panel. Next, the connectors were inserted into the individual layers of insulation.

All the full-scale panels were designed to use the same number of connectors per panel in the same configuration. The connectors for varying insulation thicknesses do vary; however, this means that while the center-to-center distances between connectors remained constant throughout all panels, the length of holes routed in the insulation for each panel did differ to accommodate the varying connector lengths.

The insulation and connector assemblies were then cut down along the edges to ensure they fit within the constructed formwork. Once all insulation and connector assemblies were adequately trimmed, all excess insulation shavings were cleaned off using an air compressor. The assemblies were then taped together using masking tape to ensure no concrete seeped in between the layers of insulation during the pour as shown in Figure 3-13. This tape was cut before testing to ensure no added shear strength was given to the specimens.

Figure 3-13 Full-Scale Panel Insulation-Connector Preparation

To lift the panels following curing of the concrete, it was determined that lifting anchors would be put in on the top faces of the panels three feet in from each edge resulting in a 16-foot total span. Due to the thin wythe thicknesses of the panels, an additional one-inch layer of insulation was cut in the insulation and connector assemblies to ensure adequate development strength for the anchor lifts. These cuts spanned the full width of the panels and were twelve inches in length, two of these recesses are shown in Figure 3-14.

Due to the even thinner wythe thicknesses of the two-inch insulation panels, all insulation was removed at these locations for the lifting anchors, and, instead, two thin sheets of linoleum were used to retain a shear plane between the wythes of concrete.

Figure 3-14 Full-Scale Panel Insulation Recess for Lifting Anchor

Steel rebar was cut and tied in preparation for construction which included longitudinal and transverse reinforcement for all panels except FS2-2 as explained above. For the first set of panels, #3 rebar was used for both the longitudinal and transverse reinforcement. Two longitudinal bars of reinforcement ran the length of the panel while transverse bars were placed in the gaps along the panel's length that were not interrupted by the connector placement. Rebar

chairs were used to ensure that the center of the longitudinal rebar would align with the center of the wythe thickness. The chairs were also tied to the rebar for convenience during construction. The rebar assemblies for the bottom wythe of the panels were inserted to the formwork after oiling the forms but prior to casting (Figure 3-15).

Chairs, which would set the center of the rebar at the center of the two-inch-thick wythe panels, were not available. The chairs that were available raised the rebar center to 1.5 inches. The legs of the chairs were sanded down until the desired height was reached that would allow the rebar to sit at the center of the two inch-thick-wythes.

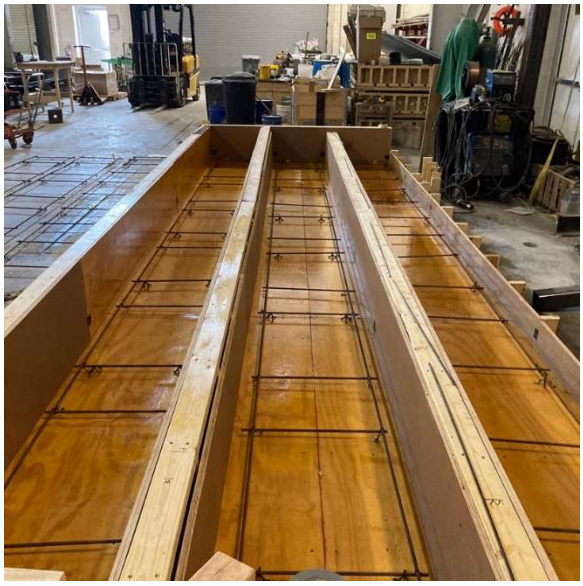

Figure 3-15 Full-Scale Panel Formwork and Reinforcement

3.3.2 Full-Scale Panel Construction

The full-scale panels were constructed by pouring the first lift of self-consolidating concrete to the desired wythe thickness and around the reinforcement. The connector-insulation assemblies were then placed into the formwork. The remaining reinforcement was then placed on top of the connector-insulation assemblies and the final lift of concrete poured on top of that. After 20 minutes, the lifting anchors were placed into the still wet concrete (shown in Figure 3-16), and the concrete was then finished using a trowel. The concrete was not vibrated during the

construction of any double shears or the first three full-scale panels because the concrete was self-consolidating. The concrete used for the series two full-scale panels, while also designated as self-consolidating concrete, was visually stiffer than the previous pours and the concrete was vibrated out of an abundance of caution to ensure the concrete would set correctly and bond to the connectors and rebar.

Figure 3-16 Placement of Lifting Anchors on Full-Scale Panels

To ensure correct wythe thicknesses, depth gauges were used; additionally, duct tape had been placed along the perimeter of the formwork to indicate the height of the concrete wythes. The concrete was covered with clear plastic sheets, and water was added, as needed, so the concrete would cure evenly. Following approximately five days of curing, cylinders were tested to attain the approximate concrete compressive strength. If the strength had reached the desired strength of 5 ksi, the panels were then demolded. After the panels were demolded, they were removed from the base of the formwork and rotated to rest on their sides until testing. The remaining cylinders were also demolded at the same time as the full-scale panels.

3.4 Material Testing

Concrete cylinders were cast during fabrication of the double shear and full-scale panel specimens. These cylinders were tested to determine the concrete compressive strength of the double shear and full-scale panel specimens. The compressive tests were performed in accordance with ASTM C39. Cylinders cast at the time as the full-scale panels were also subjected to testing of the modulus of elasticity and split tension.

3.5 Double Shear Test Setup

The double shear specimens were supported along its length on both outer wythes with two 2” thick steel plates leaving the inner wythe free to deflect under load. Two plastic strips were placed between the steel plates and outer wythes to reduce friction. The specimens were loaded using a ram and load cell centered on the inner wythe. The load was transferred to the double shear specimen through various steel plates sandwiching the load cell. Care was taken to ensure that only the inner wythe was directly loaded.

Relative displacement was measured using four separate Linear Variable Differential Transformers (LVDTs). The measurements from these four LVDTs were averaged to find the reported displacement. The LVDTs were attached to the outer wythes and were supported by a steel angle placed approximately at the mid-height section of the specimen. This steel angle was attached with washers preventing the angle from sitting flush with the concrete wythes. This was done to eliminate the chance of friction between the angle and the outer wythes. The load cell placed below the ram measured the applied load. All specimens were loaded until the ultimate strength of the specimen had been reached. Following failure each double shear was removed from the frame and the insulation was removed to visually inspect the failure of the connectors. The placements of the load cell, plates, and LVDTs are shown in Figure 3-17.

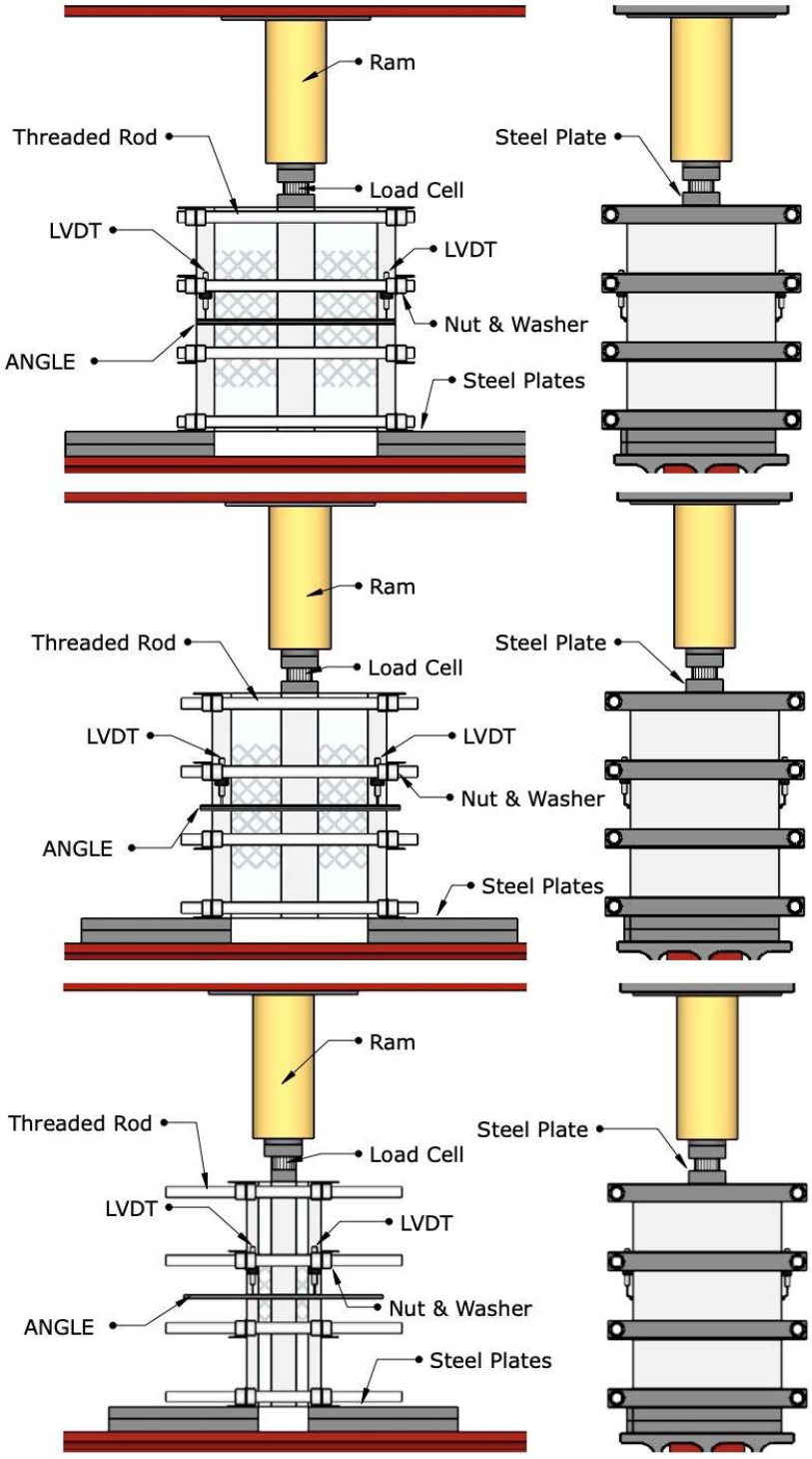

Figure 3-17 Double Shear Test Setup (F10, F8, F2 Top-Bottom)

All double shear specimens were also braced using steel angles attached directly into the outer wythes of concrete using post installed anchors. These steel angles were connected by threaded steel rod and tightened with nuts and washers. The bracing was provided to keep all wythes upright throughout the duration of the test and to prevent dangerous sudden failure due to concrete rupture of the outer wythes. The testing setups for the double shears are shown in Figure 3-18.

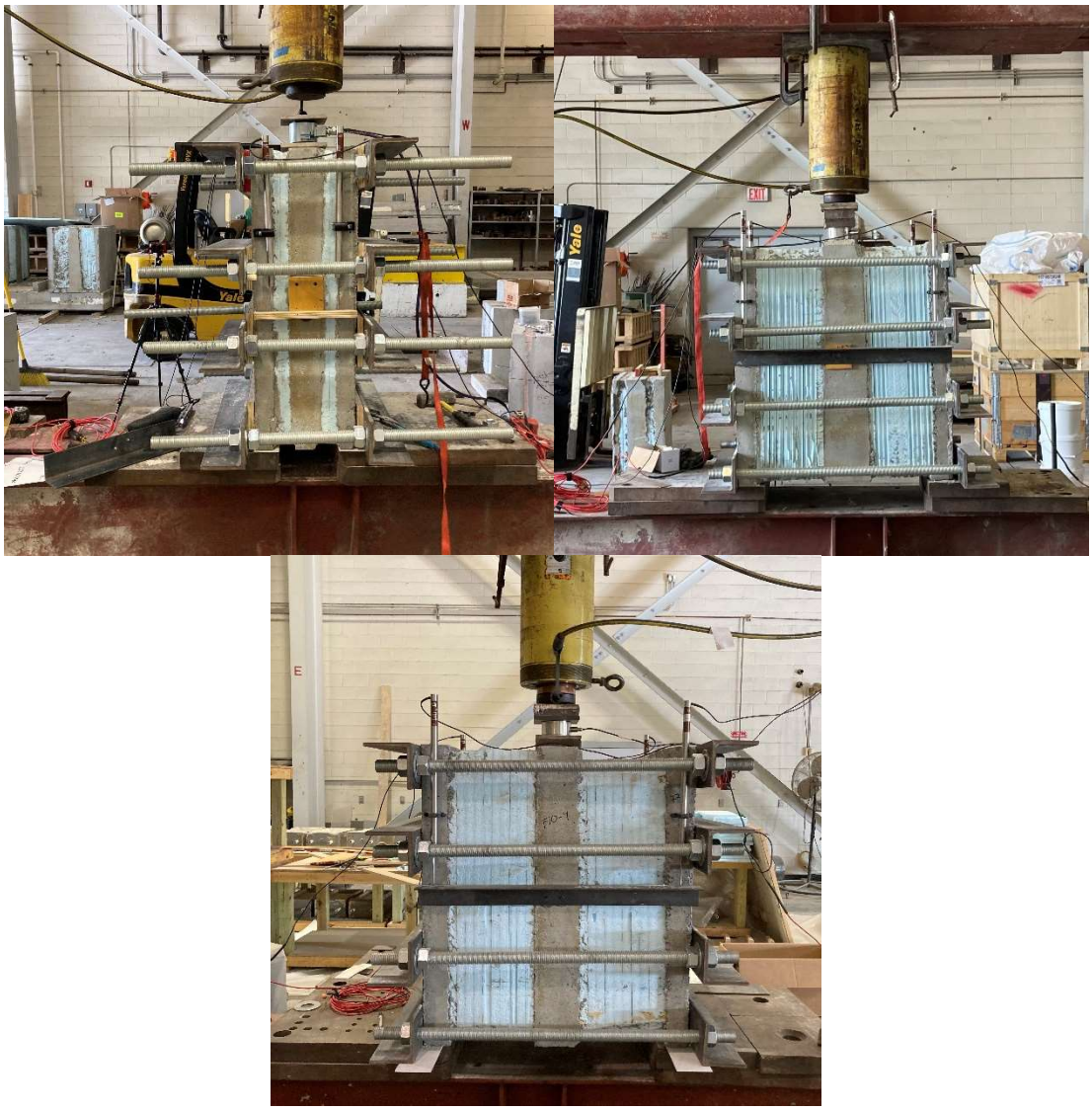

Figure 3-18 Double Shear Test Setup (F2 top-left, F8 top-right, F10 bottom)

Some modifications were made to this setup depending on the insulation thickness of the specimen being tested. As the insulation thickness varied between two and ten inches, the width of the double shear therefore varied widely as well. Frequent changes were that of the steel angles on which the LVDTs measured relative displacement. Steel angles of different lengths were used for the specimens with eight-inch and ten-inch insulation. A wood ledge was used in place of the steel angles for the specimens with two-inch thick insulation.

3.6 Full-Scale Panel Test Setup

Each full-scale panel was tested using two symmetrically loaded point loads each located approximately three feet from center span. This loading provided a constant maximum moment throughout the center six feet of the panel. A single ram was used to load the panel and an HSS spreader beam was used to split the load into the two-point loads described. A load cell sandwiched between steel plates was placed between the ram and spreader beam to measure the applied load. The number of plates varied to account for the differences in thickness between the two-inch insulation and eight- and ten-inch insulation panels. Small rollers were used to transfer the load from the spreader beam to the panel itself.

The spreader beam, ram, load cell, steel plates, and rollers were all supported using a wooden table and other dunnage to ensure they were centered vertically with the panel. The spreader beam, load cell, and plates all utilized polytetrafluoroethylene (PTFE) strips between them and their vertical supports to reduce friction during loading. Wood 2x4s were secured to the table creating two walls which prevented the ram from rolling to one side or the other. This testing setup, depicting one of the two-inch thick insulation panels, is shown in Figure 3-19.

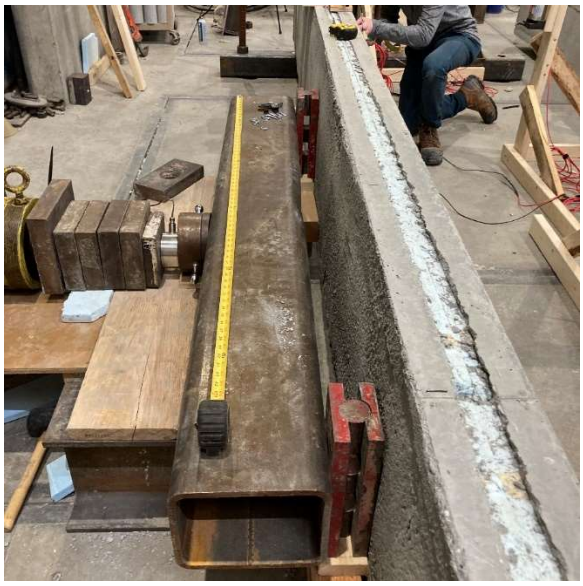

Figure 3-19 Full-Scale Panel Loading Setup

The panel was supported by two steel HSS A-frames. These A-frames were bolted into the floor of the lab using 100ksi steel rods, plates, and bolts. Steel rollers were placed at each support between the A-frame and the panel. Between each roller and the panel were two strips of PTFE which were utilized to reduce friction. The panel which sat on the bottom member of the steel A-frame was supported six inches above the lab floor. Again, PTFE strips were placed between the concrete wythes and the bottom member of the A-frame to reduce friction during testing.

Four LVDTs were placed along the top of the panel at the center of the two outermost connectors on each end to measure the slip between the wythes. Holes were drilled into the concrete and small rectangular pieces of Medium Density Overlay (MDO) board were secured using concrete screws to the top of the southern wythe of the panel. LVDTs were attached using screws to these rectangular MDO board pieces as shown in Figure 3-20. The location and identification number of each LVDT was carefully recorded. All panels were tested with the same four LVDTs, each being placed at the same relative positions on each panel to reduce confusion during the data processing stages.

Figure 3-20 Full-Scale Panel LVDT Setup

Thirteen string pots were used to measure deflection of the panel. Deflections at each reaction was measured with sensors measuring deflection at the top and bottom of the panel and on each side of the support. Additionally, deflections were measured at quarter and center spans again at top and bottom. One string pot intended for use was damaged shortly before testing began so only the top deflection was measured on the eastern quarter span. All string pots were secured to wooden A-frames that sat on the southern side of each panel and were attached to the panel using hooks and small metal angles which were glued directly to the southern face of the panel. The location and placement of all sensors are shown in Figure 3-21. The entirety of the setup is also shown in Figure 3-22.

The thicknesses of both wythes were measured and recorded at 24-inch increments along each panel's length. In addition, the depth of each panel was also measured and recorded at 24-inch increments along the panel's length to record any dimensional imperfections from formwork and casting of the specimens. The measurements of the wythe thicknesses were only taken at the top of the panel (orientation based on placement in test setup), as the panel was only raised six inches from the lab floor making accurate measurements from the bottom difficult.

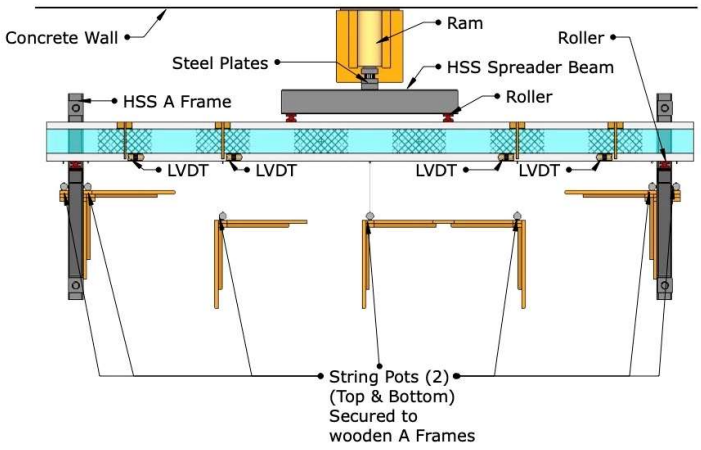

Figure 3-21 Full-Scale Panel Setup

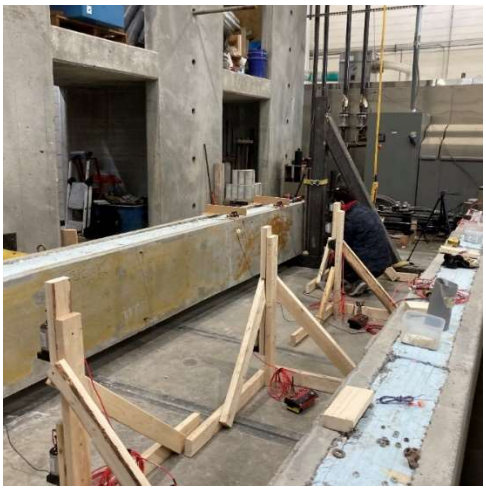

Figure 3-22 Full-Scale Panel String Pot Setup

Three different thicknesses of panel were tested varying from 6 inches to 16 inches. This difference in thickness required the use of added plates between the ram and spreader beam for the thinner panels, this difference is shown in Figure 2-3. PTFE strips were used to reduce friction under all plates in each testing configuration. The added plates were added between the ram and the load cell to reduce the friction recorded by the load cell during testing.

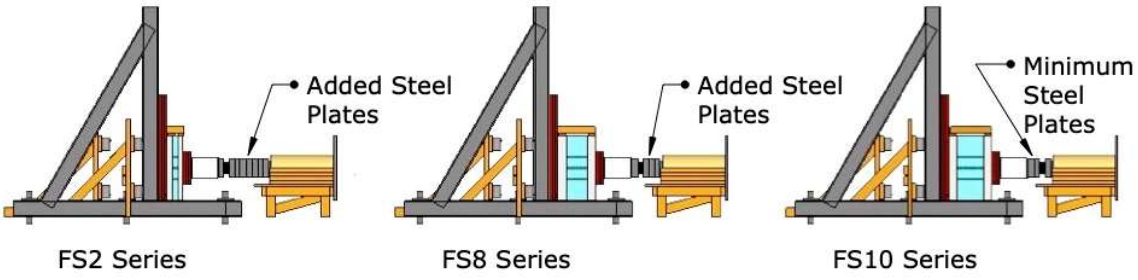

Figure 3-23 Full-Scale Panel Setup Series Comparison

3.7 Summary

This chapter describes the experimental program of this research including the design, construction, and test setup for double shear and full-scale panel specimens. All specimens were constructed and tested in the structures lab at the Peter Kiewit Institute (PKI) including the unique Fibergrate connectors which were created specifically to bridge the thick insulation. Results and analyses of the testing are found in the following chapters.

CHAPTER 4. EXPERIMENTAL RESULTS

4.1 Introduction

Fifteen double shear specimens and six full-scale panel specimens were constructed and tested to verify the feasibility of, and accuracy of, current design methods for ICSWPs with wythe and insulation thicknesses outside that of the current literature. This research included three different insulation thicknesses: two inches, eight inches, and ten inches, and two different wythe thicknesses of two inches and three inches. Connector patterns were consistent throughout the double shear and full-scale specimens. All connectors were unique Fibergrate connectors which were utilized to bridge the non-typical insulation thicknesses. The results of the testing are presented in this chapter.

4.2 Material Testing

Concrete cylinder testing was completed for both double shear specimens and the full-scale panels. Due to an effort to reduce material cost and space utilization within the lab, specimens were cast in three separate pours. The first pour consisted of nine double shear specimens. The second pour consisted of six double shear specimens and three full-scale panels, and the third pour consisted of the final three full-scale panels. Concrete cylinders were cast during each pour to determine concrete material properties for all specimens. Cylinders were cast using concrete from the middle of each pour.

Cylinders were tested for compressive stress for the double shear specimens. Compressive stress tests, modulus tests, and split tension tests were conducted on cylinders for the full-scale panel specimens. The results of this testing are found below in Table 4-1 The Fibergrate GFRP was determined to have an ultimate stress of 47,627 psi, a modulus of elasticity of 323,014 psi and a shear stress of 7696 psi.

Table 4-1 Material Properties

Specimen Designation	Compressive Stress *(psi)*	Modulus of Elasticity *(ksi)*	Tensile Strength *(psi)*
Double Shear Specimens			
F10-1	8100	-	-
F10-2	8100	-	-
F10-3	8100	-	-
F10-4	6850	-	-
F10-5	6850	-	-
F8-1	8100	-	-
F8-2	8100	-	-
F8-3	8100	-	-
F8-4	7450	-	-
F8-5	7450	-	-
F2-1	8100	-	-
F2-2	8100	-	-
F2-3	8100	-	-
F2-4	7450	-	-
F2-5	7450	-	-
Full-Scale Panels			
FS2-1	9530	5190	568
FS2-2	5080	4630	420
FS8-1	9460	5220	586
FS8-2	5080	4630	420
FS10-1	9220	5600	536
FS10-2	5080	4630	420

4.3 Double Shear Testing

All double shear specimens were tested past their ultimate capacity. Self-weight was neglected in the results for the double shear testing. The following figures, Figure 4-1, Figure 4-2, and Figure 4-3, depict the shear load and deflection relationship for all double shear specimens tested, except for specimens F2-1, F8-1, and F10-1. The load cell utilized for the first three tests was damaged and did not provide accurate data. This was discovered only after plotting the initial data. A new load cell was used for the remaining tests. Due to this sensor's malfunctioning, data

from these specimens are not included in the following figures and are not used in calculations. In addition, specimen F8-3 was poorly constructed resulting in one exterior wythe being significantly thin. During testing this wythe ruptured prematurely. The data from this specimen is plotted in Figure 4-2; however, it is not used in any calculations.

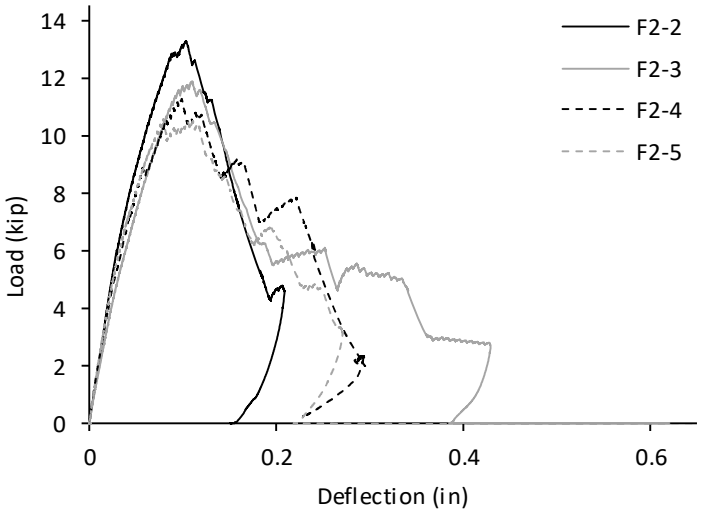

Figure 4-1 F2 Series Double Shear Results

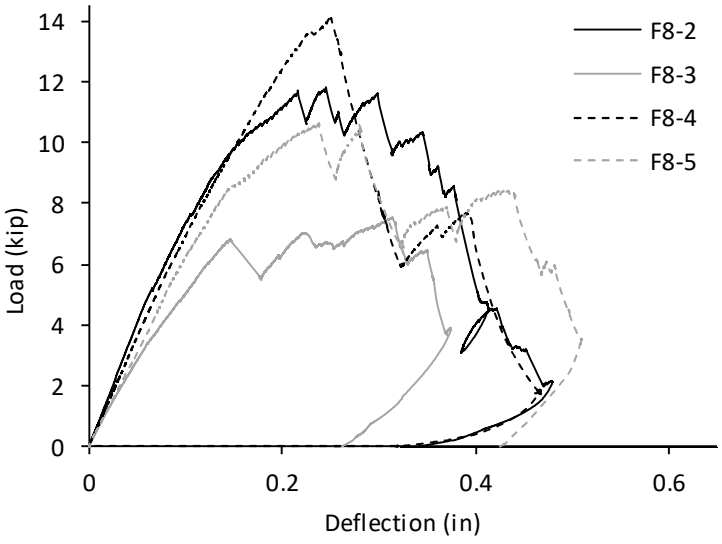

Figure 4-2 F8 Series Double Shear Results

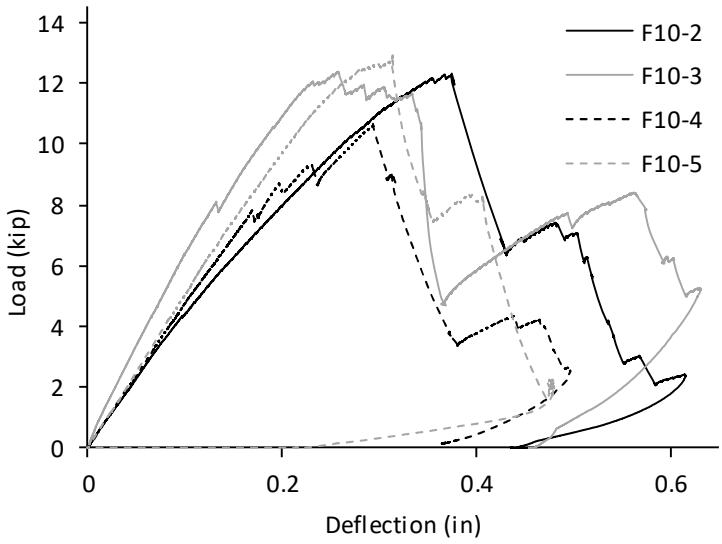

Figure 4-3 F10 Series Double Shear Results

All double shear specimens reached similar ultimate loads between 10.6 kip and 14.1 kip except for F8-3, as discussed above and seen in Table 4-2. The average maximum load for series F2 differs by only 4% from the average maximum load for series F8 (11.7 kip for series F2 and 12.2 kip for series F8). Similarly, the average maximum load for series F8 differs by only 1% from series F10 (12.2 kip for series F8 and 12.1 kip for series F10). Deflection corresponding to the ultimate load remained consistent between double shears of the same series with the exception of F10-2 which 0.06 inches further than any of the other double shears in the same series.

Some of the variability between double shears of the same series may be attributable to the use of only a single connector connecting each wythe. This single connector lacks the stability that would be more likely given two connectors connecting each wythe. Unfortunately, the lack of Fibergrate sheets necessitated the use of only a single connector connecting each wythe as described.

Table 4-2 Double Shear Specimen Test Results

Panel Designation	Wythe Thickness (in)	Insulation Thickness (in)	Maximum Load (kip)	Deflection at Maximum Load (in)
F2-2	2	2	13.26	0.10
F2-3	2	2	11.88	0.11
F2-4	2	2	11.26	0.10
F2-5	2	2	10.56	0.08
F8-2	3	8	11.82	0.25
F8-4	3	8	14.13	0.25
F8-5	3	8	10.64	0.24
F10-2	3	10	12.32	0.37
F10-3	3	10	12.38	0.26
F10-4	3	10	10.69	0.29
F10-5	3	10	12.92	0.31

4.4 Double Shear Failure Mechanisms

All the double shear specimens were loaded until failure. For all but specimen F8-3, the specimens' failures were controlled by connector failure. No tear out of the connectors was observed in any specimen. In addition, in all but specimen F8-2, the connector on one side of the specimen failed. Buckling of truss elements in compression was frequently observed as can be seen in Figure 4-4 below. Delamination of the GFRP truss elements in tension was also observed and is also shown in Figure 4-4.

Delamination and buckling were observed to occur in the eight truss elements that were used to preliminarily estimate the shear stiffness and lead to the design of each connector as described in section 3.1. Buckling was observed to be the more common of these two failure mechanisms. Specimen F8-3, as described earlier, was poorly constructed, containing a wythe that was too thin and resulted in concrete rupture prior to connector failure.

Figure 4-4 Double Shear Connector Failure (left: Buckling in F10 series, right: Delamination in F8 series)

The most complete failures occurred in the F2 series specimens. Following testing, an exterior wythe of three of the F2 series specimens completely separated from the center wythe before the insulation was able to be removed and the connector inspected for failure. This was due to the failure of each truss element in the connector. Figure 4-5 shows the near complete failure of one of the connectors in the F2 series.

Figure 4-5 Double Shear Failure of Series F2 Connector

As noted previously F8-3 failed prematurely in concrete rupture. No reinforcing was used in the double shear specimens and the thin, poorly constructed exterior wythe of this specimen ruptured vertically at the location of the connector and extended to the top and bottom of the entire wythe. This is shown in Figure 4-6.

Figure 4-6 Double Shear F8-3 Concrete Rupture

4.5 Full Scale Panel Testing

Six full-scale panels were tested past ultimate load or until concrete crushing occurred at the point of load application. The load and deflection relationship of each panel is plotted below in Figure 4-7, Figure 4-8, and Figure 4-9. Deflection values were measured at center span and averaged from sensors placed at the top and bottom of the wythe. Deflections were measured at the supports to account for settling of the panel into the testing mechanism and minor deflections caused by spacing between the bolts and steel A frames which supported the panels. The midspan deflections presented account for this settling.

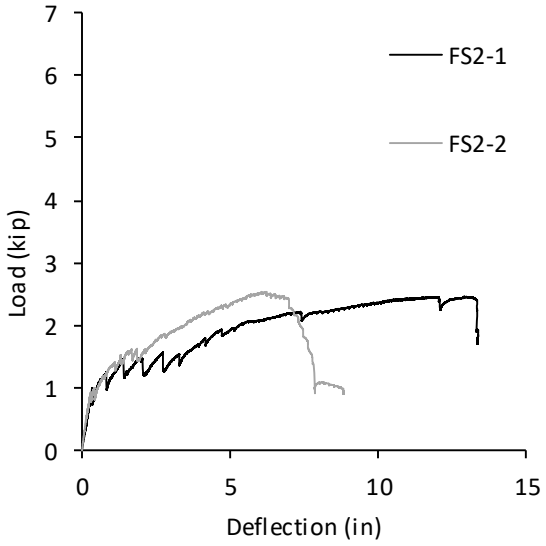

Figure 4-7 FS2 Series Deflection

FS2-1 and FS2-2 performed similarly within the elastic region but differed more in ultimate failure. FS2-1 reached its ultimate load much more slowly, and the test ended when concrete crushing at the application of load was observed. FS2-2 reached its ultimate capacity under approximately half the deflection reached by FS2-1. The difference in ultimate behavior is similar for FS8-1 and FS8-2 (Figure 4-8).

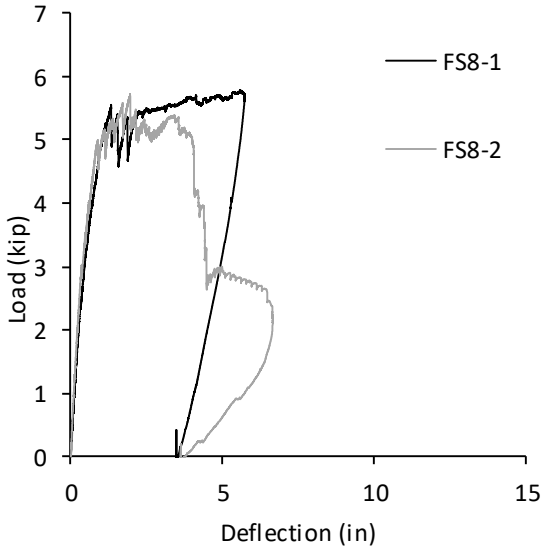

Figure 4-8 FS8 Series Deflection

FS8-1 reached ultimate capacity in a similar manner to FS2-1 and was stopped when concrete crushing was observed at the application of load. This trend for series one panels does not hold true, however, for FS10-1, which failed abruptly at a smaller deflection. It should be noted that FS10-1 was cracked prior to testing during its removal from the formwork.

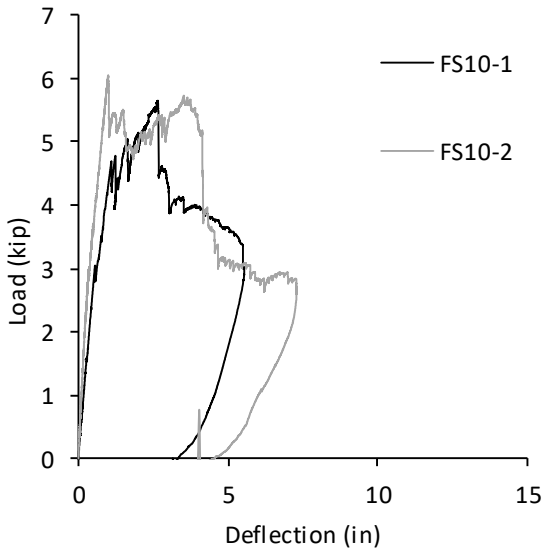

Figure 4-9 FS10 Series Deflection

The maximum load in series FS2 panels was significantly less than the maximum loads of series FS8 and FS10. All panels of the same series achieved similar maximum loading, and all max loadings are found in Table 4-3 for reference.

Table 4-3 Full-Scale Panel Results

Panel Designation	Wythe Thickness *(in)*	Insulation Thickness *(in)*	Maximum Load *(kip)*	Deflection at Maximum Load *(in)*
FS2-1	2	2	2.46	12.9
FS2-2	2	2	2.54	6.05
FS8-1	3	8	5.78	5.57
FS8-2	3	8	5.72	1.95
FS10-1	3	10	5.64	2.65
FS10-2	3	10	6.05	1.00

The relative slip between the two wythes was measured at the center of the four outermost connector locations. The load vs slip is plotted below for each panel in Figure 4-10 through Figure 4-15. The different slips were designated based on their location on the panel. East and west slips indicate the outermost connector locations and east inner and west inner slips indicate the next outermost connector locations. The data demonstrates the most perplexing information as the inner slips frequently were larger than the outermost slips.

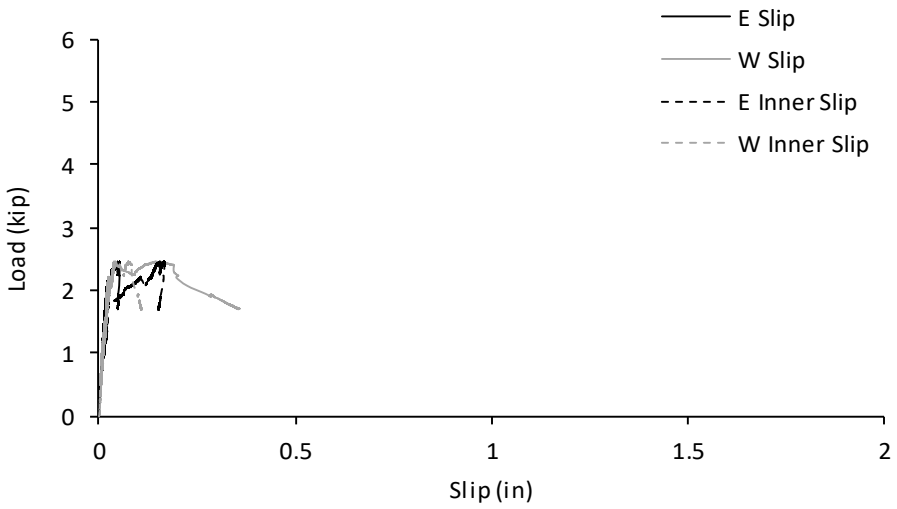

Figure 4-10 FS2-1 Load vs Slip

FS2-1 did not experience slips as large as most of the other panels. The slip of FS2-1 is most comparable to the slip experienced by FS8-1. Both had maximum slips less than 0.5 inches and the largest slips were measured on the east inner and west end connector locations. The slips measured for FS2-2 were larger than FS2-1 and seen in Figure 4-11. The largest slips measured on panel FS2-2 occurred on the east side of the panel with the inner east slip exceeding the slip at the furthest east connector location.

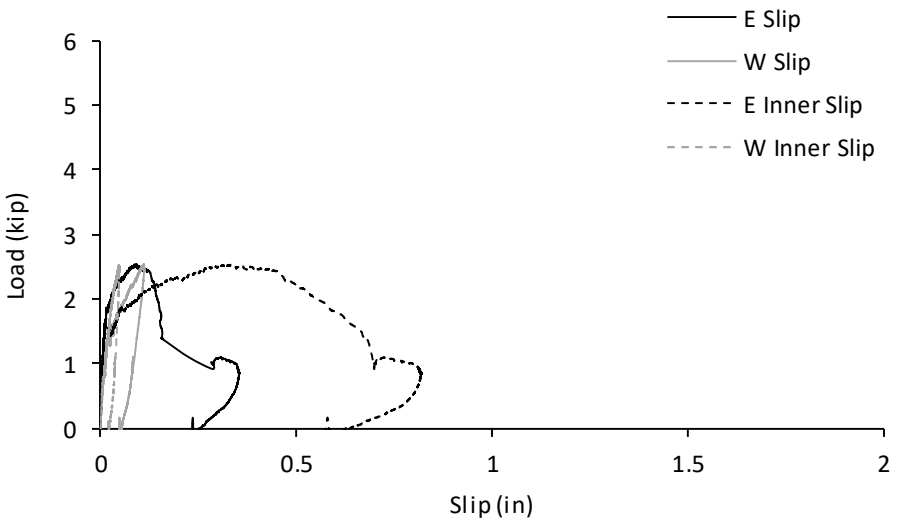

Figure 4-11 FS2-2 Load vs Slip

The slip of FS8-1 was most comparable to the slip of FS2-1, as stated. The maximum slip experienced was less than 0.5 inches. Most of the slip occurred while the load hovered around five kips.

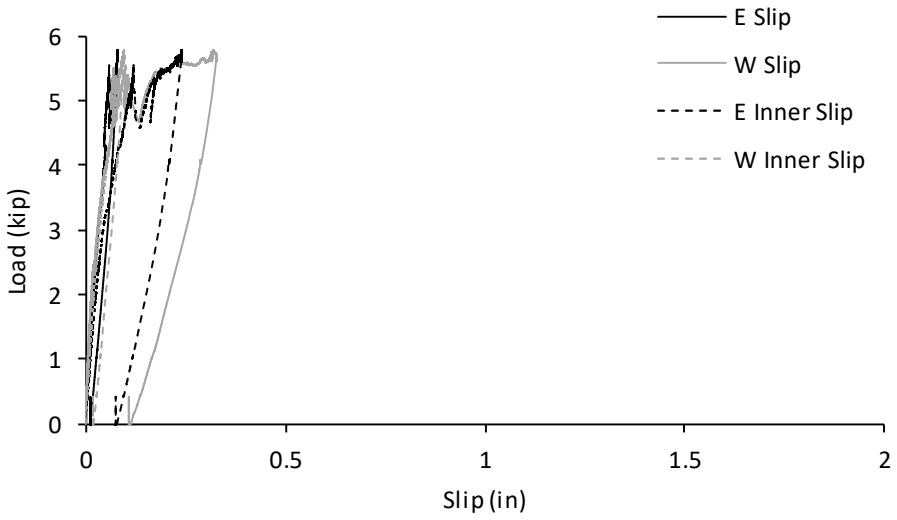

Figure 4-12 FS8-1 Load vs Slip

FS8-2 experienced larger slips than panels FS2-1, FS2-2, and FS8-1 (Figure 4-13). The maximum slip exceeded 1.5 inches, which was more than three times larger than the slip

experienced by FS2-1 and FS8-1. The largest slips measured were recorded on from the two LVDTs on the east side of the panel.

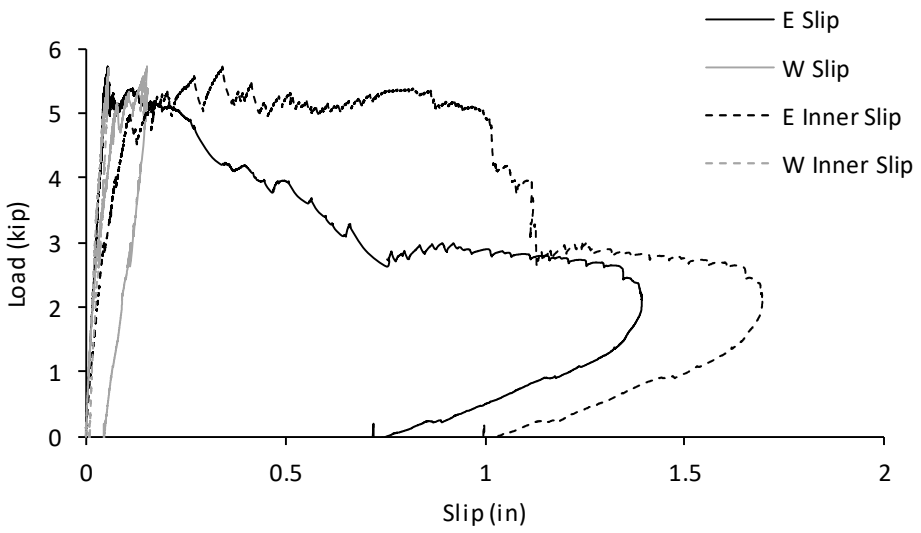

Figure 4-13 FS8-2 Load vs Slip

Frequently two or three of the slips measured never exceed 0.5 inches while the other slips measured reach significantly larger slips. This is shown clearly for the slip for FS10-1 (Figure 4-14).

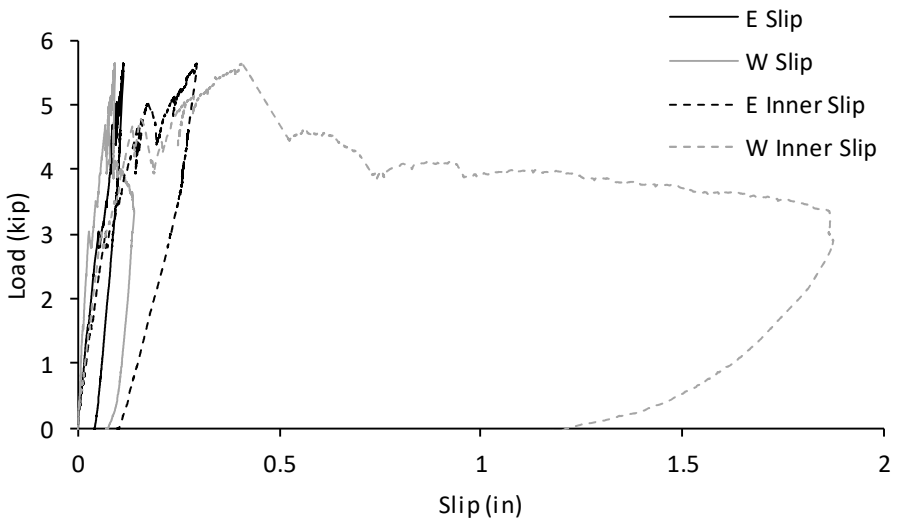

Figure 4-14 FS10-1 Load vs Slip

The slip on the west side of panel FS10-2 was measured to be significantly larger than the slip on the east side, following the same trend acknowledged in many of the other panels. The inner slip on the west side of the panel increased significantly following ultimate failure but the end slip increased prior to ultimate failure. This result differs from FS8-2 whose inner slip deflected prior to ultimate failure and the end slip increases after ultimate failure.

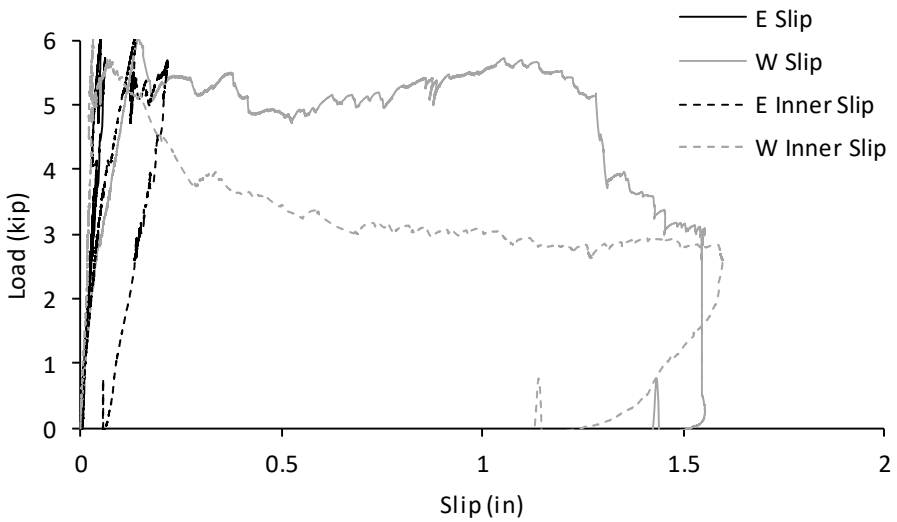

Figure 4-15 FS10-2 Load vs Slip

4.6 Full-Scale Panel Failure Mechanisms

All panels were tested past failure and or until concrete crushing occurred at the location of the application of load. During testing, all panels developed moderate to severe flexural cracking. Most commonly this cracking was observed symmetrically on both sides just within the section of the span experiencing maximum moment. An example of these flexural cracks is shown in Figure 4-16. Most of these cracks also occurred at or near the edge of a connector. In addition to this flexural cracking, flexural cracks occurred on the wythe upon which loading was applied. As can be seen in Figure 4-17, the panel is in negative bending near the end of the panel

but positive bending near center span. These cracks due to negative bending were always observed near the end of the outermost connectors.

Figure 4-16 Full-Scale Panel Flexural Cracks

Figure 4-17 Full-Scale Panel Behavior

Concrete crushing also occurred at the point of load application and is depicted in Figure 4-18. Testing was always ended when concrete crushing was observed and was most frequently the cause of the test ending. The concrete crushing often occurred after audibly observed connector failure or observed steel yielding.

Figure 4-18 Concrete Crushing

Connector failure was observed in panels FS8-1, FS8-2, FS10-1, and FS10-2 (Figure 4-19). In panels FS8-1 and FS10-1, only one connector failure was observed whereas panels FS8-2 and FS10-2 both had three connectors fail. The failed connectors were always the outermost and second outermost connectors. The connectors typically failed in compression, as seen in Figure 4-20. Panels FS2-1 and FS2-2 did not have confirmed connector failure as the tight two-inch foam was difficult to remove and could not be done prior to the removal of the tested specimens from the lab.

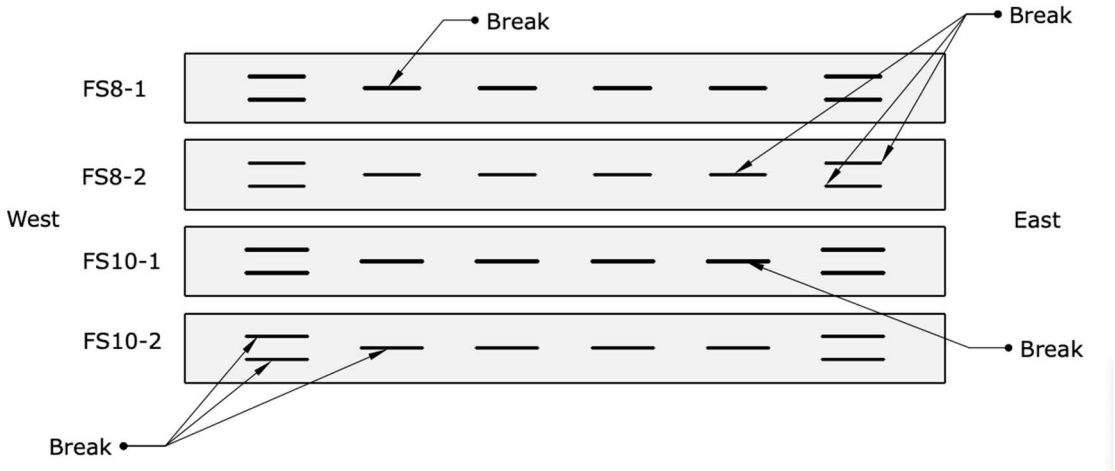

Figure 4-19 Location of Observed Connector Failures

Figure 4-20 Full-Scale Panel Connector Failure (Buckling)

Panels FS8-2 and FS10-2 both failed at peak load due to connector failures. Panel FS8-1 had only one observed connector failure and following the connector failure the panel continued to resist additional load until steel yielding was observed.

CHAPTER 5. DISCUSSION

5.1 Introduction

The results and behaviors of the experimental testing are discussed in this chapter. Included in this chapter are discussions about the behavior of the double shear specimens and the shear stiffnesses of the connectors, the behavior of the full-scale panels, their measured percent composite action, and a comparison of all testing results to existing prediction methods.

5.2 Double Shear Behavior

Double shear tests are frequently performed in conjunction with full-scale testing to determine connector shear stiffnesses. As discussed in the literature review the shear transfer mechanisms in ICSWPs are central to the behavior of the full-scale panel. Double shear tests are used to determine some principal properties of connectors. These properties, including the shear stiffness, are frequently used in analysis methods for predicting ICSWP behavior such as the beam-spring method or the SSBT method. These properties can be calculated theoretically using methods developed by Holmberg and Plem and Tomlinson, as outlined in chapter 2.

This section discusses the results of the experimental testing of the double shears and the behavior of the connectors tested. The values obtained from the experimental testing are compared to the analytical methods developed by Holmberg and Plem, and Tomlinson. Connectors typically exhibit an initial elastic response followed by an inelastic response. Load and displacement relationships are used to determine the elastic shear stiffness K_E and the inelastic shear stiffness K_{IE}. The elastic region is typically classified as the region below either of the following load limits in equations (5-1), and (5-2):

$$F_{E0.4} = 0.4 * F_u \tag{5-1}$$

or

$$F_{E0.5} = 0.5 * F_u \tag{5-2}$$

Where: F_E = elastic load limit

F_u = ultimate capacity

For design methods, both the elastic and inelastic stiffnesses are assumed to be linear. The elastic and inelastic shear stiffnesses are represented by the slopes of the load-deflection diagrams corresponding to the elastic and inelastic regions and can be calculated as follows in equations (5-3), and (5-4):

$$K_E = \frac{F_E}{\Delta_E} \tag{5-3}$$

$$K_{IE} = \frac{F_u - F_E}{\Delta_u - \Delta_E} \tag{5-4}$$

Where: K_E = elastic shear stiffness

K_{IE} = inelastic shear stiffness

Δ_E = deflection corresponding to elastic load limit F_E

Δ_u = deflection corresponding to ultimate capacity F_u

Note that the elastic stiffness and inelastic stiffness of the connector can be calculated using either the elastic stiffness based on either elastic load limit in equations (5-1) and (5-2).

Using equations (5-1) through (5-4) elastic shear stiffnesses and inelastic shear stiffnesses were calculated for each double shear specimen. The calculated stiffnesses are found below in Table 5-1.

Table 5-1 Connector Elastic and Inelastic Stiffnesses

Connector Designation	Insulation Thicknesss *(in)*	$K_{E0.4}$ (kip/in)	$K_{IE0.4}$ (kip/in)	$K_{E0.5}$ (kip/in)	$K_{IE0.4}$ (kip/in)
F2	2	193.84	96.94	181.63	90.90
F8	8	71.54	41.74	65.60	39.20
F10	10	51.80	34.33	51.08	32.44

As can readily be seen in the table above, both the elastic and inelastic stiffnesses decrease as the insulation thickness that the connectors bridge increases. It can also be noted that the elastic and inelastic shear stiffnesses are much more similar for the F8 and F10 connectors than for either the F8 or F10 compared to the F2 connector. This also indicates that the shear stiffnesses are likely a function of the insulation thicknesses they bridge. The elastic and inelastic stiffnesses based on 0.4*Peak Load are marginally larger than those based on 0.5*Peak Load for all connectors.

The methods developed by Holmberg and Plem and Tomlinson to predict connector behavior are described in section 2.3.1, and using equations (2-3), (2-4), (2-8), and (2-9), the predicted shear stiffnesses of all three connectors was calculated. As noted in section 2.3.1, the shear stiffness for Tomlinson's method is based on the current deflection of the connector. As the connector deflects, the shear stiffness changes. To account for this, the shear stiffness of the connector was determined prior to loading and at the elastic limit. These values were averaged to determine the shear stiffness based on Tomlinson's method. The difference between the two averaged values was minimal not exceeding two tenths of a kip/in. A comparison of the prediction of both methods and the experimental results based on 0.5*Peak Load and 0.4*Peak Load are shown below in Figure 5-1 Comparison of Elastic Shear Stiffnesses.

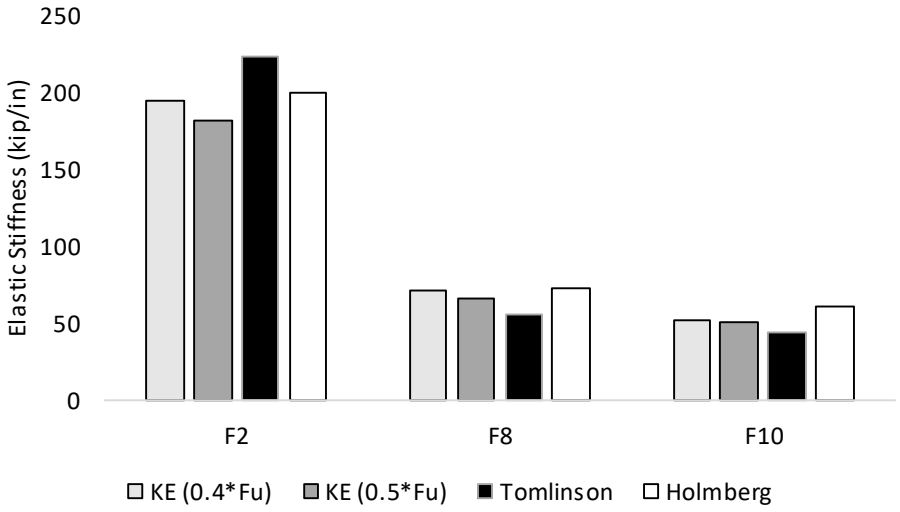

Figure 5-1 Comparison of Elastic Shear Stiffnesses

Both methods by Tomlinson and Holmberg and Plem produced shear stiffnesses like the experimental testing. Tomlinson's method overpredicted the shear stiffness of the F2 connector and underpredicted connectors F8 and F10. Holmberg and Plem's method overpredicted the shear stiffnesses of all the connectors but was closer than those of Tomlinson's method to the experimentally tested shear stiffnesses in all cases except for the F10 connector.

For further comparison, the elastic shear stiffnesses derived from both Tomlison's method and Holmberg and Plem's method are plotted against the load-displacement curves of each double shear in Figure 5-2, Figure 5-3, and Figure 5-4. These figures clearly demonstrate that both methods match the experimental data closely. Again, Tomlinson's method clearly overpredicts the shear stiffness of the F2 connector and underpredicts connector F8. However, for connector F10, the methods essentially sandwich all the experimental data between them with Holmberg overpredicting and Tomlinson underpredicting the stiffnesses.

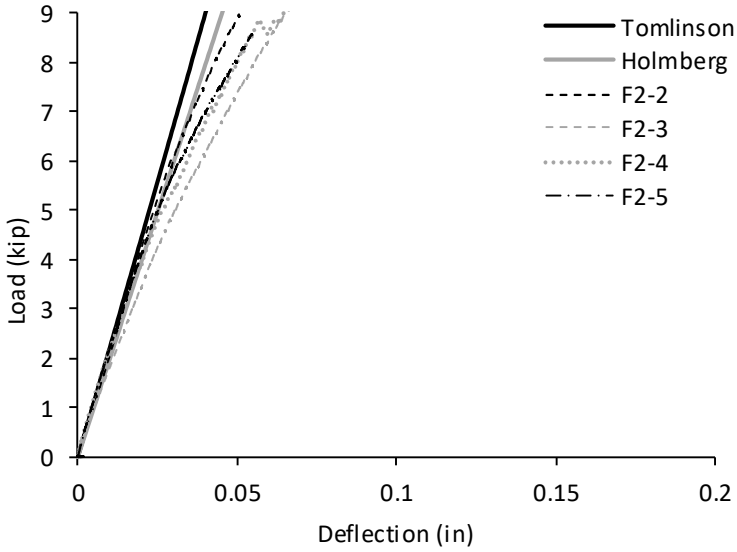

Figure 5-2 Elastic Shear Stiffness Prediction Series F2

Tomlinson's method not only overpredicts the stiffness of the F2 connector but its prediction is stiffer than any of the individual stiffnesses measured through the double shear testing. Tomlinson's method surprisingly then underpredicts the stiffness of the F8 connector as shown in Figure 5-3. Tomlinson's method predicted a stiffness that was lower than all data tested in this set of double shears except for F8-3, which failed prematurely.

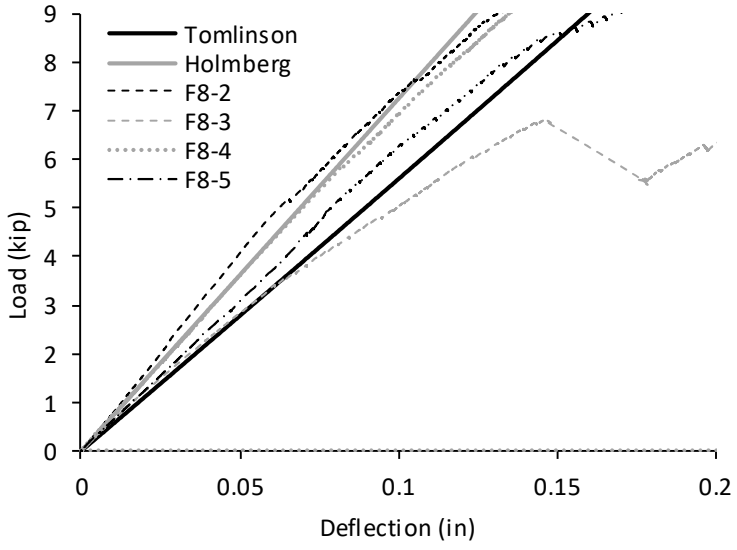

Figure 5-3 Elastic Shear Stiffness Prediction Series F8

As seen in Figure 5-4, Tomlinson's method is more accurate in predicting the F10 connector but, at smaller loads, can be seen to underpredict all measured stiffnesses. Holmberg and Plem's method overpredicted the stiffness of the F10 connector with a prediction stiffer than all but one of the double shear specimens. Holmberg and Plem's prediction was closer to the average for the other two connectors.

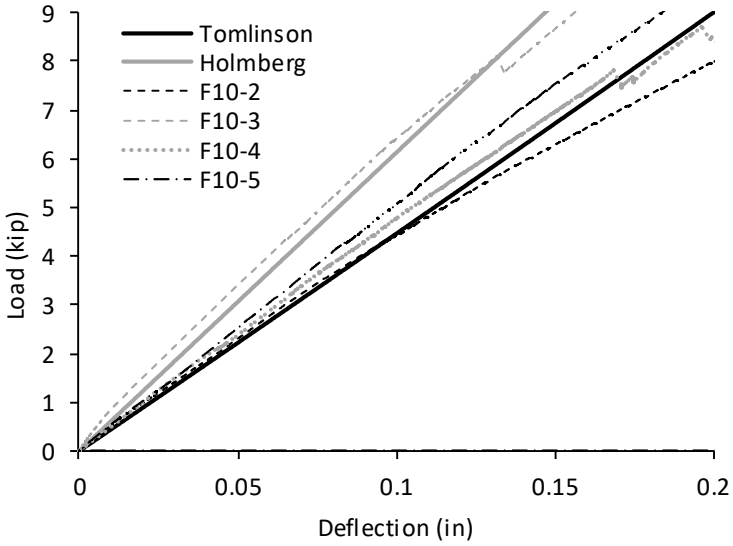

Figure 5-4 Elastic Shear Stiffness Prediction Series F10

The differences between the two methods described in chapter 2 are what result in the differences in their predictions. The method developed by Holmberg and Plem is more consistent in its prediction, as all predictions were larger than the experimental testing. Tomlinson's model was less consistent, as it switched from overpredicting to underpredicting the shear stiffnesses of the connectors.

The first difference between the methods is that Tomlinson's method calculates the shear stiffness as a function of the elongation of the connector. The shear stiffness, shown in Figure 5-2, Figure 5-3, and Figure 5-4, for Tomlinson's method includes shear stiffnesses calculated at the varying displacements at increments of 0.001 in. Again, as can be seen in the figure, the plot appears to remain linear. The non-linear behavior of Tomlinson's prediction only becomes

apparent at relatively large displacements. Because of this, for these connectors, this difference between the methods is negligible.

Another difference between the two methods is that Tomlinson does not consider the embedment depth of the truss elements of the connector into the wythes of concrete as part of the length of the elements considered in the calculations. Holmberg and Plem's method considers this difference, assuming the embedment depth is one half the wythe thickness. This assumption is accurate to our testing, as all connectors did have an embedment depth of one half the wythe thicknesses. The assumption of Holmberg and Plem may result in less accurate results for connector and wythe assemblies that do not adhere to this assumption and may be one of the reasons that Holmberg and Plem's method was shown to be marginally more accurate than that of Tomlinson.

One final difference between the two methods is that Tomlinson, in addition to considering truss action, also considers the shear contribution provided by the bonded insulation and the dowel action of the connector. Due to the truss-like behavior of our connector, the dowel action contribution was not considered when calculating the shear stiffnesses. In addition, the double shear and full-scale panel specimens were designed to utilize 1 in. thick insulation panels stacked to reach the overall insulation thickness for each specimen. This was done on purpose to allow for multiple shear planes between the insulation eliminating the shear transfer mechanism of bonded insulation. Due to this design, the shear contribution of the bonded insulation was assumed to be zero for all connectors.

While Tomlinson's model does approach similar results to Holmberg and Plem, it was concluded that Holmberg and Plem's method was found to be more accurate. The stiffnesses predicted by Holmberg and Plem all fell within one standard deviation of the average stiffness measured. Tomlinson's method predicts stiffnesses that fall outside of one standard deviation from the average for two of the three connectors and two of the predictions fall outside of the range of the measured stiffnesses with one being too high and the other being too low. Holmberg

and Plem's method also predicted stiffnesses for connectors F2 and F8 with measured to predicted ratios of 1.03 and 1.01, respectively. The most accurate prediction by Tomlinson's method resulted in a measured to predicted ratio of 0.86.

5.3 Full-Scale Apparent Percent Composite

Percent or degree of composite action is a common metric used to describe the behavior of partially composite ICSWPs. Percent composite action describes how close certain behavioral aspects of the panel perform when compared to how the panel would perform given its behavior as non-composite or fully composite. Percent composite action is frequently calculated based on three separate behaviors: cracking moment, ultimate moment, and deflection within the elastic region.

The percent composite action for each panel and for each behavior described above was calculated and shown in Figure 5-5. The strength and deflection based on cracking was not calculated for panel FS10-1 as the panel had cracked prior to testing. As can be seen in Figure 5-5, panels FS2-1, FS8-1, and FS10-1 all exceeded 100% composite action for ultimate strength behavior. While the strengths measured did in fact result in an exceedance of 100% composite action, the panel is not capable of truly exceeding 100% composite action. The excess of 100% composite action occurs frequently in ICSWPs and is typically attributed to steel having a larger yield stress than was measured in testing or provided by mill verification. This discrepancy results in an underpredicted ultimate panel strength. One trend that can be seen from the above figure is that series 1 panels all performed at or near 100% composite action while all series 2 panels performed closer to 20% composite action. The difference in the composite action reached is due to the difference in steel reinforcement outlined in CHAPTER 3.

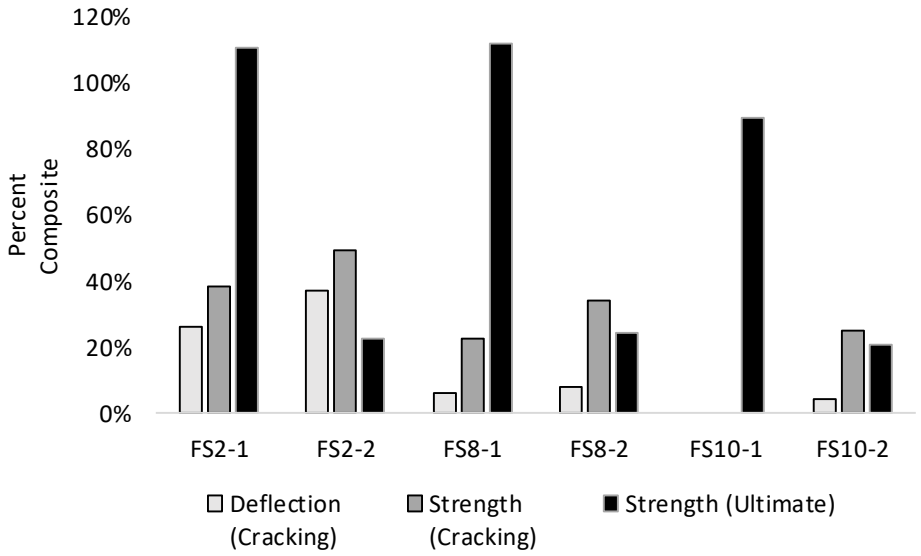

Figure 5-5 Percent Composite Action

The series 1 panels were designed to fail in reinforcement yielding prior to connector failure and the series 2 panels were designed to exhibit connector failure. This difference in intended failure was done to allow the study of the ability of various existing methods to predict the ultimate failure mechanism. All panels failed as expected except for panels FS2-2 and FS10-1. The discussion on ultimate panel failure is further expounded in section 5.5.

From the figure, it is shown that some panels including panels FS8-1, FS8-2, and FS10-2 did not perform with a high percent composite action based on deflection. In fact, as can be seen in Table 5-2 below, these panels performed with 6%, 8%, and 4% composite action respectively. The low percentages of composite action could likely be misinterpreted by many as an indication of a poorly designed partially composite panel, but the low percent can be deceiving. Despite the low percent composite action, panels FS8-1, FS8-2, and FS10-2 were 3.6, 4.2, and 3.1 times stiffer than non-composite panels of their same dimensions, or, in other words, partial composite action resulted in an increase in stiffness of 263%, 322%, and 211%, respectively. Unfortunately, using percent composite action to describe panel behavior can unintentionally undersell the performance of partially composite ICSWPs.

Table 5-2 Composite Action (Deflection)

Panel Designation	I_{NC} (in^4)	I_{FC} (in^4)	$I_{equivalent}$ (in^4)	Percent Comp.	Percent Increase
FS2-1	32	418	134	26%	315%
FS2-2	31	386	163	37%	424%
FS8-1	98	4274	355	6%	263%
FS8-2	105	4387	442	8%	322%
FS10-1	109	6257	NA	NA	NA
FS10-2	146	7182	454	4%	211%

Table 5-3 below outlines the relevant information needed for calculating the percent composite action based on cracking. Again, an additional column in the table is included outlining the percent increase in cracking moment from the cracking moment of a non-composite panel to the measured cracking moment. An interesting trend can be seen in this table, as the percent composite decreases as panel insulation increases but the percent increase of the cracking moment increases as insulation thickness increases. In fact, the cracking moment increased 1,378% for panel FS8-2 or in other words was nearly 15 times higher than that of the same panel performing non-compositely.

Table 5-3 Composite Action (Cracking)

Panel Designation	$M_{cr\ NC}$ (kip-in)	$M_{cr\ FC}$ (kip-in)	M_{cr} (kip-in)	Percent Comp.	Percent Increase
FS2-1	7.9	102	44	38%	461%
FS2-2	6.2	77	41	49%	557%
FS8-1	10.1	442	108	23%	966%
FS8-2	9.0	377	133	34%	1378%
FS10-1	9.8	563	NA	NA	NA
FS10-2	10.2	502	131	25%	1190%

Table 5-4 shows the breakdown of percent composite and percent increase of all panels based on the panels' ultimate moment capacity. This table highlights some of the same trends

discussed above about the differences between series 1 and series 2 panels. The difference in reinforcement accounts for most of the differences between series 1 and series 2 panels. As described in this section, the ultimate capacity of non-composite and fully composite panels are calculated based on internal equilibrium and strain compatibility. Series 2 panels have an increased bar size and, therefore, the steel is capable of resisting more tensile forces resulting in a larger ultimate moment capacity of the panel.

Table 5-4 Composite Action (Ultimate)

Panel Designation	$M_{u\,NC}$ (kip-in)	$M_{u\,FC}$ (kip-in)	M_u (kip-in)	Percent Comp.	Percent Increase
FS2-1	29	90	96	111%	226%
FS2-2	69	203	99	22%	43%
FS8-1	43	206	226	112%	426%
FS8-2	114	560	223	25%	96%
FS10-1	45	242	220	89%	393%
FS10-2	126	663	236	20%	87%

Percent composite is commonly used to describe ICSWP behavior but it can be misleading in the overall performance of panels. This misleading nature of percent composite may disproportionately discourage the use of thick insulation ICSWPs. A key advantage to using thick insulation ICSWPs is the increase in depth of the wall panel when resisting flexure. The deep section of thick insulation ICSWPs dramatically increases the moment of inertia of the section. This is because the moment of inertia of a section is a function of a section's depth to the third power.

The exponential increase in fully composite moment of inertia of thick insulation ICSWPs results in the fact that thick insulation ICSWPs do not need to reach the same percent composite as thinner panels to increase the overall capacity of the panel to similar degrees. This is true specifically for deflection and cracking moment which are both functions of a section's moment of inertia. This is illustrated in the above figures and tables. For example, Table 5-2

shows that the thin insulation panels reached 26% to 37% composite action while the thick insulation panels only reached 4% to 8% composite action, but the percent increase from non-composite behavior between all panels were much more comparable.

5.4 Full Scale Elastic Prediction

Three elastic prediction methods, which were described in chapter 2, were used to model the expected behavior of each of the six full-scale panels tested. The three methods used were the beam-spring method, the ISBT method, and the method developed by Holmberg and Plem. The results of each prediction are plotted jointly with the measured results in Figure 5-6, Figure 5-7, and Figure 5-8. The methods of prediction used material properties obtained from concrete cylinder testing including concrete compressive strength and modulus of elasticity. The modulus of rupture of the concrete was obtained using the ACI equation. The shear stiffness of the connectors was calculated using the average of the stiffness values obtained at 0.4 times each connector's ultimate load.

As described in section 3.6, wythe thickness measurements were taken for each panel specimen. The thinner of the two wythe thickness measurements taken nearest the first observed crack was used for the thickness of the tension wythe. The depth of the wythes was taken as the depth measured at the corresponding wythe measurement used for the tension wythe. The thickness of the compression wythe was taken as the average measured wythe thickness. These dimensions were chosen to accurately model the actual behavior of the panel at cracking. There are two exceptions to the use of the above dimensions. The first exception is made for panel FS10-1. Panel FS10-1 was cracked prior to testing, so there was no observed first crack, instead nominal dimensions are used for panel FS10-1's wythe thicknesses. The other exception was made because Holmberg & Plem's method assumes equal wythe thicknesses. For Holmberg and Plem, the wythe thickness used for the tension wythe was also used in the compression wythe as explained later in this section.

The Beam Spring and ISBT methods are robust methods capable of modeling ICSWPs with different wythe thicknesses for tension and compression wythes, discrete or continuous connectors, and any loading condition. The method developed by Holmberg and Plem, as discussed in CHAPTER 2, makes several assumptions which resulted in a method that is not capable of adapting to various loading conditions, discrete connectors, and different compression and tension wythe thicknesses. Several assumptions and adaptations were made in order to use the method developed by Holmberg and Plem to predict the behavior of the panels tested in this research and are listed below.

- Incompatibility between loading conditions: The panels tested in this research were subjected to symmetrical two-point loading whereas Holmberg and Plem's method assumes a uniform load. In order to compare loading, the two-point loading was converted to an equivalent uniform load by calculating the maximum moment caused by the two-point loading and calculating an equivalent uniform load that would result in the same maximum moment.
- Different Tension and Compression Wythe Thicknesses: Due to errors in construction, the compression and tension wythe thicknesses in some panels differed from one another. These slight differences were accounted for using the other methods to accurately model the tested panels. The method of Holmberg and Plem assumes equal wythe thicknesses, therefore, making it impossible to account for these discrepancies by modeling the varying wythe thicknesses. For both compression and tension wythe thicknesses, the measured tension wythe thickness as described previously in this section was used for both the tension and compression wythes.
- Discrete Connector Incompatibility: The panels tested in this research utilize discrete connectors instead of continuous connectors, as the method of Holmberg and Plem assumes. In addition, Holmberg and Plem assume a uniform panel stiffness, the panels in

this research have nonuniform stiffness due to both the use of discrete connectors and the use of two rows of connectors at the edges of the panels and only a single row otherwise. Despite the discrete nature of the connectors in the panels, it was assumed for this method that the panel had a uniform stiffness that was calculated using the following equations.

$$K_{E.Panel} = \frac{N * K_E}{b * l} \tag{5-5}$$

Where: $K_{E.Panel}$ = uniform panel stiffness

K_E = elastic shear stiffness of a single connector

N = number of connectors

b = panel width

l = span length

The results calculated using Holmberg and Plem's method with the above stated adaptations are presented in this thesis alongside the other methods. It is recognized that any poor correlation between the predictions from Holmberg and Plem's method and the measured results may be the result of the above assumptions and adaptations.

5.4.1 Elastic Stiffness Predictions

Figure 5-6 shows the predicted results of Holmberg and Plem, Beam Spring, and ISBT methods for panels FS2-1 and FS2-2. The stiffnesses of both panels were higher than were predicted using all three methods. All methods agree closely with one another on the expected stiffness of the panel with their respective responses nearly overlapping for both panels.

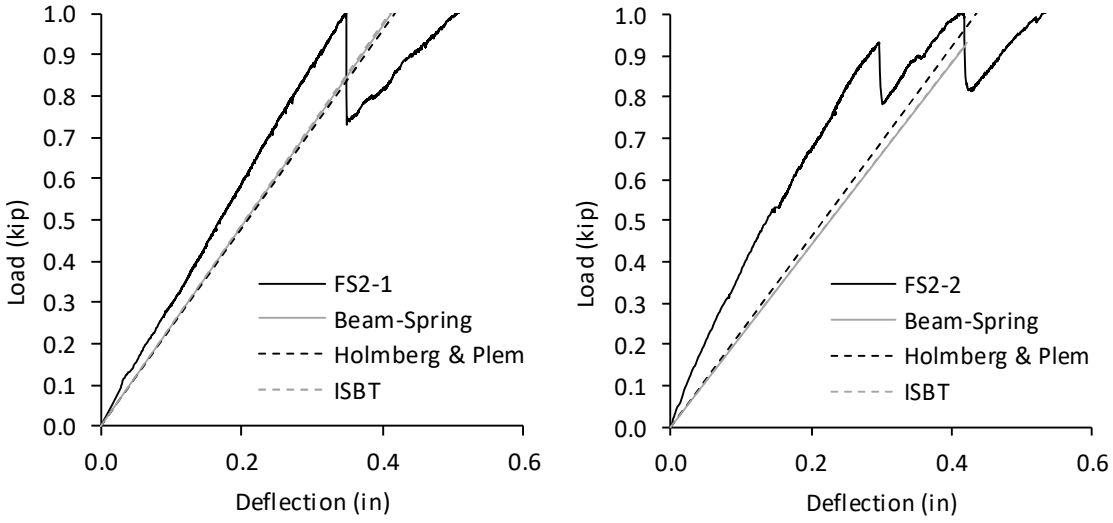

Figure 5-6 Full Scale Elastic Prediction (FS2-1 left, FS2-2 right)

The results and predictions for FS2-2 differ much more widely with the measured results demonstrating stiffer behavior than any prediction. The cracking load, however, is still accurately represented. The larger stiffness from the measured results is likely due to an unintentional section of concrete connecting both wythes. This section of concrete was located at the increased wythe depth at the concrete anchor lifting locations described in Chapter 3. Great efforts were made to maintain a separation between the two wythes at these locations, but efforts were unsuccessful in this instance. This concrete section connecting the two wythes was observed during testing. No similar concrete section was observed in panel FS2-1; however, it is possible a smaller concrete section existed which may account for the difference in stiffness between the predictions and measured results.

The elastic stiffness predictions for panels FS8-1 and FS8-2 are shown in Figure 5-7 below. All three prediction methods again follow closely to one another; however, of FS8-1 and FS8-2, the stiffnesses predicted match closer to the measured response. The measured stiffness for panel FS8-2 varies a little from the prediction near the beginning of the test and may be the result of unintended friction introduced into the test.

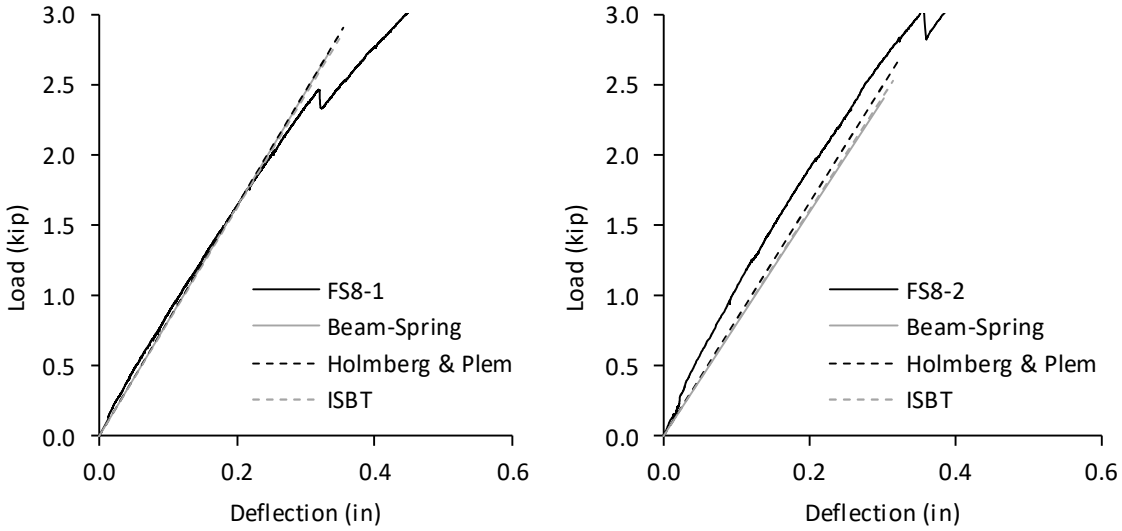

Figure 5-7 Full-Scale Elastic Prediction (FS8-1 left, FS8-2 right)

The predictions and measured results for FS10-1 and FS10-2 are plotted in Figure 5-8. As noted previously, FS10-1 was cracked prior to testing, and the cracked concrete resulted in a reduction in stiffness which can be seen in the difference between the measured results and the predictions. Like the other panel predictions, all three methods predicted very similar stiffnesses and, in the case of panel FS8-2, appear to model the measured behavior well. Panel FS8-2 did lose stiffness prior to cracking, and this slight change favors the Beam Spring method and the ISBT method because their predictions fell below the measured results until this reduction in stiffness. Despite having been cracked prior to testing, FS10-1 appears to have experienced a large crack at approximately the same load as panels FS8-1, FS8-2, and FS10-2.

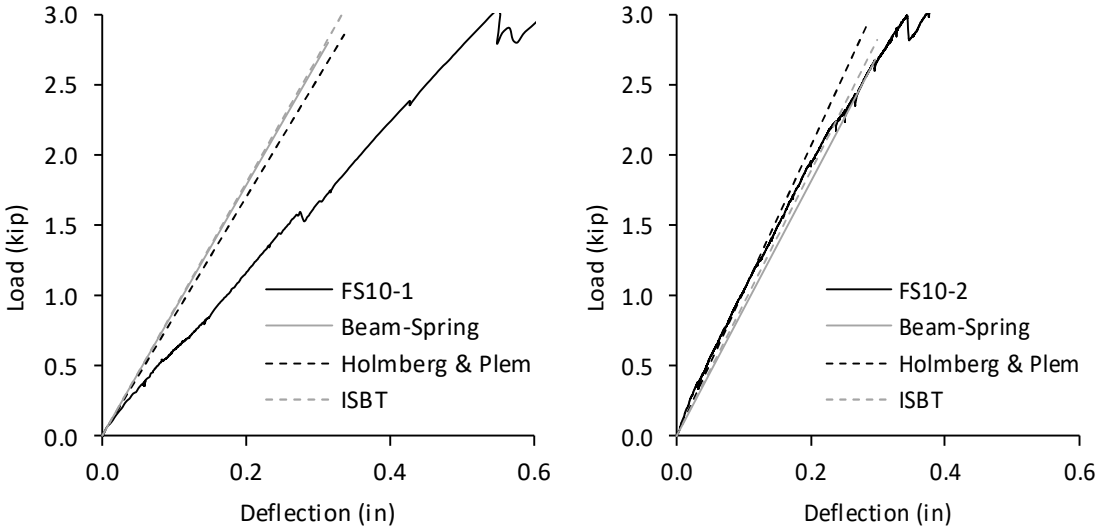

Figure 5-8 Full-Scale Elastic Prediction (FS10-1 left, FS10-2 right)

Table 5-5 shows the measured stiffness and compares this to the predictions for each panel from all three methods. The percent difference of the predicted method compared to the measured stiffness is also shown. The observed stiffness displayed was calculated based on the load and deflection of each panel measured at the first observed crack. The Beam Spring method and the ISBT methods agree almost identically for all panels except for panel FS10-2. All three methods adequately predict the elastic stiffness of the thick insulation panels with the percent difference from the observed elastic stiffness being less than 8% for all panels and methods with only one exception.

This exception is the prediction provided by Holmberg and Plem for panel FS10-2. This difference can likely be attributed to some of the assumptions described earlier, namely the assumption of using the same wythe thickness for both tension and compression wythes. Panel FS10-2 was poorly cast and the tension wythe was measured to be, on average, over ½ inch thicker than the compression wythe. This discrepancy between the actual panel dimensions and fitting the measured dimensions to Holmberg and Plem's assumptions likely contributes to the over-estimation of elastic stiffness.

Table 5-5 Predicted Full-Scale Panel Elastic Stiffness

Panel Designation	Observed Stiffness (kip/in)	Beam Spring Method		Holmberg and Plem		ISBT Method	
		Predicted Stiffness (kip/in)	Percent Difference	Predicted Stiffness (kip/in)	Percent Difference	Predicted Stiffness (kip/in)	Percent Difference
FS2-1	2.9	2.4	-16%	2.4	-17%	2.4	-15%
FS2-2	3.1	2.2	-30%	2.3	-27%	2.2	-29%
FS8-1	7.7	8.2	6%	8.2	6%	8.1	5%
FS8-2	8.5	7.9	-7%	8.3	-3%	8.0	-6%
FS10-2	8.7	9.0	4%	10.3	18%	9.4	8%

Disregarding the data from FS2-2, due to the concrete section described previously, the average percent difference for each method are -3%, 1%, and -2% for the Beam Spring method, Holmberg and Plem, and ISBT method, respectively. The differences between the predicted stiffnesses are negligible because a variety of factors could result in measured results that differ within these margins of differences such as unintended introduction of friction. Therefore, the recommended method would be the ISBT method or Beam Spring method.

5.4.2 Cracking Moment Prediction

All three elastic prediction methods can also be used to predict the cracking moment of partially composite panels. For the Beam-Spring method, this is done by using the FEA model to find the largest stress in the beam elements in tension and use the linear relationship between load and stress to determine the load necessary for this stress to reach the modulus of rupture of the concrete. For the ISBT method, it is required to assume at what location the highest stress will accumulate and use the linear relationship between load and stress and extrapolate the applied load in the same manner as with the Beam Spring method that will cause stress to equal the concrete modulus of rupture. In a similar manner, Holmberg and Plem's method can also be used to find the cracking load. This is done using the relationship between the force applied to the panel and the total shear force within the tension wythe. This force can be converted to a stress

using the cross-sectional area of the tension wythe and compared to the concrete modulus of rupture.

The predicted cracking moment for each panel was calculated using Holmberg and Plem, Beam Spring, and ISBT methods and are shown in Table 5-6. The percent difference of the predicted cracking moment from the measured cracking moment was also calculated and included in the table. All methods predicted the cracking moment for all panels within 21% of the measured cracking moment. The average percent difference between predicted and measured cracking load are -2%, 6%, and 2% for the Beam Spring, Holmberg and Plem, and ISBT methods, respectively.

Table 5-6 Predicted Cracking Moment

Panel Designation	Measured M_{cr} (kip-in)	Beam Spring Method		Holmberg and Plem		ISBT Method	
		Predicted M_{cr} (kip-in)	Percent Difference	Predicted M_{cr} (kip-in)	Percent Difference	Predicted M_{cr} (kip-in)	Percent Difference
FS2-1	44.1	48.7	10%	50.3	14%	51.7	17%
FS2-2	41.0	40.7	-1%	45.2	10%	41.0	0%
FS8-1	108.2	119.3	10%	127.6	18%	124.2	15%
FS8-2	133.0	105.6	-21%	125.7	-5%	111.1	-16%
FS10-2	131.5	117.7	-10%	129.9	-1%	123.8	-6%

5.4.3 Elastic Slip Predictions

As described in section 3.6, LVDTs were placed on each full-scale panel to measure the relative slip between wythes at the locations of the outermost connectors. This section investigates the accuracy of the Beam Spring method and ISBT methods in predicting slip within the elastic behavior region of thin wythe and thick insulation ICSWPs. The Beam Spring method utilizes an FEA model, and it is possible to obtain the theoretical slip of the panel at each connector location by identifying the lateral displacement of the link elements used in the model. The relationship between slip at connector locations and the force in each connector is key to the

ISBT method and, as such, can easily be obtained following necessary iterations and convergence reached. Holmberg and Plem's method assumes a total panel rigidity and does not consider slip within its method, and, therefore, is not used in the slip comparisons in this section.

The theoretical slip at these connector locations is plotted against the measured slips recorded by the LVDTs in Figure 5-9, Figure 5-10, and Figure 5-11. All slips are compared to the slips measured or predicted at a constant load that is demonstrably within the elastic region of the panel's behavior. Panels FS2-1 and FS2-2 compare slip values measured or predicted corresponding to an applied load of 0.8 kip, which is less than the applied load measured at cracking as seen in Figure 5-6 and within the elastic behavior region of both panels. Similarly, FS8-1, FS8-2, FS10-1, and FS10-2 all compare slip corresponding to an applied load of 2 kip. The connector locations were measured from east to west.

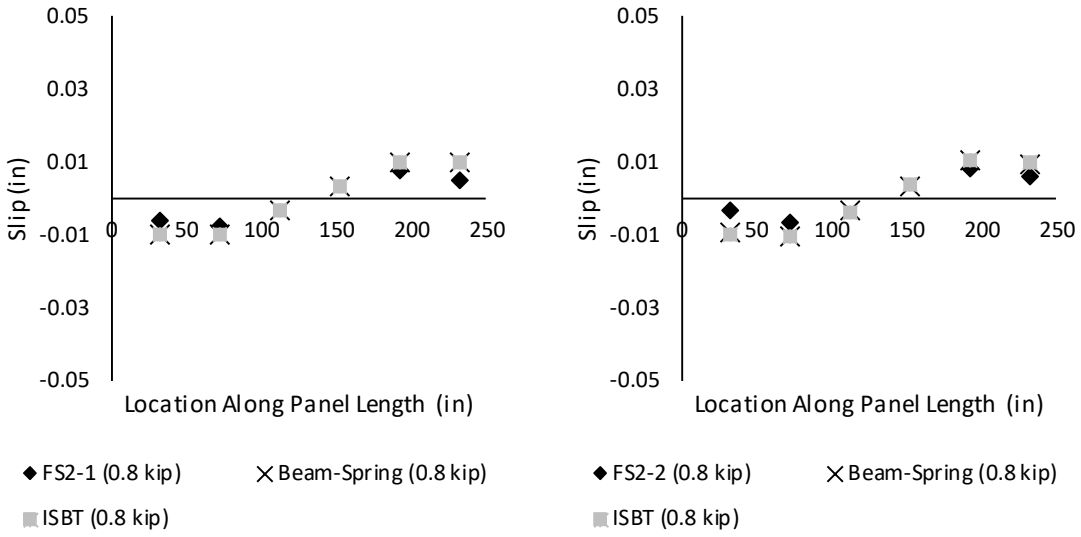

Figure 5-9 Elastic Slip Predictions (FS2-1 left, FS2-2 right)

As can be seen in Figure 5-9, the slip of panels FS2-1 and FS2-2 behaved non-linearly. The non-linear behavior was followed by the predictions of the ISBT and Beam Spring methods. The predictions of both methods overestimate the slip in all instances for panels FS2-1 and FS2-2

with a larger overestimation on the end connectors. The figure clearly shows that the wythes slipped less at the end connectors than they did at the connectors set inward of the end connectors. This is because the end connectors had two connectors at this location, and all other connector locations only had one connector.

Figure 5-10 shows the predicted and measured slips for panels FS8-1 and FS8-2. A similar trend can be seen for the 8-inch-thick insulation panels as for the 2-inch-thick insulation panels with the wythes slipping less at the end connectors than at the next inset connectors. There is one exception to this with the slip on the west end of FS8-2.

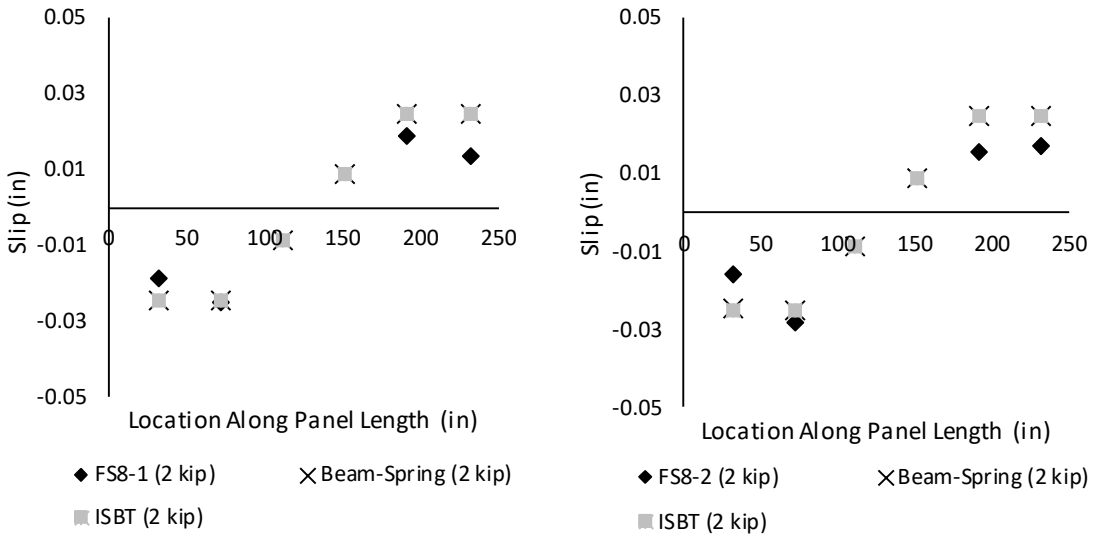

Figure 5-10 Elastic Slip Predictions (FS8-1 left, FS8-2 right)

Figure 5-11 shows the predicted and measured slips for panels FS10-1 and FS10-2. The same trend regarding the slip at the end connectors being less than that shown at the location of the connectors set just inward of the end connectors is manifested in these figures as well. This trend is magnified for panel FS10-1, showing the slip at the end connectors to be approximately half of the slip measured at the connectors set just inward of the end connectors.

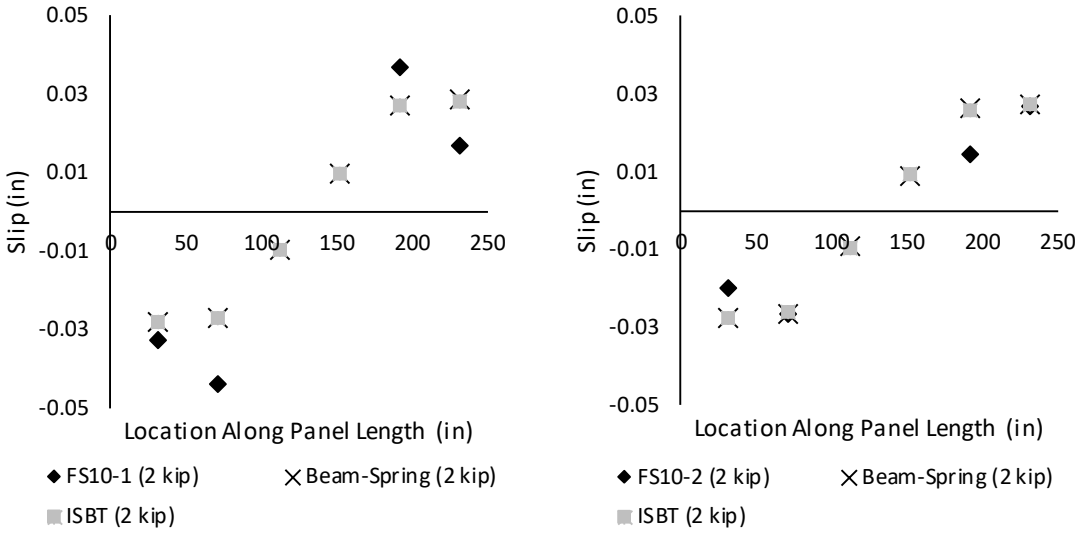

Figure 5-11Elastic Slip Predictions (FS10-1 left, FS10-2 right)

The methods all predict slips that are symmetrical about the center of the panel as the panel dimensions, connector placements and loading were symmetrical as well. The measured slips do not exhibit perfectly symmetrical behavior indicating minor errors in the dimensions, connector placements, and possibly loading placement of the tested specimens. This trend is seen throughout all the slips measured. Another trend common among all the panels is that the ISBT method and Beam Spring method predict the same slip for each connector.

The average difference between the predicted and measured slip was 0.002 inches, the average difference between the east and west measured slips was 0.004 inches. This indicates that the predicted slips are well within the margin of error due to imperfections in testing and that both the Beam Spring and ISBT methods are adequate prediction methods for slip within the elastic region.

5.5 Full Scale Ultimate Strength Prediction

The results of the tested panels were compared to predictions of ultimate behavior and capacity from two methods: shear flow, and a modified shear flow method.

5.5.1 Shear Flow

Shear flow is a common method used to predict the ultimate strength of a panel assuming the failure is dictated by connector failure. The method is based on principles of mechanics and compares the shear flow capacity and demand along the panel length.

The shear flow capacity and demand were calculated for each panel and the results are plotted in Figure 5-12, Figure 5-13, and Figure 5-14 for the two inch thick insulation, eight inch thick insulation, and 10 inch thick insulation panels, respectively. As can be seen in the figures, the method predicts that the connectors located 72 inches in from the panel ends will fail in the FS2-2 panel but that no connector failure will occur in any of the other panels. It is possible that the same connectors will fail in panel FS2-1, as the shear flow and shear demand are very close and small variations in measurements could easily account for the miniscule difference. As discussed in section 4.5, the insulation was removed from the eight- and ten-inch insulation panels but not from the two-inch-thick insulation panels, and, therefore, no visual confirmation was made regarding connector failure in these specimens.

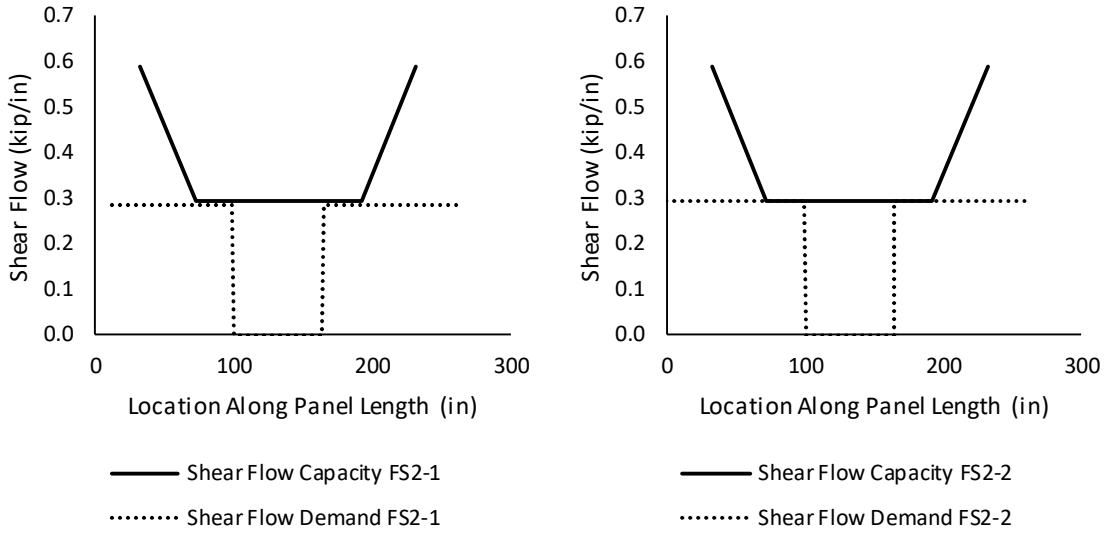

Figure 5-12 Standard Shear Flow (FS2-1 left, FS2-2 right)

The results shown in Figure 5-13, however, are demonstrably incorrect in predicting connector failure. The shear flow method predicted that, at maximum loading, the connectors would only be subjected to 260 lbf/in and that the connectors would have at minimum a shear flow capacity of 310 lbf/in leaving a gap of 50 lbf/in necessary to reach connector failure. This is demonstrably false as connector failures were visually confirmed in panel FS8-2. Connector failures were observed in the connector 72 inches from the panel's east end and also for the two connectors 32 inches from the panel's east end.

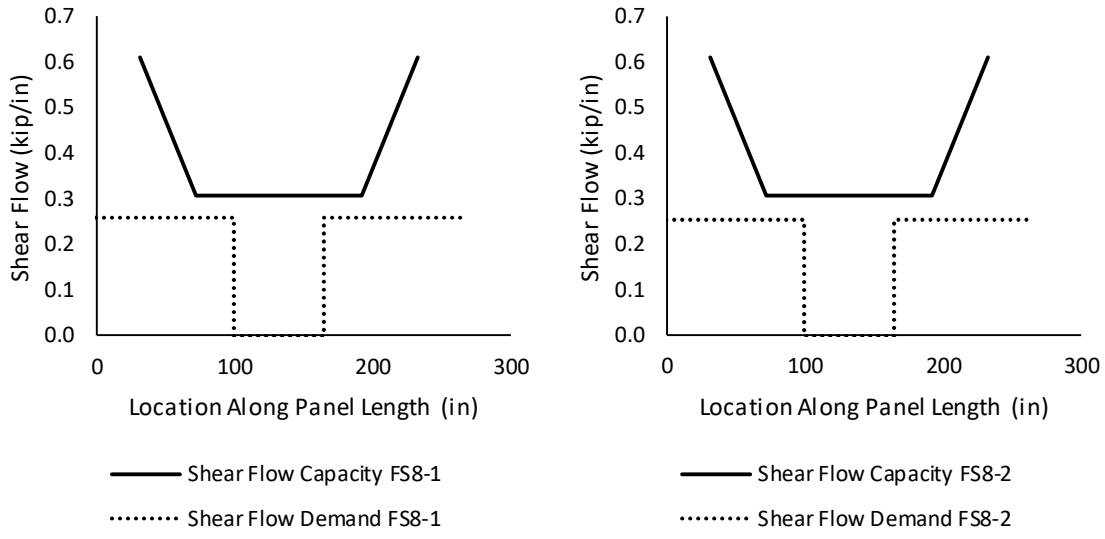

Figure 5-13 Standard Shear Flow (FS8-1 left, FS8-2 right)

Figure 5-14 shows similar results for panels FS10-1 and FS10-2 with even larger gaps between the shear flow capacity and shear flow demand at maximum loading. Both predictions can also be proven incorrect as connector failures were visually observed in both FS10-1 and FS10-2.

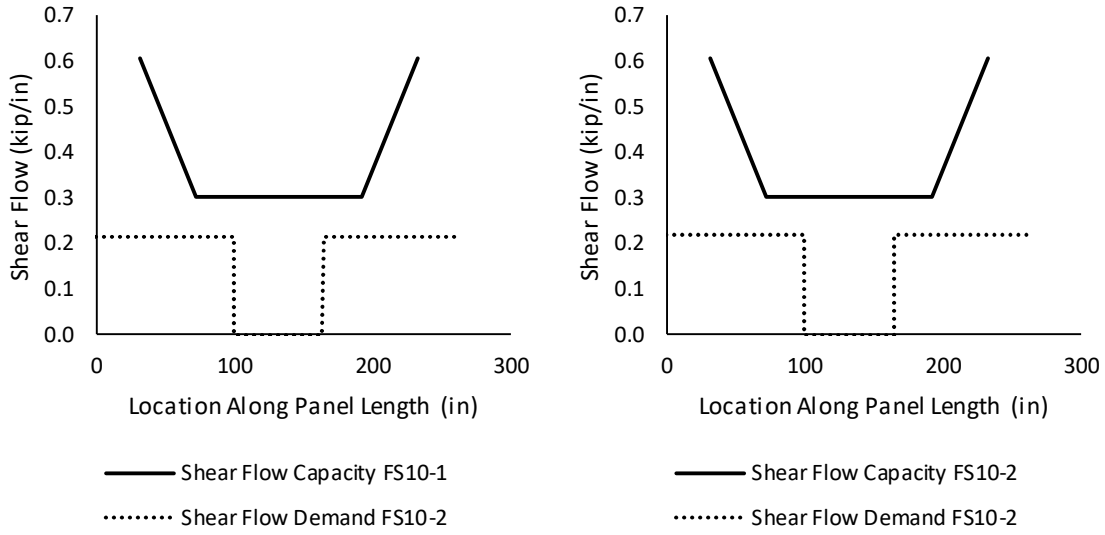

Figure 5-14 Standard Shear Flow (FS10-1 left, FS10-2 right)

The standard shear flow method did not adequately predict or describe the ultimate failure of the thick-insulation panels overpredicting the connector's capacity for both eight and ten-inch-thick insulation panels. Following this conclusion, a modified shear flow model was used which incorporated a few new assumptions and lead to results which were more compatible with the measured results. The standard shear flow method calculates the shear flow capacity of a single connector by dividing the connector ultimate shear strength by the connector spacing in the panel. Assuming a tributary width in place of the connector spacing and recognizing the directional nature of shear flow, we assume that the shear closest to the applied load and originally distributed to the center connector will be distributed in an outward manner, thereby, increasing the total shear flow attributed specifically to the second connector location. A similar tributary width is assumed for the end connectors also recognizing that no shear force should be present on the 12-inch overhang at the supports. Figure 5-15 below shows the shear diagram with respect to the panel and connector locations in addition to depicting the tributary width described.

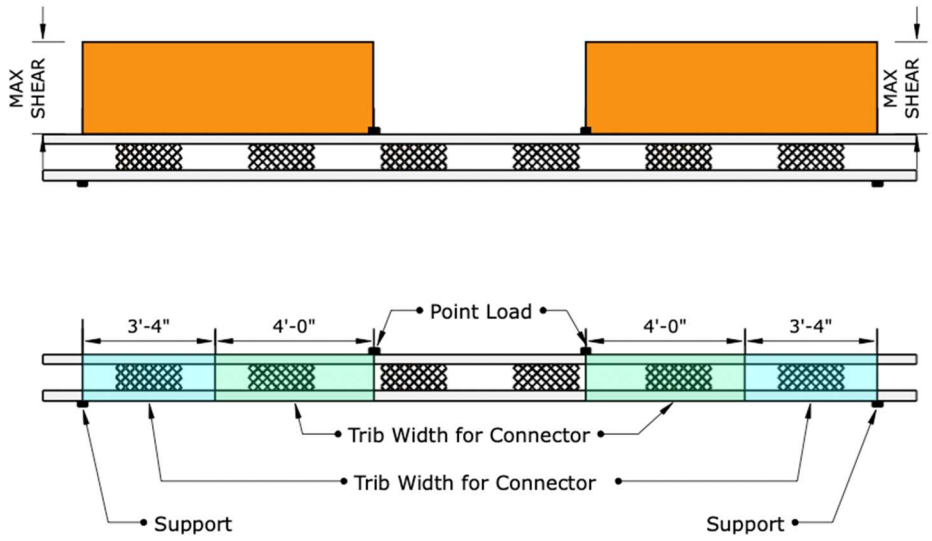

Figure 5-15 Modified Shear Flow Tributary Width

The modified shear flow compares the shear capacity of the connectors directly to the shear flow times the tributary width described above. The shear capacity and demand are calculated for each connector. The method is described in the following equations:

$$V_{demand} = \frac{V_{max} * Q_{FC} * w_{tribv}}{I_{FC}} \tag{5-6}$$

$$V_{nc} = F_{uc} * N \tag{5-7}$$

Where: V_{demand} = shear demand based on shear flow

V_{max} = maximum shear force due to applied load

Q_{FC} = first moment of area calculated with fully composite section properties

w_{tribv} = tributary width for shear flow

I_{FC} = fully composite moment of inertia

V_{nc} = shear capacity at connector location

F_{uc} = ultimate shear capacity of a single connector

N = number of shear connectors

The modified shear flow was calculated for all full-scale panels, and the results are shown in Figure 5-16, Figure 5-17, and Figure 5-18. This method underpredicts the shear capacity of the connectors for panels FS2-1, FS2-2, and FS8-1 and overpredicts the shear capacity of panels FS10-1 and FS10-2. This indicates that the method tends to underpredict the thinner insulation panels and overpredict the thicker insulation panels.

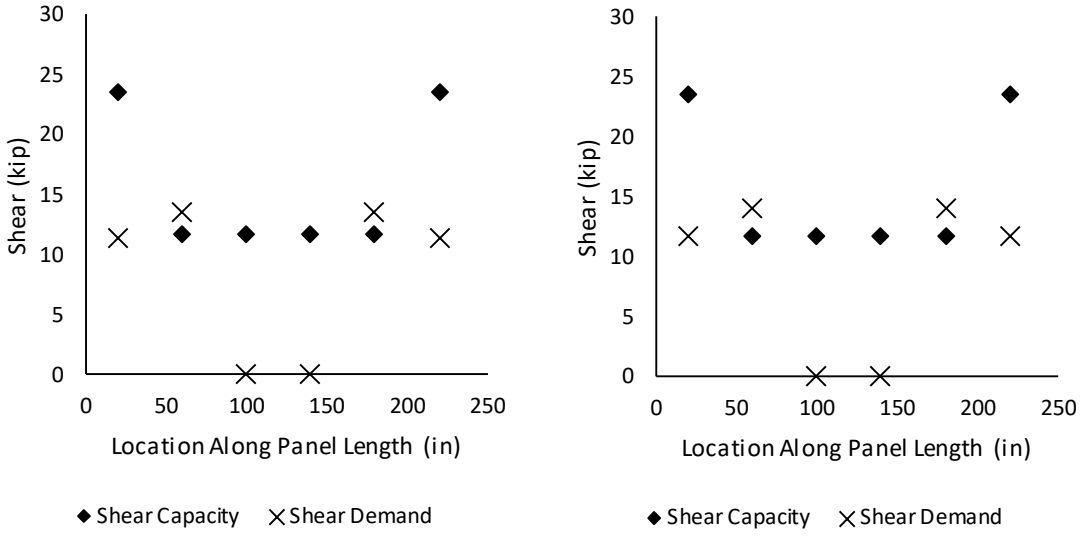

Figure 5-16 Modified Shear Flow (FS2-1 left, FS2-2 right)

Figure 5-17 shows the modified shear flow results for FS8-1 and FS8-2. The modified shear flow method's prediction was nearly exact for both panels. This method does predict connector failure at the second connector location on both sides of the panel.

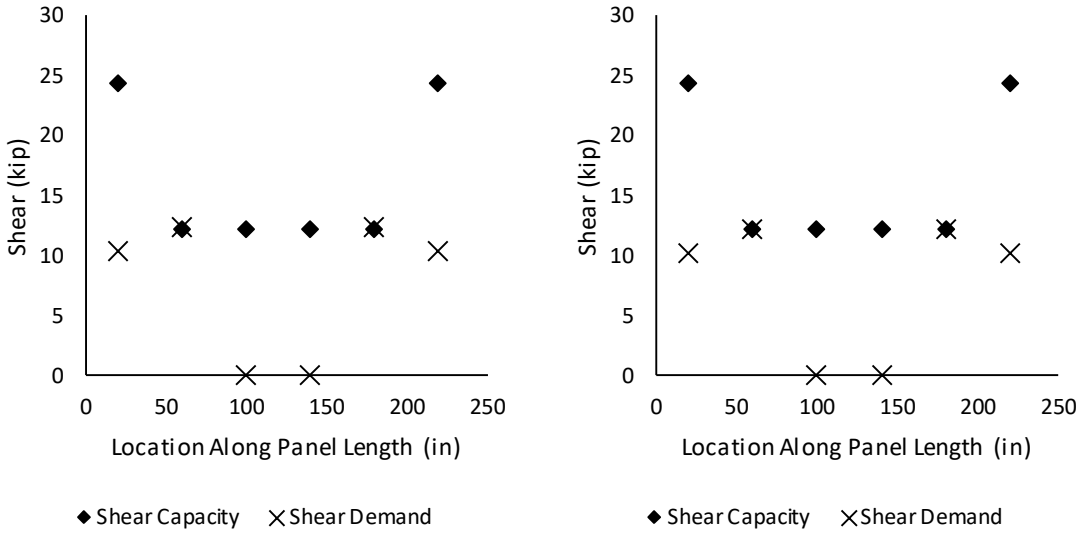

Figure 5-17 Modified Shear Flow (FS8-1 left, FS8-2 right)

Figure 5-18 shows the results of the modified shear flow method for FS10-1 and FS10-2. As described above, the method appears to overpredict the capacity of the connectors for the thicker insulation panels with the connectors breaking before the shear demand reached the expected shear capacity.

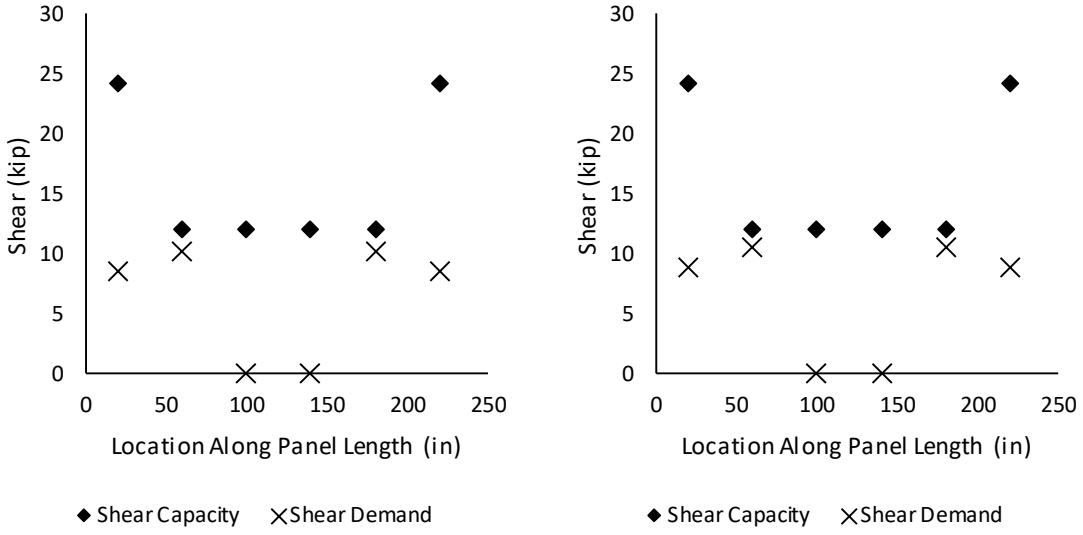

Figure 5-18 Modified Shear Flow (FS10-1 left, FS10-2 right)

Using the modified shear flow method, the load required to reach connector failure for each panel was calculated and the results of these calculations are included in Table 5-7. In addition, the measured-to-predicted ratio for each panel was included. The average measured-to-predicted ratio between the panels is 1.02.

Table 5-7 Modified Shear Flow Measured to Predicted Comparison

Panel Designation	P_u (kip)	$P_{predicted}$ (kip)	Measured/Predicted Ratio
FS2-1	2.46	2.12	1.16
FS2-2	2.54	2.13	1.19
FS8-1	5.78	5.67	1.02
FS8-2	5.72	5.72	1.00
FS10-1	5.64	6.66	0.85
FS10-2	6.05	6.90	0.88

5.6 Viability of Thick Insulation and Thin Wythe ICSWPs

For the purposes of this thesis, the viability of the use of thin wythe and thick insulation concrete sandwich wall panels was defined as the capability to adequately design and construct such wall panels for typical real-world use cases. This section discusses these three criteria to determine if thin wythe and thick insulation concrete sandwich wall panels are viable. The cost of materials, design, and construction do not fall within the provided definition of viability and are, therefore, not considered in this thesis.

Currently, there are no commercially available shear ties which are capable of bridging eight- and ten-inch-thick insulation and such shear ties would need to be specially manufactured. As shown by this research, such ties could be manufactured. The shear capacity of such connectors would need to be determined either by experimental testing or determined analytically. Commercially available shear ties are available that require embedment depths less than 2 inches and can be used for thin wythe sandwich wall panels. All other materials including

concrete, insulation, and reinforcement would be readily available for the construction of both thin wythe and thick insulation ICSWPs.

This research concluded that current methods of design are adequate in predicting elastic behavior of thin wythe and thick insulation ICSWPs. Current methods of design were found to be inadequate in predicting the ultimate behavior of thin wythe and thick insulation ICSWPs. Therefore, only panels subjected to forces within their elastic regions could be adequately designed.

All panels tested ultimately withstood loading equivalent to pressures ranging from 26-to-65 psf which is sufficient for common wind pressures found within the United States. Unfortunately, as confidence in the design of these panels is limited to the elastic region, the loads would need to be restricted to the elastic region. While the thin wythe panels tested within this research did not resist loads equivalent to common wind pressures within the elastic region, it would still be possible to design thin wythe panels to resist such loads. This could be accomplished by increasing the concrete strength and its rupture strength or by increasing the percent composite behavior through additional connectors.

Considering the ability to adequately construct and design thin wythe and thick insulation ICSWPs under common loading, it was concluded that thin wythe and thick insulation ICSWPs are viable given they are conservatively designed only within their elastic behavior.

CHAPTER 6. CONCLUSIONS

6.1 Verification of Existing Prediction Methods

Fifteen double shear specimens and six full-scale panels were tested. The testing was completed to validate current prediction methods for insulated concrete sandwich wall panels (ICSWPs) for specimens designated within this research as thin wythe (two-inches or less) and thick insulation (eight-inches or more). All specimens tested within this research incorporated only mild reinforcement. The use of prestressed strands could contribute to enhanced performance of the full-scale panels.

6.1.1 Elastic Stiffness of Shear Connectors

Two methods were used to predict the elastic behavior of the shear connectors and compared to the experimental double shear testing. The methods which were used were developed by Holmberg and Plem and Tomlinson. The following conclusions can be made from the comparison of these methods and the experimental results of the double shear specimens:

- Holmberg and Plem's method accurately predicted the elastic shear stiffnesses of all three connectors in the study with all predictions falling within one standard deviation of the average measured stiffness.
- Tomlinson's method predicted shear stiffnesses that approached the measured values but ultimately was found to be less accurate than the method of Holmberg and Plem
- The shear stiffness of the Fibergrate connector used in this research was able to be accurately predicted based on the assumed truss action, section properties, and given material modulus of elasticity.

6.1.2 Elastic Behavior of Full-Scale Panels

Three methods were used to model the elastic behavior of the full-scale panels and compared to the measured experimental full-scale panel testing behavior. The methods used for comparison included the ISBT method, the Beam-Spring model, both developed by Al-Rubaye, and the method developed by Holmberg and Plem. The following conclusions can be made from the comparison of these methods and the experimental results of the full-scale panels:

- All three methods used to predict the elastic behavior of the full-scale panels were accurate in their predictions with their average percent differences from the measured stiffnesses within 3% for all methods.
- All three methods used to predict the cracking moment of the full-scale panels were accurate in their predictions with their average percent differences from the measured cracking moments within 6% for all methods.
- The two methods (ISBT and Beam-Spring) used to predict the slip at the connectors were accurate in their predictions for all panels tested. The average differences between the predicted and measured slips (0.002 inches) were less than the average difference of the symmetrically corresponding measured slips on the East and West end of the panels (0.004 inches).
- The ISBT method, the Beam-Spring method, and the method of Holmberg and Plem adequately predict behavior of thin wythe and thick insulation ICSWPs within the elastic region.

6.1.3 Ultimate Behavior of Full-Scale Panels

Two methods were used to predict the ultimate strength and behavior of the full-scale panels and compared to the measured experimental full-scale panel testing behavior. The methods included two differing shear flow analyses. The following conclusions can be made from the comparison of these methods and the experimental results of the full-scale panels:

- The standard method of shear flow did not accurately predict the ultimate capacity of the thick insulation full-scale panels overpredicting the shear capacity of the connectors with an average measured to predicted ratio of 1.29.
- The modified shear flow method accurately predicted the connector failure of the full-scale panels with an average measured to predicted ratio of 1.02.

6.2 Future Research

1. Perform a comparative cost analysis on the use of thin wythe and thick insulation ICSWPs.
2. Investigate the severity of thermal bowing due to temperature differentials in thick insulation ICSWPs.
3. Verify the accuracy of braced double shear tests in determining ultimate shear strength of shear connectors.
4. Verify the modified shear flow method using existing testing data from available literature.
5. Investigate the shear contribution from insulation in thick insulation ICSWPs with the insulation produced in eight- and ten-inch thicknesses and bonded to both wythes.

REFERENCES

Al-Rubaye, S. (2017). *Experimental and simplified analytical investigation of full scale sandwich panel walls* [Master's thesis, Utah State University]. All Graduate Theses and Dissertations. 6825. https://digitalcommons.usu.edu/etd/6825

Al-Rubaye, S., Sorensen, T. J., & Maguire, M. (2017). Investigating composite action at ultimate for commercial sandwich panel composite connectors.

Al-Rubaye, S., Sorensen, T., Dorafshan, S., & Maguire, M. (2018). Matrix model accuracy of partially composite concrete sandwich panels. *PCI/NBC*.

Al-Rubaye, S., Sorensen, T., Olsen, J., & Maguire, M. (2018). Evaluating elastic behavior for partially composite precast concrete sandwich wall panels. *PCI Journal*.

Al-Rubaye, S., Sorensen, T., Thomas, R. J., & Maguire, M. (2019). Generalized beam–spring model for predicting elastic behavior of partially composite concrete sandwich wall panels. Engineering Structures, 198, 109533.

Allen, H. G. (1969). Analysis and design of structural sandwich panels.

Benayoune, A., Samad, A. A. A., Abang Ali, A. A., Trikha, D. N. (2007). Response of pre-cast reinforced composite sandwich panels to axial loading. *Construction and Building Materials*, *21*(3), 677-685. https://doi.org/10.1016/j.conbuildmat.2005.12.011

Bunn, W. G. (2011). CFRP grid/rigid foam shear transfer mechanism for precast, prestressed concrete sandwich wall panels [Master's thesis, North Carolina State University]. repository.lib.ncsu.edu

Choi, I., Kim, J., & Kim, H. (2015). Composite behavior of insulated concrete sandwich wall panels subjected to wind pressure and suction. *Materials*, *8*, 1264-1282. DOI: 10.3390/ma8031264

Choi, I., Kim, J., & You, Y. (2016). Effect of cyclic loading on composite behavior of insulated concrete sandwich panels with GFRP shear connectors. *Composites Part B: Engineering*, *96*, 7-19. https://doi.org/10.1016/j.compositesb.2016.04.030

Choi, K., Choi, W., Feo, L., Jan, S., & Yun, H. (2015). In-plane shear behavior of insulated precast concrete sandwich panels reinforced with corrugated GFRP shear connectors. *Composites Part B: Engineering*, *79*, 419-429. https://doi.org/10.1016/j.compositesb.2015.04.056

Choi, W., Jang, S., & Yun, H. (2019). Design properties of insulated precast concrete sandwich panels with composite shear connectors. *Composites Part B: Engineering*, *157*, 36-42. https://doi.org/10.1016/j.compositesb.2018.08.081

Cox, B., Syndergaard, P., Al-Rubaye, S., Pozo-Lora, F. F., Tawadrous, R., & Maguire, M. (2019). Lumped GFRP star connector system for partial composite action in insulated precast concrete sandwich panels. *Journal of Composite Structures*, *229*, 1-13. https://doi.org/10.1016/j.compstruct.2019.111465

Fernando, P. L. N., Jayasinghe, M. T. R., & Jayasinghe, C. (2017). Structural feasibility of expanded polystyrene (EPS) based lightweight concrete sandwich wall panels. *Construction and Building Materials*, *139*, 45-51. http://dx.doi.org/10.1016/j.conbuildmat.2017.02.027

Frankl, B. A., Lucier, G. W., Hassan, T. K., & Rizkall, S. H. (2011). Behavior of precast, prestressed concrete sandwich wall panels reinforced with CFRP shear grid. *PCI Journal*, *56*(2), 42-54.

Gombeda, M. J., Trasborg, P., Naito, C. J., & Quiel, S. E. (2017). Simplified model for partially-composite precast concrete insulated wall panels subjected to lateral loading. *Engineering Structures*, *138*, 367-380. https://doi.org/10.1016/j.engstruct.2017.01.065

Granholm, H. (1949). On composite beams and columns with particular regard to nailed timber structures. *Chalmer Technical University.*

He, A., Pan, P., Ren, J., & Wang, H. (2020). Experimental and numerical investigation of novel I-shaped GFRP connectors for insulated precast concrete sandwich wall panels. *Journal of Composites for Construction*, *24*(5), 1-14. DOI: 10.1061/(ASCE)CC.1943-5614.0001053

Hodicky, K., Sopal, G. Rizkall, S., Hulin, T., & Stang, H. (2015). Experimental and numerical investigation of the FRP shear mechanism for concrete sandwich panels. *Journal of Composites for Construction*, *19*(5), 1-12. DOI: 10.1061/(ASCE)CC.1943-5614.0000554

Holmberg, A., & Plem, E. (1965). *Behaviour of load-bearing sandwich-type structures*. Nat. Swed, Cncl. Bldg. Res.

Jensen, K., Al-Rubaye, S., Thomas, R. J., & Maguire, M. (2020, February). Mechanics-Based model for elastic Bending, Axial, thermal Deformations, and asymmetry of concrete composite sandwich wall panels. In Structures (Vol. 23, pp. 459-471). Elsevier.

Kim, J., & You, Y. (2015). Composite behavior of a novel insulated concrete sandwich wall panel reinforced with GFRP shear grids: Effects of insulation types. *Materials*, *8*, 899-913. DOI: 10.3390/ma8030899

Maguire, M., & Pozo-Lora, F. F. (2020). Partially composite concrete sandwich wall panels: What is “percent composite”? *Concrete International*, *42*(10), 47–52.

Mlynarczyk, A., & Pessiki, S. (2000). Experimental evaluation of the composite behavior of precast concrete sandwich wall panels. *ATLSS Reports*. ATLSS report number 00-07:. http://preserve.lehigh.edu/engr-civil-environmental-atlss-reports/7

Naito, C. Hoemann, J., Beacraft, M., & Bewick, B. (2012). Performance and characterization of shear ties for use in insulated precast concrete sandwich wall panels. *Journal of Structural Engineering*, *138*(1), 52-61. DOI: 10.1061/(ASCE)ST.1943-541S.0000430

Naito, C. J., Hoemann, J. M., Shull, J. S., Saucier, A., Salim, H. A., Bewick, B. T., & Hammons, M. I. (2011). Precast/prestressed concrete experiments performance on non-load bearing sandwich wall panels. AFRL-RX-TY-TR-2011-0021. Distribution A.

Newmark, N. M., Siess, C. P., & Viest, I. M. (1951). Tests and analysis of composite beams with in-complete interaction. *Proceedings of the Society for Experimental Stress Analysis*, *9*(1), 75-92.

Olsen, J., Al-Rubaye, S., Sorensen, T., & Maguire, M. (2017). Developing a general methodology for evaluating composite action in insulated wall panels.
(A report to the precast/prestressed concrete institute PCI)

Pantelides, C. P., Surapaneni, R., & Reaveley, L. D. (2008). Structural performance of hybrid GFRP/steel concrete sandwich panels. *Journal of Composites for Construction*, *12*(5), 570-576. DOI: 10.1061/(ASCE)1090-0268(2008)12:5(570)

Pessiki, S., & Mlynarczyk, A. (2003). Experimental evaluation of the composite behavior of precast concrete sandwich wall panels. *PCI Journal*, 54-71.

Pozo, F. (2018). *On thermal bowing of concrete sandwich wall panels with flexible shear connectors* [Master's thesis, Utah State University]. All Graduate Theses and Dissertations. 7133. https://digitalcommons.usu.edu/etd/7133

Pozo-Lora, F., & Maguire, M. (2019a). Flexural behavior of continuous non-loadbearing insulated wall panels. 2019 PCI/NBC, PCI, Chicago, IL, 15.

Pozo-Lora, F., & Maguire, M. (2019b). Thermal bowing testing of precast concrete sandwich wall panels. UTC Report 01-2019.

Pozo-Lora, F., & Maguire, M. (2020). Thermal bowing of concrete sandwich panels with flexible shear connectors. *Journal of Building Engineering*, *29*, 101124.

Salmon, D. C., & Einea, A. (1995). Partially composite sandwich panel deflections. *Journal of Structural Engineering*, *121*(4), 778-783.

Salmon, D. C., Einea, A., Tadros, M. K., & Culp, T. D. (1997). Full scale testing of precast concrete sandwich panels. *Structural Journal*, *94*(4), 354-362.

Sorensen, T., Dorafshan, S., & Maguire, M. (2017). Thermal Evaluation of Common Locations of Heat Loss in Sandwich Wall Panels. In *Congress on Technical Advancement* 2017 (pp. 173-184).

Tomlinson, D. G. (2015). *Behavior of partially composite precast concrete sandwich panels under flexural and axial loads* [Doctoral dissertation, Queen's University]. Queen's Graduate Theses and Dissertations Department of Civil Engineering Graduate Theses. http://hdl.handle.net/1974/13745

Tomlinson, D., & Fam, A. (2015). Flexural behavior of precast concrete sandwich wall panels with basalt FRP and steel reinforcement. *60*(6), 51-71. https://doi.org/10.15554/pcij.11012015.51.71

Tomlinson, D. G., Teixeira, N., & Fam, A. (2016). New shear connector design for insulated concrete sandwich panels using basalt fiber-reinforced polymer bars. *Journal of Composites for Construction*, *20*(4), 1-13. DOI: 10.1061/(ASCE)CC.1943-5614.0000662

Trasborg, P. A. (2014). Analytical and experimental evaluation of precast sandwich wall panels subjected to blast, breach, and ballistic demands [Doctoral dissertation, Lehigh University]. Theses and Dissertations. Paper 1656.

Woltman, G., Tomlinson, D., & Fam, A. (2013). Investigation of various GFRP shear connectors of insulated precast concrete sandwich wall panels. *Journal of Composites for Construction*, *17*(5), 711-721. DOI: 10.1061/(ASCE)CC.1943-5614.0000373

APPENDIX

Table 6-1 Double Shear and Push Through Testing in Literature

Reference	Designation	Wythe 1 (in)	Wythe 2 (in)	Central Wythe (in)	Insulation Thickness (in)	Height (in)	f'_c (psi)	Connector Type
(Naito et al., 2012)	A1	3	3	5	1.97	18	66800	GFRP Truss
(Naito et al., 2012)	A2	3	3	5	1.97	18	68720	GFRP Truss
(Naito et al., 2012)	A3	3	3	5	1.97	18	70390	GFRP Truss
(Naito et al., 2012)	B1	3	3	5	1.97	18	66800	GFRP Composite Pin
(Naito et al., 2012)	B2	3	3	5	1.97	18	68940	GFRP Composite Pin
(Naito et al., 2012).	B3	3	3	5	1.97	18	70390	GFRP Composite Pin
(Naito et al., 2012)	C1	3	3	5	1.97	18	66800	GFRP non-composite Pin
(Naito et al., 2012)	C2	3	3	5	1.97	18	68940	GFRP non-composite Pin
(Naito et al., 2012)	C3	3	3	5	1.97	18	70390	GFRP non-composite Pin
(Naito et al., 2012)	E1	3	3	5	1.97	18	67060	GFRP Pin
(Naito et al., 2012)	E2	3	3	5	1.97	18	68940	GFRP Pin
(Naito et al., 2012)	E3	3	3	5	1.97	18	70190	GFRP Pin
(Naito et al., 2012)	F1	3	3	5	1.97	18	67060	BFRP bar
(Naito et al., 2012)	F2	3	3	5	1.97	18	68940	BFRP bar
(Naito et al., 2012)	F3	3	3	5	1.97	18	70390	BFRP bar
(Naito et al., 2012)	G1	3	3	5	1.97	18	67060	Galvanized C Clip
(Naito et al., 2012)	G2	3	3	5	1.97	18	68940	Galvanized C Clip
(Naito et al., 2012)	G3	3	3	5	1.97	18	70390	Galvanized C Clip
(Naito et al., 2012)	H11	3	3	5	1.97	18	40560	Galvanized C Clip
(Naito et al., 2012)	H21	3	3	5	1.97	18	40560	Stainless C Clip
(Naito et al., 2012)	H22	3	3	5	1.97	18	40560	Stainless C Clip
(Naito et al., 2012)	H23	3	3	5	1.97	18	40560	Stainless C Clip
(Naito et al., 2012)	H24	3	3	5	1.97	18	51100	Stainless C Clip

Table 6-1 Continued

Reference	Designation	Wythe 1 (in)	Wythe 2 (in)	Central Wythe (in)	Insulation Thickness (in)	Height (in)	f'_c (psi)	Connector Type
(Naito et al., 2012)	I1	3	3	5	1.97	18	40560	M type
(Naito et al., 2012)	I2	3	3	5	1.97	18	40560	M type
(Naito et al., 2012)	I3	3	3	5	1.97	18	40560	M type
(Naito et al., 2012)	D11	3	3	5	1.97	18	103570	CFRP Truss
(Naito et al., 2012)	D12	3	3	5	1.97	18	103570	CFRP Truss
(Naito et al., 2012)	D21	3	3	5	1.97	18	103570	CFRP Truss
(Naito et al., 2012)	D22	3	3	5	1.97	18	103570	CFRP Truss
(Naito et al., 2012)	D23	3	3	5	1.97	18	103570	CFRP Truss
(Naito et al., 2012)	J1	3	3	5	1.97	18	51100	Truss Girder
(Naito et al., 2012)	J2	3	3	5	1.97	18	51100	Truss Girder
(Naito et al., 2012)	J3	3	3	5	1.97	18	51100	Truss Girder
(Naito et al., 2012)	K1	3	3	5	1.97	18	40560	Wire Truss
(Naito et al., 2012)	K2	3	3	5	1.97	18	40560	Wire Truss
(Naito et al., 2012)	K3	3	3	5	1.97	18	40560	Wire Truss
(Naito et al., 2012)	L1	3	3	5	1.97	18	40560	Ladder Truss
(Naito et al., 2012)	L2	3	3	5	1.97	18	40560	Ladder Truss
(Naito et al., 2012)	L3	3	3	5	1.97	18	40560	Ladder Truss
(Woltman et al., 2013)	P1	2.01	2.01	2.95	5.98	35.43	8992	Steel
(Woltman et al., 2013)	P2_1*	2.01	2.01	2.95	5.98	35.43	8992	Steel
(Woltman et al., 2013)	P2_2*	2.01	2.01	2.95	5.98	35.43	8992	Steel
(Woltman et al., 2013)	P2_3*	2.01	2.01	2.95	5.98	35.43	8992	Steel
(Woltman et al., 2013)	P3_1*	2.01	2.01	2.95	5.98	35.43	8992	GFRP
(Woltman et al., 2013)	P3_2*	2.01	2.01	2.95	5.98	35.43	8992	GFRP
(Woltman et al., 2013)	P3_3*	2.01	2.01	2.95	5.98	35.43	8992	GFRP
(Woltman et al., 2013)	P4_1*	2.01	2.01	2.95	5.98	35.43	8992	GFRP

Table 6-1 continued

Reference	Designation	Wythe 1 (in)	Wythe 2 (in)	Central Wythe (in)	Insulation Thickness (in)	Height (in)	f'_c (psi)	Connector Type
(Woltman et al., 2013).	P4_2*	2.01	2.01	2.95	5.98	35.43	8992	GFRP
(Woltman et al., 2013)	P4_3*	2.01	2.01	2.95	5.98	35.43	6092	GFRP
(Woltman et al., 2013)	P5_1*	2.01	2.01	2.95	5.98	35.43	8992	GFRP
(Woltman et al., 2013)	P5_2*	2.01	2.01	2.95	5.98	35.43	8992	GFRP
(Woltman et al., 2013)	P5_3*	2.01	2.01	2.95	5.98	35.43	8992	GFRP
(Woltman et al., 2013)	P6_1*	2.01	2.01	2.95	5.98	35.43	8992	GFRP
(Woltman et al., 2013)	P6_2*	2.01	2.01	2.95	5.98	35.43	8992	GFRP
(Woltman et al., 2013)	P6_3*	2.01	2.01	2.95	5.98	35.43	8992	GFRP
(Woltman et al., 2013)	P7_1*	2.01	2.01	2.95	5.98	35.43	8992	GFRP
(Woltman et al., 2013)	P7_2*	2.01	2.01	2.95	5.98	35.43	8992	GFRP
(Woltman et al., 2013)	P7_3*	2.01	2.01	2.95	5.98	35.43	8992	GFRP
(Woltman et al., 2013)	P8	2.01	2.01	2.95	5.98	35.43	6092	GFRP
(Woltman et al., 2013)	P9_1*	2.01	2.01	2.95	5.98	35.43	6092	GFRP
(Woltman et al., 2013)	P9_2*	2.01	2.01	2.95	5.98	35.43	8992	GFRP
(Woltman et al., 2013)	P9_3*	2.01	2.01	2.95	5.98	35.43	8992	GFRP
(Woltman et al., 2013)	P10_1*	2.01	2.01	2.95	5.98	35.43	8992	GFRP
(Woltman et al., 2013)	P10_2*	2.01	2.01	2.95	5.98	35.43	8992	GFRP
(Woltman et al., 2013)	P10_3*	2.01	2.01	2.95	5.98	35.43	8992	GFRP
(Woltman et al., 2013)	P11_1*	2.01	2.01	2.95	5.98	35.43	8992	GFRP
(Woltman et al., 2013)	P11_2*	2.01	2.01	2.95	5.98	35.43	8992	GFRP
(Woltman et al., 2013)	P11_3*	2.01	2.01	2.95	5.98	35.43	8992	GFRP
(Woltman et al., 2013)	P12_1*	2.01	2.01	2.95	5.98	35.43	6092	GFRP
(Woltman et al., 2013)	P12_2*	2.01	2.01	2.95	5.98	35.43	8992	GFRP
(Woltman et al., 2013)	P12_3*	2.01	2.01	2.95	5.98	35.43	8992	GFRP
(Woltman et al., 2013)	P13_1*	2.01	2.01	2.95	5.98	35.43	8992	GFRP

Table 6-1 continued

Reference	Designation	Wythe 1 (in)	Wythe 2 (in)	Central Wythe (in)	Insulation Thickness (in)	Height (in)	f'_c (psi)	Connector Type
(Woltman et al., 2013)	P13_2*	2.01	2.01	2.95	5.98	35.43	8992	GFRP
(Woltman et al., 2013)	P13_3*	2.01	2.01	2.95	5.98	35.43	8992	GFRP
(Woltman et al., 2013)	P14_1*	2.01	2.01	2.95	5.98	35.43	8992	GFRP
(Woltman et al., 2013)	P14_2*	2.01	2.01	2.95	5.98	35.43	8992	GFRP
(Woltman et al., 2013)	P14_3*	2.01	2.01	2.95	5.98	35.43	8992	GFRP
(Woltman et al., 2013)	P15_1*	2.01	2.01	2.95	5.98	35.43	8992	GFRP
(Woltman et al., 2013)	P15_2*	2.01	2.01	2.95	5.98	35.43	8992	GFRP
(Woltman et al., 2013)	P15_3*	2.01	2.01	2.95	5.98	35.43	8992	GFRP
(Woltman et al., 2013)	P16_1*	2.01	2.01	2.95	5.98	35.43	8992	GFRP
(Woltman et al., 2013)	P16_2*	2.01	2.01	2.95	5.98	35.43	8992	GFRP
(Woltman et al., 2013)	P16_3*	2.01	2.01	2.95	5.98	35.43	8992	GFRP
(Woltman et al., 2013)	P17	2.01	2.01	2.95	5.98	35.43	6092	GFRP
(Woltman et al., 2013)	P18	2.01	2.01	2.95	5.98	35.43	6092	GFRP
(Woltman et al., 2013)	P19	2.01	2.01	2.95	5.98	35.43	6092	GFRP
(Woltman et al., 2013)	P20	2.01	2.01	2.95	5.98	35.43	6092	Polymer
(Woltman et al., 2013)	P21	2.01	2.01	2.95	5.98	35.43	6092	Polymer
(Woltman et al., 2013)	P22	2.01	2.01	2.95	5.98	35.43	6092	Polymer
(Tomlinson et al., 2016)	B30C4	2.36	2.36	2.36	5.91	19.69	5685	BFRP
(Tomlinson et al., 2016)	B45C4_1*	2.36	2.36	2.36	5.91	19.69	5685	BFRP
(Tomlinson et al., 2016)	B45C4_2*	2.36	2.36	2.36	5.91	19.69	5685	BFRP
(Tomlinson et al., 2016)	B60C4	2.36	2.36	2.36	5.91	19.69	5685	BFRP
(Tomlinson et al., 2016)	B30T4	2.36	2.36	2.36	5.91	19.69	5685	BFRP
(Tomlinson et al., 2016)	B45T4_1*	2.36	2.36	2.36	5.91	19.69	5685	BFRP
(Tomlinson et al., 2016)	B45T4_2*	2.36	2.36	2.36	5.91	19.69	5685	BFRP
(Tomlinson et al., 2016)	B60T4	2.36	2.36	2.36	5.91	19.69	5685	BFRP

Table 6-1 continued

Reference	Designation	Wythe 1 (in)	Wythe 2 (in)	Central Wythe (in)	Insulation Thickness (in)	Height (in)	f'_c (psi)	Connector Type
(Tomlinson et al., 2016)	B30C6	2.36	2.36	2.36	5.91	19.69	5685	BFRP
(Tomlinson et al., 2016)	B45C6	2.36	2.36	2.36	5.91	19.69	5685	BFRP
(Tomlinson et al., 2016)	B45C6a_1*	2.36	2.36	2.36	5.91	19.69	5685	BFRP
(Tomlinson et al., 2016)	B45C6a_2*	2.36	2.36	2.36	5.91	19.69	5685	BFRP
(Tomlinson et al., 2016)	B60C6	2.36	2.36	2.36	5.91	19.69	5685	BFRP
(Tomlinson et al., 2016)	B30T6	2.36	2.36	2.36	5.91	19.69	5685	BFRP
(Tomlinson et al., 2016)	B45T6	2.36	2.36	2.36	5.91	19.69	5685	BFRP
(Tomlinson et al., 2016)	B45T6a_1*	2.36	2.36	2.36	5.91	19.69	5685	BFRP
(Tomlinson et al., 2016)	B45T6a_2*	2.36	2.36	2.36	5.91	19.69	5685	BFRP
(Tomlinson et al., 2016)	B60T6	2.36	2.36	2.36	5.91	19.69	5685	BFRP
(Tomlinson et al., 2016)	B30C8	2.36	2.36	2.36	5.91	19.69	5685	BFRP
(Tomlinson et al., 2016)	B45C8_1*	2.36	2.36	2.36	5.91	19.69	5685	BFRP
(Tomlinson et al., 2016)	B45C8_2*	2.36	2.36	2.36	5.91	19.69	5685	BFRP
(Tomlinson et al., 2016)	B60C8	2.36	2.36	2.36	5.91	19.69	5685	BFRP
(Tomlinson et al., 2016)	B30T8	2.36	2.36	2.36	5.91	19.69	5685	BFRP
(Tomlinson et al., 2016)	B45T8_1*	2.36	2.36	2.36	5.91	19.69	5685	BFRP
(Tomlinson et al., 2016)	B45T8_2*	2.36	2.36	2.36	5.91	19.69	5685	BFRP
(Tomlinson et al., 2016)	B60T8	2.36	2.36	2.36	5.91	19.69	5685	BFRP
(Tomlinson et al., 2016)	S30C	2.36	2.36	2.36	5.91	19.69	5685	Steel
(Tomlinson et al., 2016)	S45C_1*	2.36	2.36	2.36	5.91	19.69	5685	Steel
(Tomlinson et al., 2016)	S45C_2*	2.36	2.36	2.36	5.91	19.69	5685	Steel
(Tomlinson et al., 2016)	S45Ca_1*	2.36	2.36	2.36	5.91	19.69	5685	Steel
(Tomlinson et al., 2016)	S45Ca_2*	2.36	2.36	2.36	5.91	19.69	5685	Steel
(Tomlinson et al., 2016)	S60C	2.36	2.36	2.36	5.91	19.69	5685	Steel
(Tomlinson et al., 2016)	S30T	2.36	2.36	2.36	5.91	19.69	5685	Steel

Table 6-1 continued

Reference	Designation	Wythe 1 (in)	Wythe 2 (in)	Central Wythe (in)	Insulation Thickness (in)	Height (in)	f'_c (psi)	Connector Type
(Tomlinson et al., 2016)	S45T_1*	2.36	2.36	2.36	5.91	19.69	5685	Steel
(Tomlinson et al., 2016)	S45T_2*	2.36	2.36	2.36	5.91	19.69	5685	Steel
(Tomlinson et al., 2016)	S45Ta_1*	2.36	2.36	2.36	5.91	19.69	5685	Steel
(Tomlinson et al., 2016)	S45Ta_2*	2.36	2.36	2.36	5.91	19.69	5685	Steel
(Tomlinson et al., 2016)	S60T	2.36	2.36	2.36	5.91	19.69	5685	Steel
(Choi et al., 2019)	XPS-A50_1*	2.36	2.36	5.12	1.97	47.24	4351	GFRP Grid
(Choi et al., 2019)	XPS-A50_2*	2.36	2.36	5.12	1.97	47.24	4351	GFRP Grid
(Choi et al., 2019)	XPS-A100_1*	2.36	2.36	5.12	3.94	47.24	4351	GFRP Grid
(Choi et al., 2019)	XPS-A100_2*	2.36	2.36	5.12	3.94	47.24	4351	GFRP Grid
(Choi et al., 2019)	XPS-A100_3*	2.36	2.36	5.12	3.94	47.24	4351	GFRP Grid
(Choi et al., 2019)	XPS-A150_1*	2.36	2.36	5.12	5.91	47.24	4351	GFRP Grid
(Choi et al., 2019)	XPS-A150_2*	2.36	2.36	5.12	5.91	47.24	4351	GFRP Grid
(Choi et al., 2019)	XPS-A150_3*	2.36	2.36	5.12	5.91	47.24	4351	GFRP Grid
(Choi et al., 2019)	XPS-B100_1*	2.36	2.36	5.12	3.94	47.24	4351	GFRP Grid
(Choi et al., 2019)	XPS-B100_2*	2.36	2.36	5.12	3.94	47.24	4351	GFRP Grid
(Choi et al., 2019)	XPS-B100_3*	2.36	2.36	5.12	3.94	47.24	4351	GFRP Grid
(Choi et al., 2019)	EPS-A50_1*	2.36	2.36	5.12	1.97	47.24	4351	GFRP Grid
(Choi et al., 2019)	EPS-A50_2*	2.36	2.36	5.12	1.97	47.24	4351	GFRP Grid
(Choi et al., 2019)	EPS-A100_1*	2.36	2.36	5.12	3.94	47.24	4351	GFRP Grid
(Choi et al., 2019)	EPS-A100_2*	2.36	2.36	5.12	3.94	47.24	4351	GFRP Grid
(Choi et al., 2019)	EPS-A100_3*	2.36	2.36	5.12	3.94	47.24	4351	GFRP Grid
(Choi et al., 2019)	EPS-A150_1*	2.36	2.36	5.12	5.91	47.24	4351	GFRP Grid
(Choi et al., 2019)	EPS-A150_2*	2.36	2.36	5.12	5.91	47.24	4351	GFRP Grid
(Choi et al., 2019)	EPS-A150_3*	2.36	2.36	5.12	5.91	47.24	4351	GFRP Grid
(Choi et al., 2019)	EPS-B100_1*	2.36	2.36	5.12	3.94	47.24	4351	GFRP Grid

Table 6-1 continued

Reference	Designation	Wythe 1 (in)	Wythe 2 (in)	Central Wythe (in)	Insulation Thickness (in)	Height (in)	f'_c (psi)	Connector Type
(Choi et al., 2019)	EPS-B100_2*	2.36	2.36	5.12	3.94	47.24	4351	GFRP Grid
(Choi et al., 2019)	EPS-B100_3*	2.36	2.36	5.12	3.94	47.24	4351	GFRP Grid
(Cox et al., 2019)	HS50P1	2.76	2.76	5.51	1.97	42.13	5453	GFRP Star
(Cox et al., 2019)	HS50P2	2.76	2.76	5.51	1.97	42.13	5453	GFRP Star
(Cox et al., 2019)	HS50P3	2.76	2.76	5.51	1.97	42.13	5453	GFRP Star
(Cox et al., 2019)	HS50P4	2.76	2.76	5.51	1.97	42.13	5453	GFRP Star
(Cox et al., 2019)	HS50P5	2.76	2.76	5.51	1.97	42.13	5453	GFRP Star
(Cox et al., 2019)	HS50P6	2.76	2.76	5.51	1.97	42.13	5453	GFRP Star
(Cox et al., 2019)	HS100P1	2.76	2.76	5.51	3.94	42.13	5453	GFRP Star
(Cox et al., 2019)	HS100P2	2.76	2.76	5.51	3.94	42.13	5453	GFRP Star
(Cox et al., 2019)	HS100P3	2.76	2.76	5.51	3.94	42.13	5453	GFRP Star
(Cox et al., 2019)	HS100P4	2.76	2.76	5.51	3.94	42.13	5453	GFRP Star
(Cox et al., 2019)	HS100P5	2.76	2.76	5.51	3.94	42.13	5453	GFRP Star
(Cox et al., 2019)	LS50P1	2.76	2.76	5.51	1.97	42.13	2489	GFRP Star
(Cox et al., 2019)	LS50P2	2.76	2.76	5.51	1.97	42.13	2489	GFRP Star
(Cox et al., 2019)	LS50P3	2.76	2.76	5.51	1.97	42.13	2489	GFRP Star
(Cox et al., 2019)	LS50P4	2.76	2.76	5.51	1.97	42.13	2489	GFRP Star
(Cox et al., 2019)	LS50P5	2.76	2.76	5.51	1.97	42.13	2489	GFRP Star
(Cox et al., 2019)	LS100P1	2.76	2.76	5.51	3.94	42.13	2489	GFRP Star
(Cox et al., 2019)	LS100P2	2.76	2.76	5.51	3.94	42.13	2489	GFRP Star
(Cox et al., 2019)	LS100P3	2.76	2.76	5.51	3.94	42.13	2489	GFRP Star
(Cox et al., 2019)	LS100P4	2.76	2.76	5.51	3.94	42.13	2489	GFRP Star
(Cox et al., 2019)	LS100P5	2.76	2.76	5.51	3.94	42.13	2489	GFRP Star
(Cox et al., 2019)	LS100P6	2.76	2.76	5.51	3.94	42.13	2489	GFRP Star
(Cox et al., 2019)	HS50P1D	2.76	2.76	5.51	1.97	42.13	5453	GFRP Star

Table 6-1 continued

Reference	Designation	Wythe 1 (in)	Wythe 2 (in)	Central Wythe (in)	Insulation Thickness (in)	Height (in)	f'_c (psi)	Connector Type
(Cox et al., 2019)	HS50P2D	2.76	2.76	5.51	1.97	42.13	5453	GFRP Star
(Cox et al., 2019)	HS50P3D	2.76	2.76	5.51	1.97	42.13	5453	GFRP Star
(Cox et al., 2019)	HS50P4D	2.76	2.76	5.51	1.97	42.13	5453	GFRP Star
(Cox et al., 2019)	HS50P5D	2.76	2.76	5.51	1.97	42.13	5453	GFRP Star
(Cox et al., 2019)	HS50P6D	2.76	2.76	5.51	1.97	42.13	5453	GFRP Star
(Cox et al., 2019)	HS100P1D	2.76	2.76	5.51	3.94	42.13	5453	GFRP Star
(Cox et al., 2019)	HS100P2D	2.76	2.76	5.51	3.94	42.13	5453	GFRP Star
(Cox et al., 2019)	HS100P3D	2.76	2.76	5.51	3.94	42.13	5453	GFRP Star
(Cox et al., 2019)	HS100P4D	2.76	2.76	5.51	3.94	42.13	5453	GFRP Star
(Cox et al., 2019)	HS100P5D	2.76	2.76	5.51	3.94	42.13	5453	GFRP Star
(Cox et al., 2019)	HS100P6D	2.76	2.76	5.51	3.94	42.13	5453	GFRP Star
(Cox et al., 2019)	LS50T1	-	-	-	1.97	-	-	GFRP Star
(Cox et al., 2019)	LS50T2	-	-	-	1.97	-	-	GFRP Star
(Cox et al., 2019)	LS50T3	-	-	-	1.97	-	-	GFRP Star
(Cox et al., 2019)	LS50T4	-	-	-	1.97	-	-	GFRP Star
(Cox et al., 2019)	LS50T5	-	-	-	1.97	-	-	GFRP Star
(Cox et al., 2019)	LS50T6	-	-	-	1.97	-	-	GFRP Star
(Cox et al., 2019)	LS100T1	-	-	-	3.94	-	-	GFRP Star
(Cox et al., 2019)	LS100T2	-	-	-	3.94	-	-	GFRP Star
(Cox et al., 2019)	LS100T3	-	-	-	3.94	-	-	GFRP Star
(Cox et al., 2019)	LS100T4	-	-	-	3.94	-	-	GFRP Star
(Cox et al., 2019)	LS100T5	-	-	-	3.94	-	-	GFRP Star
(Cox et al., 2019)	LS100T6	-	-	-	3.94	-	-	GFRP Star
(Cox et al., 2019)	HS50T1	-	-	-	1.97	-	-	GFRP Star
(Cox et al., 2019)	HS50T2	-	-	-	1.97	-	-	GFRP Star

Table 6-1 continued

Reference	Designation	Wythe 1 (in)	Wythe 2 (in)	Central Wythe (in)	Insulation Thickness (in)	Height (in)	f'_c (psi)	Connector Type
(Cox et al., 2019)	HS50T3	-	-	-	1.97	-	-	GFRP Star
(Cox et al., 2019)	HS50T4	-	-	-	1.97	-	-	GFRP Star
(Cox et al., 2019)	HS50T5	-	-	-	1.97	-	-	GFRP Star
(Cox et al., 2019)	HS50T6	-	-	-	1.97	-	-	GFRP Star
(Cox et al., 2019)	HS100T1	-	-	-	3.94	-	-	GFRP Star
(Cox et al., 2019)	HS100T2	-	-	-	3.94	-	-	GFRP Star
(Cox et al., 2019)	HS100T3	-	-	-	3.94	-	-	GFRP Star
(Cox et al., 2019)	HS100T4	-	-	-	3.94	-	-	GFRP Star
(Cox et al., 2019)	HS100T5	-	-	-	3.94	-	-	GFRP Star
(Choi et al. (b), 2015)	XPS-V_1*	2.36	2.36	5.12	3.94	47.24	4351	Corrugated GFRP
(Choi et al. (b), 2015)	XPS-V_2*	2.36	2.36	5.12	3.94	47.24	4351	Corrugated GFRP
(Choi et al. (b), 2015)	XPS-V_3*	2.36	2.36	5.12	3.94	47.24	4351	Corrugated GFRP
(Choi et al. (b), 2015)	XPS-A30_1*	2.36	2.36	5.12	3.94	47.24	4351	Corrugated GFRP
(Choi et al. (b), 2015)	XPS-A30_2*	2.36	2.36	5.12	3.94	47.24	4351	Corrugated GFRP
(Choi et al. (b), 2015)	XPS-A30_3*	2.36	2.36	5.12	3.94	47.24	4351	Corrugated GFRP
(Choi et al. (b), 2015)	XPS-A40_1*	3.15	3.15	5.12	3.94	47.24	4351	Corrugated GFRP
(Choi et al. (b), 2015)	XPS-A40_2*	3.15	3.15	5.12	3.94	47.24	4351	Corrugated GFRP
(Choi et al. (b), 2015)	XPS-B30_1*	2.36	2.36	5.12	3.94	47.24	4351	Corrugated GFRP
(Choi et al. (b), 2015)	XPS-B30_2*	2.36	2.36	5.12	3.94	47.24	4351	Corrugated GFRP
(Choi et al. (b), 2015)	XPS-B40_1*	3.15	3.15	5.12	3.94	47.24	4351	Corrugated GFRP
(Choi et al. (b), 2015)	XPS-B40_2*	3.15	3.15	5.12	3.94	47.24	4351	Corrugated GFRP
(Choi et al. (b), 2015)	XPS-B40_3*	3.15	3.15	5.12	3.94	47.24	4351	Corrugated GFRP
(Choi et al. (b), 2015)	XPS-C50_1*	3.15	3.15	5.12	3.94	47.24	4351	Corrugated GFRP
(Choi et al. (b), 2015)	XPS-C50_2*	3.15	3.15	5.12	3.94	47.24	4351	Corrugated GFRP
(Choi et al. (b), 2015)	XPS-C50_3*	3.15	3.15	5.12	3.94	47.24	4351	Corrugated GFRP

Table 6-1 continued

Reference	Designation	Wythe 1 (in)	Wythe 2 (in)	Central Wythe (in)	Insulation Thickness (in)	Height (in)	f'_c (psi)	Connector Type
(Choi et al. (b), 2015)	EPS-V_1*	2.36	2.36	5.12	3.94	47.24	4351	Corrugated GFRP
(Choi et al. (b), 2015)	EPS-V_2*	2.36	2.36	5.12	3.94	47.24	4351	Corrugated GFRP
(Choi et al. (b), 2015)	EPS-V_3*	2.36	2.36	5.12	3.94	47.24	4351	Corrugated GFRP
(Choi et al. (b), 2015)	EPS-A30_1*	2.36	2.36	5.12	3.94	47.24	4351	Corrugated GFRP
(Choi et al. (b), 2015)	EPS-A30_2*	2.36	2.36	5.12	3.94	47.24	4351	Corrugated GFRP
(Choi et al. (b), 2015)	EPS-A30_3*	2.36	2.36	5.12	3.94	47.24	4351	Corrugated GFRP
(Choi et al. (b), 2015)	EPS-A40_1*	3.15	3.15	5.12	3.94	47.24	4351	Corrugated GFRP
(Choi et al. (b), 2015)	EPS-A40_2*	3.15	3.15	5.12	3.94	47.24	4351	Corrugated GFRP
(Choi et al. (b), 2015)	EPS-B30_1*	2.36	2.36	5.12	3.94	47.24	4351	Corrugated GFRP
(Choi et al. (b), 2015)	EPS-B30_2*	2.36	2.36	5.12	3.94	47.24	4351	Corrugated GFRP
(Choi et al. (b), 2015)	EPS-B40_1*	3.15	3.15	5.12	3.94	47.24	4351	Corrugated GFRP
(Choi et al. (b), 2015)	EPS-B40_2*	3.15	3.15	5.12	3.94	47.24	4351	Corrugated GFRP
(Choi et al. (b), 2015)	EPS-B40_3*	3.15	3.15	5.12	3.94	47.24	4351	Corrugated GFRP
(Choi et al. (b), 2015)	EPS-C50_1*	3.15	3.15	5.12	3.94	47.24	4351	Corrugated GFRP
(Choi et al. (b), 2015)	EPS-C50_2*	3.15	3.15	5.12	3.94	47.24	4351	Corrugated GFRP
(Choi et al. (b), 2015)	EPS-C50_3*	3.15	3.15	5.12	3.94	47.24	4351	Corrugated GFRP
(Hodicky et al., 2015)	24.EPS.NONE.2	1.97	1.97	3.94	1.97	72.05	6005	None
(Hodicky et al., 2015)	48.EPS.NONE.2	1.97	1.97	3.94	1.97	72.05	6005	None
(Hodicky et al., 2015)	24.EPS.NONE.4	1.97	1.97	3.94	3.94	72.05	6005	None
(Hodicky et al., 2015)	48.EPS.NONE.4	1.97	1.97	3.94	3.94	72.05	6005	None
(Hodicky et al., 2015)	24.EPS.NONE.6	1.97	1.97	3.94	5.91	72.05	6005	None
(Hodicky et al., 2015)	48.EPS.NONE.6	1.97	1.97	3.94	5.91	72.05	6005	None
(Hodicky et al., 2015)	24.EPS.12.2_1*	1.97	1.97	3.94	1.97	72.05	6005	CFRP Grid
(Hodicky et al., 2015)	24.EPS.12.2_2*	1.97	1.97	3.94	1.97	72.05	6005	CFRP Grid
(Hodicky et al., 2015)	48.EPS.24.2_1*	1.97	1.97	3.94	1.97	72.05	6005	CFRP Grid

Table 6-1 continued

Reference	Designation	Wythe 1 (in)	Wythe 2 (in)	Central Wythe (in)	Insulation Thickness (in)	Height (in)	f'_c (psi)	Connector Type
(Hodicky et al., 2015)	48.EPS.24.2_2*	1.97	1.97	3.94	1.97	72.05	6005	CFRP Grid
(Hodicky et al., 2015)	96.EPS.48.2_1*	1.97	1.97	3.94	1.97	72.05	6005	CFRP Grid
(Hodicky et al., 2015)	96.EPS.48.2_2*	1.97	1.97	3.94	1.97	72.05	6005	CFRP Grid
(Hodicky et al., 2015)	96.EPS.48.2_3*	1.97	1.97	3.94	1.97	72.05	6005	CFRP Grid
(Hodicky et al., 2015)	96.EPS.48.2_4*	1.97	1.97	3.94	1.97	72.05	6005	CFRP Grid
(Hodicky et al., 2015)	96.EPS.48.2_5*	1.97	1.97	3.94	1.97	72.05	6005	CFRP Grid
(Hodicky et al., 2015)	24.EPS.12.4_1*	1.97	1.97	3.94	3.94	72.05	6005	CFRP Grid
(Hodicky et al., 2015)	24.EPS.12.4_2*	1.97	1.97	3.94	3.94	72.05	6005	CFRP Grid
(Hodicky et al., 2015)	48.EPS.24.4_1*	1.97	1.97	3.94	3.94	72.05	6005	CFRP Grid
(Hodicky et al., 2015)	48.EPS.24.4_2*	1.97	1.97	3.94	3.94	72.05	6005	CFRP Grid
(Hodicky et al., 2015)	48.EPS.24.4_3*	1.97	1.97	3.94	3.94	72.05	6005	CFRP Grid
(Hodicky et al., 2015)	48.EPS.24.4_4*	1.97	1.97	3.94	3.94	72.05	6005	CFRP Grid
(Hodicky et al., 2015)	48.EPS.24.4_5*	1.97	1.97	3.94	3.94	72.05	6005	CFRP Grid
(Hodicky et al., 2015)	96.EPS.48.4_1*	1.97	1.97	3.94	3.94	72.05	6005	CFRP Grid
(Hodicky et al., 2015)	96.EPS.48.4_2*	1.97	1.97	3.94	3.94	72.05	6005	CFRP Grid
(Hodicky et al., 2015)	96.EPS.48.4_3*	1.97	1.97	3.94	3.94	72.05	6005	CFRP Grid
(Hodicky et al., 2015)	96.EPS.48.4_4*	1.97	1.97	3.94	3.94	72.05	6005	CFRP Grid
(Hodicky et al., 2015)	96.EPS.48.4_5*	1.97	1.97	3.94	3.94	72.05	6005	CFRP Grid
(Hodicky et al., 2015)	24.EPS.12.6_1*	1.97	1.97	3.94	5.91	72.05	6005	CFRP Grid
(Hodicky et al., 2015)	24.EPS.12.6_2*	1.97	1.97	3.94	5.91	72.05	6005	CFRP Grid
(Hodicky et al., 2015)	48.EPS.24.6_1*	1.97	1.97	3.94	5.91	72.05	6005	CFRP Grid
(Hodicky et al., 2015)	48.EPS.24.6_2*	1.97	1.97	3.94	5.91	72.05	6005	CFRP Grid
(Hodicky et al., 2015)	96.EPS.48.6_1*	1.97	1.97	3.94	5.91	72.05	6005	CFRP Grid
(Hodicky et al., 2015)	96.EPS.48.6_2*	1.97	1.97	3.94	5.91	72.05	6005	CFRP Grid
(Hodicky et al., 2015)	96.EPS.48.6_3*	1.97	1.97	3.94	5.91	72.05	6005	CFRP Grid

Table 6-1 continued

Reference	Designation	Wythe 1 (in)	Wythe 2 (in)	Central Wythe (in)	Insulation Thickness (in)	Height (in)	f'_c (psi)	Connector Type
(Hodicky et al., 2015)	96.EPS.48.6_4*	1.97	1.97	3.94	5.91	72.05	6005	CFRP Grid
(Hodicky et al., 2015)	96.EPS.48.6_5*	1.97	1.97	3.94	5.91	72.05	6005	CFRP Grid
(He et al., 2020)	VS300 -1	2.36	2.36	5.91	11.81	27.56	5192	I-Shaped GFRP
(He et al., 2020)	VS300 -2	2.36	2.36	5.91	11.81	27.56	5192	I-Shaped GFRP
(He et al., 2020)	VS150 -1	2.36	2.36	5.91	5.91	27.56	5192	I-Shaped GFRP
(He et al., 2020)	VS150 -2	2.36	2.36	5.91	5.91	27.56	5192	I-Shaped GFRP
(He et al., 2020)	VS120 -1	2.36	2.36	5.91	4.72	27.56	5192	I-Shaped GFRP
(He et al., 2020)	VS120 -2	2.36	2.36	5.91	4.72	27.56	5192	I-Shaped GFRP
(He et al., 2020)	VS60 -1	2.36	2.36	5.91	2.36	27.56	5192	I-Shaped GFRP
(He et al., 2020)	VS60 -2	2.36	2.36	5.91	2.36	27.56	5192	I-Shaped GFRP
(He et al., 2020)	HS300 -1	2.36	2.36	5.91	11.81	27.56	5192	I-Shaped GFRP
(He et al., 2020)	HS300 -2	2.36	2.36	5.91	11.81	27.56	5192	I-Shaped GFRP
(He et al., 2020)	HS150 -1	2.36	2.36	5.91	5.91	27.56	5192	I-Shaped GFRP
(He et al., 2020)	HS150 -2	2.36	2.36	5.91	5.91	27.56	5192	I-Shaped GFRP
(He et al., 2020)	HS120 -1	2.36	2.36	5.91	4.72	27.56	5192	I-Shaped GFRP
(He et al., 2020)	HS120 -2	2.36	2.36	5.91	4.72	27.56	5192	I-Shaped GFRP
(He et al., 2020)	HS60 -1	2.36	2.36	5.91	2.36	27.56	5192	I-Shaped GFRP
(He et al., 2020)	HS60 -2	2.36	2.36	5.91	2.36	27.56	5192	I-Shaped GFRP
(Bunn, 2011)	24EPS.12.2.A	2	2	4	2	72	6610	CFRP Grid
(Bunn, 2011)	24EPS.12.2.B	2	2	4	2	72	7000	CFRP Grid
(Bunn, 2011)	24EPS.12.4.A	2	2	4	4	72	6570	CFRP Grid
(Bunn, 2011)	24EPS.12.4.B	2	2	4	4	72	6920	CFRP Grid
(Bunn, 2011)	24EPS.12.6.A	2	2	4	6	72	7385	CFRP Grid
(Bunn, 2011)	24EPS.12.6.B	2	2	4	6	72	7980	CFRP Grid
(Bunn, 2011)	36EPS.18.2.A	2	2	4	2	72	5800	CFRP Grid

Table 6-1 continued

Reference	Designation	Wythe 1 (in)	Wythe 2 (in)	Central Wythe (in)	Insulation Thickness (in)	Height (in)	f'_c (psi)	Connector Type
(Bunn, 2011)	36EPS.18.2.B	2	2	4	2	72	6400	CFRP Grid
(Bunn, 2011)	36EPS.18.4.A	2	2	4	4	72	7980	CFRP Grid
(Bunn, 2011)	36EPS.18.4.B	2	2	4	4	72	7410	CFRP Grid
(Bunn, 2011)	36EPS.18.6.A	2	2	4	6	72	7745	CFRP Grid
(Bunn, 2011)	36EPS.18.6.B	2	2	4	6	72	7265	CFRP Grid
(Bunn, 2011)	48EPS.24.2.A	2	2	4	2	72	7980	CFRP Grid
(Bunn, 2011)	48EPS.24.2.B	2	2	4	2	72	7410	CFRP Grid
(Bunn, 2011)	48EPS.24.4.A	2	2	4	4	72	7980	CFRP Grid
(Bunn, 2011)	48EPS.24.4.B	2	2	4	4	72	7410	CFRP Grid
(Bunn, 2011)	48EPS.24.6.A	2	2	4	6	72	7160	CFRP Grid
(Bunn, 2011)	48EPS.24.6.B	2	2	4	6	72	6180	CFRP Grid
(Bunn, 2011)	48EPS.24.8.A	2	2	4	8	72	6180	CFRP Grid
(Bunn, 2011)	48EPS.24.8.B	2	2	4	8	72	7385	CFRP Grid
(Bunn, 2011)	72EPS.36.2.A	2	2	4	2	72	7790	CFRP Grid
(Bunn, 2011)	72EPS.36.2.B	2	2	4	2	72	6435	CFRP Grid
(Bunn, 2011)	72EPS.36.4.A	2	2	4	4	72	6435	CFRP Grid
(Bunn, 2011)	72EPS.36.4.B	2	2	4	4	72	7790	CFRP Grid
(Bunn, 2011)	72EPS.36.6.A	2	2	4	6	72	7300	CFRP Grid
(Bunn, 2011)	72EPS.36.6.B	2	2	4	6	72	6615	CFRP Grid
(Bunn, 2011)	24XPS.12.2.A	2	2	4	2	72	6450	CFRP Grid
(Bunn, 2011)	24XPS.12.2.B	2	2	4	2	72	7020	CFRP Grid
(Bunn, 2011)	24XPS.12.4.A	2	2	4	4	72	7980	CFRP Grid
(Bunn, 2011)	24XPS.12.4.B	2	2	4	4	72	7265	CFRP Grid
(Bunn, 2011)	36XPS.18.2.A	2	2	4	2	72	6100	CFRP Grid
(Bunn, 2011)	36XPS.18.2.B	2	2	4	2	72	6550	CFRP Grid

Table 6-1 continued

Reference	Designation	Wythe 1 (in)	Wythe2 (in)	Central Wythe (in)	Insulation Thickness (in)	Height (in)	f'_c (psi)	Connector Type
(Bunn, 2011)	36XPS.18.4.A	2	2	4	4	72	6570	CFRP Grid
(Bunn, 2011)	36XPS.18.4.B	2	2	4	4	72	7745	CFRP Grid
(Bunn, 2011)	48XPS.24.2.A	2	2	4	2	72	7160	CFRP Grid
(Bunn, 2011)	48XPS.24.2.B	2	2	4	2	72	7745	CFRP Grid
(Bunn, 2011)	48XPS.24.4.A	2	2	4	4	72	6570	CFRP Grid
(Bunn, 2011)	48XPS.24.4.B	2	2	4	4	72	6920	CFRP Grid
(Bunn, 2011)	72XPS.36.2.A	2	2	4	2	72	7300	CFRP Grid
(Bunn, 2011)	72XPS.36.2.B	2	2	4	2	72	6615	CFRP Grid
(Bunn, 2011)	72XPS.36.4.A	2	2	4	4	72	7300	CFRP Grid
(Bunn, 2011)	72XPS.36.4.B	2	2	4	4	72	6230	CFRP Grid
(Bunn, 2011)	48EPS.24.2.DEBOND.A	2	2	4	2	72	7160	CFRP Grid
(Bunn, 2011)	48EPS.24.2.DEBOND.B	2	2	4	2	72	7745	CFRP Grid
(Bunn, 2011)	48EPS.24.4.DEBOND.A	2	2	4	4	72	6435	CFRP Grid
(Bunn, 2011)	48EPS.24.4.DEBOND.B	2	2	4	4	72	7790	CFRP Grid
(Bunn, 2011)	48XPS.24.2.DEBOND.A	2	2	4	2	72	7790	CFRP Grid
(Bunn, 2011)	48XPS.24.2.DEBOND.B	2	2	4	2	72	6910	CFRP Grid
(Bunn, 2011)	48XPS.24.4.DEBOND.A	2	2	4	4	72	6910	CFRP Grid
(Bunn, 2011)	48XPS.24.4.DEBOND.B	2	2	4	4	72	6615	CFRP Grid
(Bunn, 2011)	48EPS.36.2.TRANS.A	2	2	4	2	72	7790	CFRP Grid
(Bunn, 2011)	48EPS.36.2.TRANS.B	2	2	4	2	72	6435	CFRP Grid
(Bunn, 2011)	48XPS.36.2.TRANS.A	2	2	4	2	72	6910	CFRP Grid
(Bunn, 2011)	48XPS.36.2.TRANS.B	2	2	4	2	72	6230	CFRP Grid
(Bunn, 2011)	36EPS.18.2.GAP.A	2	2	4	2	72	7745	CFRP Grid
(Bunn, 2011)	36EPS.18.2.GAP.B	2	2	4	2	72	7410	CFRP Grid
(Bunn, 2011)	36EPS.18.4.GAP.A	2	2	4	4	72	6910	CFRP Grid

Table 6-1 continued

Reference	Designation	Wythe 1 (in)	Wythe2 (in)	Central Wythe (in)	Insulation Thickness (in)	Height (in)	f'_c (psi)	Connector Type
(Bunn, 2011)	36EPS.18.4.GAP.B	2	2	4	4	72	6230	CFRP Grid
(Bunn, 2011)	36XPS.18.2.GAP.A	2	2	4	2	72	7385	CFRP Grid
(Bunn, 2011)	36XPS.18.2.GAP.B	2	2	4	2	72	7980	CFRP Grid
(Bunn, 2011)	36XPS.18.4.GAP.A	2	2	4	4	72	7790	CFRP Grid
(Bunn, 2011)	36XPS.18.4.GAP.B	2	2	4	4	72	6435	CFRP Grid
(Bunn, 2011)	48EPS.NONE.2.A	2	2	4	2	72	6570	CFRP Grid
(Bunn, 2011)	48EPS.NONE.2.B	2	2	4	2	72	6180	CFRP Grid
(Bunn, 2011)	48XPS.NONE.2.A	2	2	4	2	72	7265	CFRP Grid
(Bunn, 2011)	48XPS.NONE.2.B	2	2	4	2	72	7980	CFRP Grid
(Bunn, 2011)	20EPS.2.CREEP.A	2	2	4	2	72	-	CFRP Grid
(Bunn, 2011)	20EPS.2.CREEP.B	2	2	4	2	72	-	CFRP Grid
(Bunn, 2011)	20EPS.2.CREEP.C	2	2	4	2	72	-	CFRP Grid
(Bunn, 2011)	20EPS.2.CREEP.D	2	2	4	2	72	-	CFRP Grid
(Bunn, 2011)	20XPS.2.CREEP.A	2	2	4	2	72	-	CFRP Grid
(Bunn, 2011)	20XPS.2.CREEP.B	2	2	4	2	72	-	CFRP Grid
(Bunn, 2011)	20XPS.2.CREEP.C	2	2	4	2	72	-	CFRP Grid
(Bunn, 2011)	20XPS.2.CREEP.D	2	2	4	2	72	-	CFRP Grid

*Designation was modified to account for multiple identically designated specimens

Table 6-2 Full-Scale Panel Testing in Literature

Reference	Panel Designation	Wythe 1 (in)	Wythe 2 (in)	Insulation (in)	Span (ft)	Width (ft)	Foam Type	Connector Type	f'c (ksi)	Reinforcing Type
(Salmon et al., 1997)		2.52	2.52	2.99	30.00	8.00	EPS	#3 Nu V1	6.29	Prestressed
(Salmon et al., 1997)		2.52	2.52	2.99	30.00	8.00	EPS	#3 Nu V1	6.29	Prestressed
(Naito et al., 2011)	PCS1-A	3.00	3.00	2.00	10.00	2.67	EPS	Stainless C-Clip	8.22	Prestressed
(Naito et al., 2011)	PCS1-B	3.00	3.00	2.00	10.00	2.67	EPS	Stainless C-Clip	8.22	Prestressed
(Naito et al., 2011)	PCS1-C	3.00	3.00	2.00	10.00	2.67	EPS	Stainless C-Clip	8.22	Prestressed
(Naito et al., 2011)	PCS2-A	3.00	3.00	2.00	10.00	2.67	EPS	C-Grid	8.41	Prestressed
(Naito et al., 2011)	PCS2-B	3.00	3.00	2.00	10.00	2.67	EPS	C-Grid	8.41	Prestressed
(Naito et al., 2011)	PCS2-C	3.00	3.00	2.00	10.00	2.67	EPS	C-Grid	8.41	Prestressed
(Naito et al., 2011)	PCS3-A	3.00	3.00	2.00	10.00	2.67	EPS	C-Grid	8.40	Prestressed
(Naito et al., 2011)	PCS3-B	3.00	3.00	2.00	10.00	2.67	EPS	C-Grid	8.40	Prestressed
(Naito et al., 2011)	PCS3-C	3.00	3.00	2.00	10.00	2.67	EPS	C-Grid	8.40	Prestressed
(Naito et al., 2011)	PCS3-D	3.00	3.00	2.00	10.00	2.67	EPS	C-Grid	8.40	Prestressed
(Naito et al., 2011)	PCS3-E	3.00	3.00	2.00	10.00	2.67	EPS	C-Grid	8.40	Prestressed
(Naito et al., 2011)	PCS3-F	3.00	3.00	2.00	10.00	2.67	EPS	C-Grid	8.40	Prestressed
(Naito et al., 2011)	PCS4-A	3.00	3.00	3.00	10.00	2.67	XPS	Carbon C-Clip	8.82	Prestressed
(Naito et al., 2011)	PCS4-B	3.00	3.00	3.00	10.00	2.67	XPS	Carbon C-Clip	8.82	Prestressed
(Naito et al., 2011)	PCS4-C	3.00	3.00	3.00	10.00	2.67	XPS	Carbon C-Clip	8.82	Prestressed
(Naito et al., 2011)	PCS5-A	3.00	3.00	3.00	10.00	2.67	XPS	CC	8.80	Prestressed
(Naito et al., 2011)	PCS5-B	3.00	3.00	3.00	10.00	2.67	XPS	CC	8.80	Prestressed
(Naito et al., 2011)	PCS5-C	3.00	3.00	3.00	10.00	2.67	XPS	CC	8.80	Prestressed
(Naito et al., 2011)	PCS6-A	3.00	3.00	3.00	10.00	2.67	XPS	C-Grid	8.70	Prestressed
(Naito et al., 2011)	PCS6-B	3.00	3.00	3.00	10.00	2.67	XPS	C-Grid	8.70	Prestressed
(Naito et al., 2011)	PCS6-C	3.00	3.00	3.00	10.00	2.67	XPS	C-Grid	8.70	Prestressed

Table 6-2 continued

Reference	Panel Designation	Wythe 1 (in)	Wythe 2 (in)	Insulation (in)	Span (ft)	Width (ft)	Foam Type	Connector Type	f'c (ksi)	Reinforcing Type
(Naito et al., 2011)	PCS7-A	3.00	3.00	3.00	10.00	2.67	XPS	CC	8.85	Mild
(Naito et al., 2011)	PCS7-B	3.00	3.00	3.00	10.00	2.67	XPS	CC	8.85	Mild
(Naito et al., 2011)	PCS7-C	3.00	3.00	3.00	10.00	2.67	PIMA	CC	8.85	Mild
(Naito et al., 2011)	PCS8-A	3.00	3.00	3.00	10.00	2.67	PIMA	CC	8.82	Prestressed
(Naito et al., 2011)	PCS8-B	3.00	3.00	3.00	10.00	2.67	PIMA	CC	8.82	Prestressed
(Naito et al., 2011)	PCS8-C	3.00	3.00	3.00	10.00	2.67	PIMA	CC	8.82	Prestressed
(Naito et al., 2011)	PCS9-A	3.00	3.00	3.00	10.00	2.67	PIMA	C-Grid	8.62	Prestressed
(Naito et al., 2011)	PSC9-B	3.00	3.00	3.00	10.00	2.67	PIMA	C-Grid	8.62	Prestressed
(Naito et al., 2011)	PSC9-C	3.00	3.00	3.00	10.00	2.67	PIMA	C-Grid	8.62	Prestressed
(Naito et al., 2011)	TS1-A	6.00	3.00	2.00	10.00	1.33	XPS	N-CC	5.22	Mild
(Naito et al., 2011)	TS1-B	6.00	3.00	2.00	10.00	1.33	XPS	N-CC	5.22	Mild
(Naito et al., 2011)	TS1-C	6.00	3.00	2.00	10.00	1.33	XPS	N-CC	5.22	Mild
(Naito et al., 2011)	TS2-A	3.00	3.00	2.00	10.00	1.33	XPS	CC	4.93	Mild
(Naito et al., 2011)	TS2-B	3.00	3.00	2.00	10.00	1.33	XPS	CC	4.93	Mild
(Naito et al., 2011)	TS2-C	3.00	3.00	2.00	10.00	1.33	XPS	CC	4.93	Mild
(Naito et al., 2011)	Tin1-A	3.00	3.00	4.00	10.00	2.67	XPS	MB Truss Girder	8.46	Prestressed
(Naito et al., 2011)	Tin1-B	3.00	3.00	4.00	10.00	2.67	XPS	MB Truss Girder	8.46	Prestressed
(Naito et al., 2011)	Tin1-C	3.00	3.00	4.00	10.00	2.67	XPS	MB Truss Girder	8.46	Prestressed
(Naito et al., 2011)	Tin2-A	3.00	3.00	4.00	10.00	2.67	XPS	MB Truss Girder	8.47	Prestressed
(Naito et al., 2011)	Tin2-B	3.00	3.00	4.00	10.00	2.67	XPS	MB Truss Girder	8.47	Prestressed
(Naito et al., 2011)	Tin2-C	3.00	3.00	4.00	10.00	2.67	XPS	MB Truss Girder	8.47	Prestressed
(Trasborg, 2014)	PtEG2_1*	3.00	3.00	2.00	10.00	2.67	EPS	C-Grid	6.96	Prestressed
(Trasborg, 2014)	PtEG2_2*	3.00	3.00	2.00	10.00	2.67	EPS	C-Grid	6.96	Prestressed
(Trasborg, 2014)	PtEG2_3*	3.00	3.00	2.00	10.00	2.67	EPS	C-Grid	6.96	Prestressed

Table 6-2 continued

Reference	Panel Designation	Wythe 1 (in)	Wythe 2 (in)	Insulation (in)	Span (ft)	Width (ft)	Foam Type	Connector Type	f'c (ksi)	Reinforcing Type
(Trasborg, 2014)	RtXN_1*	3.00	3.00	2.00	10.00	2.67	XPS	#3 Nu V5	4.93	GFRP
(Trasborg, 2014)	RtXN_2*	3.00	3.00	2.00	10.00	2.67	XPS	#3 Nu V5	4.93	GFRP
(Trasborg, 2014)	RtXN_3*	3.00	3.00	2.00	10.00	2.67	XPS	#3 Nu V5	4.93	GFRP
(Trasborg, 2014)	PtXN_1*	3.00	3.00	2.00	10.00	2.67	XPS	#3 Nu V5	4.93	Prestressed
(Trasborg, 2014)	PtXN_2*	3.00	3.00	2.00	10.00	2.67	XPS	#3Nu V5	4.93	Prestressed
(Trasborg, 2014)	PtXN_3*	3.00	3.00	2.00	10.00	2.67	XPS	#3 Nu V5	4.93	Prestressed
(Trasborg, 2014)	RtXX_1*	3.00	3.00	2.00	10.00	2.67	XPS	X and CC	6.00	Mild
(Trasborg, 2014)	RtXX_2*	3.00	3.00	2.00	10.00	2.67	XPS	X and CC	6.00	Mild
(Trasborg, 2014)	RtXX_3*	3.00	3.00	2.00	10.00	2.67	XPS	X and CC	6.00	Mild
(Trasborg, 2014)	PtXX_1*	3.00	3.00	2.00	10.00	2.67	XPS	X and CC	6.00	Prestressed
(Trasborg, 2014)	PtXX_2*	3.00	3.00	2.00	10.00	2.67	XPS	X and CC	6.00	Prestressed
(Trasborg, 2014)	PtXX_3*	3.00	3.00	2.00	10.00	2.67	XPS	X and CC	6.00	Prestressed
(Al-Rubaye 2017)	A2	3.00	3.00	4.00	15.00	4.00	XPS	#3 Nu V5	10.43	Prestressed
(Al-Rubaye 2017)	A4	3.00	3.00	4.00	15.00	4.00	XPS	#3 Nu V5	10.43	Prestressed
(Al-Rubaye 2017)	D1	4.00	4.00	3.00	14.00	3.00	XPS	HK	9.22	Mild
(Al-Rubaye 2017)	D2	4.00	4.00	3.00	14.00	3.00	XPS	HK	9.22	Mild
(Al-Rubaye 2017)	BC1	4.00	4.00	3.00	14.00	3.00	XPS	HK	9.22	Mild
(Al-Rubaye 2017)	BC2	4.00	4.00	3.00	14.00	3.00	XPS	HK	9.22	Mild
(Pozo-Lora & Maguire, 2019)	P1	3.00	3.00	3.00	16.00	4.00	XPS	CF	8.75	Mild
(Pozo-Lora & Maguire, 2019)	P2	3.00	3.00	1.97	20.00	3.00	XPS	S	10.53	Mild
(Cox et al., 2019)	70-50-70-3.3	2.76	2.76	1.97	10.83	5.91	XPS	GFRP star	-	Mild
(Cox et al., 2019)	70-50-70-4.2	2.76	2.76	1.97	13.78	5.91	XPS	GFRP star	-	Mild
(Cox et al., 2019)	90-50-90-3.3	3.54	3.54	1.97	10.83	5.91	XPS	GFRP star	-	Mild

Table 6-2 continued

Reference	Panel Designation	Wythe 1 (in)	Wythe 2 (in)	Insulation (in)	Span (ft)	Width (ft)	Foam Type	Connector Type	f'c (ksi)	Reinforcing Type
(Cox et al., 2019)	90-100-90-3.3	3.54	3.54	3.94	13.78	5.91	XPS	GFRP star	-	Mild
(Cox et al., 2019)	90-50-90-4.2	3.54	3.54	1.97	10.83	5.91	XPS	GFRP star	-	Mild
(Cox et al., 2019)	90-100-90-4.2	3.54	3.54	3.94	13.78	5.91	XPS	GFRP star	-	Mild
(Choi et al. (a), 2015)	XPSST2_P	2.36	2.36	3.94	11.81	3.94	XPS	GFRP Shear Grid	6.53	Wire Mesh
(Choi et al. (a), 2015)	XPSST3_P	2.36	2.36	3.94	11.81	3.94	XPS	GFRP Shear Grid	6.53	Wire Mesh
(Choi et al. (a), 2015)	XPSST4_P	2.36	2.36	3.94	11.81	3.94	XPS	GFRP Shear Grid	6.53	Wire Mesh
(Choi et al. (a), 2015)	XPSNB2_P	2.36	2.36	3.94	11.81	3.94	XPS	GFRP Shear Grid	5.22	Wire Mesh
(Choi et al. (a), 2015)	XPSNB3_P	2.36	2.36	3.94	11.81	3.94	XPS	GFRP Shear Grid	5.22	Wire Mesh
(Choi et al. (a), 2015)	XPSNB4_P	2.36	2.36	3.94	11.81	3.94	XPS	GFRP Shear Grid	5.22	Wire Mesh
(Choi et al. (a), 2015)	EPS2_P	2.36	2.36	3.94	11.81	3.94	EPS	GFRP Shear Grid	5.22	Wire Mesh
(Choi et al. (a), 2015)	EPS3_P	2.36	2.36	3.94	11.81	3.94	EPS	GFRP Shear Grid	5.22	Wire Mesh
(Choi et al. (a), 2015)	EPS4_P	2.36	2.36	3.94	11.81	3.94	EPS	GFRP Shear Grid	5.22	Wire Mesh
(Choi et al. (a), 2015)	XPSST2_N	2.36	2.36	3.94	11.81	3.94	XPS	GFRP Shear Grid	6.53	Wire Mesh
(Choi et al. (a), 2015)	XPSST3_N	2.36	2.36	3.94	11.81	3.94	XPS	GFRP Shear Grid	6.53	Wire Mesh
(Choi et al. (a), 2015)	XPSST4_N	2.36	2.36	3.94	11.81	3.94	XPS	GFRP Shear Grid	6.53	Wire Mesh
(Choi et al. (a), 2015)	XPSNB2_N	2.36	2.36	3.94	11.81	3.94	XPS	GFRP Shear Grid	6.38	Wire Mesh
(Choi et al. (a), 2015)	XPSNB3_N	2.36	2.36	3.94	11.81	3.94	XPS	GFRP Shear Grid	6.38	Wire Mesh
(Choi et al. (a), 2015)	XPSNB4_N	2.36	2.36	3.94	11.81	3.94	XPS	GFRP Shear Grid	6.38	Wire Mesh
(Choi et al. (a), 2015)	EPS2_N	2.36	2.36	3.94	11.81	3.94	EPS	GFRP Shear Grid	6.53	Wire Mesh
(Choi et al. (a), 2015)	EPS3_N	2.36	2.36	3.94	11.81	3.94	EPS	GFRP Shear Grid	6.53	Wire Mesh
(Choi et al. (a), 2015)	EPS4_N	2.36	2.36	3.94	11.81	3.94	EPS	GFRP Shear Grid	6.53	Wire Mesh
(Pessiki & Mlynarczyk, 2003)	1	3.00	3.00	2.00	35.00	6.00	EPS	Steel M Ties and Concrete Sections	6.93	Prestressed
(Pessiki & Mlynarczyk, 2003)	2	3.00	3.00	2.00	35.00	6.00	EPS	Steel M Ties	8.76	Prestressed

Table 6-2 continued

Reference	Panel Designation	Wythe 1 (in)	Wythe 2 (in)	Insulation (in)	Span (ft)	Width (ft)	Foam Type	Connector Type	f'c (ksi)	Reinforcing Type
(Pessiki & Mlynarczyk, 2003)	3	3.00	3.00	2.00	35.00	6.00	EPS	Concrete Sections	6.24	Prestressed
(Pessiki & Mlynarczyk, 2003)	4	3.00	3.00	2.00	35.00	6.00	EPS	None	7.00	Prestressed
(Kim & You, 2015)	XPS0	2.36	2.36	3.94	11.81	3.94	XPS	GFRP Shear Grid	6.53	Wire Mesh
(Kim & You, 2015)	XPS1	2.36	2.36	3.94	11.81	3.94	XPS	GFRP Shear Grid	6.53	Wire Mesh
(Kim & You, 2015)	XPS2	2.36	2.36	3.94	11.81	3.94	XPS	GFRP Shear Grid	6.53	Wire Mesh
(Kim & You, 2015)	XPS3	2.36	2.36	3.94	11.81	3.94	XPS	GFRP Shear Grid	6.53	Wire Mesh
(Kim & You, 2015)	XPSC	2.36	2.36	3.94	11.81	3.94	XPS	GFRP Shear Grid	6.53	Wire Mesh
(Kim & You, 2015)	EPS0	2.36	2.36	3.94	11.81	3.94	EPS	GFRP Shear Grid	5.51	Wire Mesh
(Kim & You, 2015)	EPS1	2.36	2.36	3.94	11.81	3.94	EPS	GFRP Shear Grid	5.51	Wire Mesh
(Kim & You, 2015)	EPS2	2.36	2.36	3.94	11.81	3.94	EPS	GFRP Shear Grid	5.51	Wire Mesh
(Kim & You, 2015)	EPS3	2.36	2.36	3.94	11.81	3.94	EPS	GFRP Shear Grid	5.51	Wire Mesh
(Kim & You, 2015)	EPS4	2.36	2.36	3.94	11.81	3.94	EPS	GFRP Shear Grid	5.51	Wire Mesh
(Frankl et al., 2011)	EPS1	2.00	2.00	4.00	20.00	12.00	EPS	CFRP Shear Grid	7.62	-
(Frankl et al., 2011)	EPS2	2.00	2.00	4.00	20.00	12.00	EPS	CFRP Shear Grid	7.67	-
(Frankl et al., 2011)	XPS1	2.00	2.00	4.00	20.00	12.00	XPS	CFRP Shear Grid and Concrete Sections	10.08	-
(Frankl et al., 2011)	XPS2	4.00	2.00	2.00	20.00	12.00	XPS	CFRP Shear Grid	8.79	-
(Frankl et al., 2011)	XPS3	2.00	2.00	4.00	20.00	12.00	XPS	CFRP Shear Grid	7.67	-
(Frankl et al., 2011)	XPS4	2.00	2.00	4.00	20.00	12.00	XPS	CFRP Shear Grid	7.34	-
(Choi et al., 2016)	GEL01_M	2.36	2.36	3.94	14.76	6.89	EPS	GFRP Shear Grid	5.60	Wire Mesh
(Choi et al., 2016)	GXL01_M	2.36	2.36	3.94	14.76	6.89	XPSST	GFRP Shear Grid	5.12	Wire Mesh
(Choi et al., 2016)	GEL01_C	2.36	2.36	3.94	14.76	6.89	EPS	GFRP Shear Grid	5.12	Wire Mesh

Table 6-2 continued

Reference	Panel Designation	Wythe 1 (in)	Wythe 2 (in)	Insulation (in)	Span (ft)	Width (ft)	Foam Type	Connector Type	f'c (ksi)	Reinforcing Type
(Choi et al., 2016)	GXL01_C	2.36	2.36	3.94	14.76	6.89	XPSST	GFRP Shear Grid	5.22	Wire Mesh
(Fernando et al., 2017)	Compression-Type-1-1	-	-	-	2.26	1.97	EPS	None	-	-
(Fernando et al., 2017)	Compression-Type-1-2	-	-	-	2.26	1.97	EPS	None	-	-
(Fernando et al., 2017)	Compression-Type-1-3	-	-	-	2.26	1.97	EPS	None	-	-
(Fernando et al., 2017)	Compression-Type-2-1	-	-	-	2.26	1.97	EPS	None	-	-
(Fernando et al., 2017)	Compression-Type-2-2	-	-	-	2.26	1.97	EPS	None	-	-
(Fernando et al., 2017)	Compression-Type-2-3	-	-	-	2.26	1.97	EPS	None	-	-
(Fernando et al., 2017)	Compression-Full-Type-1-1	-	-	-	7.87	1.97	EPS	None	-	-
(Fernando et al., 2017)	Compression-Full-Type-1-2	-	-	-	7.87	1.97	EPS	None	-	-
(Fernando et al., 2017)	Compression-Full-Type-2-1	-	-	-	7.87	1.97	EPS	None	-	-
(Fernando et al., 2017)	Compression-Full-Type-2-2	-	-	-	7.87	1.97	EPS	None	-	-
(Fernando et al., 2017)	Flexure-Type-1	-	-	-	7.87	1.97	EPS	None	-	-

Table 6-2 continued

Reference	Panel Designation	Wythe 1 (in)	Wythe 2 (in)	Insulation (in)	Span (ft)	Width (ft)	Foam Type	Connector Type	f'c (ksi)	Reinforcing Type
(Fernando et al., 2017)	Flexure-Type-2	-	-	-	7.87	1.97	EPS	None	-	-
(Pantiledes et al., 2008)	Epoxy-cured GFRP single-cage	2.52	2.52	2.99	14.50	2.00	EPS	Hybrid GFRP/Steel Cages	4.06	Mild
(Pantiledes et al., 2008)	Urethane-cured GFRP Single-Cage	2.52	2.52	2.99	14.50	2.00	EPS	Hybrid GFRP/Steel Cages	4.06	Mild
(Pantiledes et al., 2008)	Epoxy-cured GFRP Double-Cage	2.52	2.52	2.99	14.50	2.00	EPS	Hybrid GFRP/Steel Cages	4.06	Mild
(Pantiledes et al., 2008)	Urethane-cured GFRP Double-Cage	2.52	2.52	2.99	14.50	2.00	EPS	Hybrid GFRP/Steel Cages	4.06	Mild
(Benayoune, 2007)	P11	1.57	1.57	1.57	6.56	2.46	-	Steel Truss	-	-
(Benayoune, 2007)	P12	1.57	1.57	1.57	6.56	2.46	-	Steel Truss	-	-
(Benayoune, 2007)	P21	1.57	1.57	1.57	4.92	4.92	-	Steel Truss	-	-
(Benayoune, 2007)	P22	1.57	1.57	1.57	4.92	4.92	-	Steel Truss	-	-
(Benayoune, 2007)	P23	1.57	1.57	1.57	3.28	1.64	-	Steel Truss	-	-
(Benayoune, 2007)	P24	1.57	1.57	1.57	3.28	1.64	-	Steel Truss	-	-

*Designation was modified to account for multiple identically designated specimens.